ELECTRIC AND MICROFLUIDIC MANIPUILATION OF MOLECULES AND PARTICLES IN MICROFABRICATED DEVICES

by

Kyung Eun Sung

A dissertation submitted in partial fulfillment
of the requirements for the degree of
Doctor of Philosophy
(Chemical Engineering)
in the University of Michigan
2007

Doctoral Committee:

        Professor Mark A. Burns, Chair
        Professor David T. Burke
        Professor Ronald G. Larson
        Assistant Professor Joerg Lahann

To my parents

ACKNOWLEDGEMENTS

First, I offer my sincerest thanks and deepest appreciation to my advisor, Professor Mark A. Burns for his undying assistance and support during my Ph.D. study. I arrived in Ann Arbor, MI in the fall of 2002 from Korea. Having never resided on a long-term basis in any foreign country, I was lost during my first semester prior to meeting professor Burns. He has aptly guided me through my research projects and provided extensive research freedom and opportunities. Moreover, he encouraged me, times too numerous to mention, when I experienced difficulties and glitches during my studies. His consistent aid immensely impacted successful completion of my doctoral study. Actually, he has been more than a research advisor to me. Whenever I experienced concerns and troubles beyond research related problems, I felt assurance talking to Mark. Consistently, he gave me excellent suggestions and recommendations, as those a close family member would contribute.

Moreover, I would like to thank my committee members, Professors Larson, Burke, and Lahann, for the numerous suggestions and assistance with my dissertation work. When I was involved in the DNA stretching project, I had several meetings with Professor Larson and Burke, and I obtained many great instructions, facilitating experimental proceedings. Professor Lahann posed excellent questions at my preliminary examination and data meeting, which caused me to reevaluate problems previously not

considered in depth. Moreover, his suggestions were invaluable in finishing the works presented in this dissertation.

It is my pleasure to acknowledge Professors Solomon and Mirecki-Millunchick, as we have worked together intensively on the anisotropic particle synthesis. The project would not have been successful without their expertise. Actually, Professor Solomon has unofficially acted as a second advisor during my fourth and fifth years of Ph.D. study, when I was actively involved in the particle synthesis project. I was greatly impressed at his enthusiasm and endeavor at the research, and I have learned organizational skills under his tutelage. It was always pleasurable to work with Professor Mirecki-Millunchick as her personality elicits warmth and encouragement in every meeting. Likewise, she has contributed enormous knowledge regarding material sciences and nanofabrication to the project group.

In addition, I would like to extend thanks to current and previous Burns research group members and a special thank you to Brian Johnson, our Lab Manager. Having the Burns Research Group without Brian's knowledge and support is unimaginable. I received tremendous assistance from him during my study with fabrication and experimental set-ups. I would also like to thank previous research staffs in our group, Zafar, K.C., Dylan, Ken, and Razi. They put forth enormous effort to maintain a clean room and labs for the Burns group. Furthermore, I want to acknowledge my senior members, Rohit, Ming, Nimisha, Zheng, and Prasanna, all of whom are great people. I will sincerely miss the times spent with them in the lab. In addition, I extend thanks to current lab members, Dustin, Sean, Minsoung, Fang, Akshat, Jihyang, and Ramsey for sharing great lab and office experiences.

Furthermore, sincere appreciation is extended to the people in MNF, especially, Onnop, Sanghyun, Jaeyoong, Jongmun, Venkat, Xiaoyang, Jaehyun, Sangwon, and Greg for their tremendous assistance in the area of fabrication. Every one of them is knowledgeable and skillful and has taught me many 'know-how's' unattainable through regular classroom training, and these helps have expedited my processes.

Additionally, I want to acknowledge PCM project group members, Siva, Desh, and Hugh. I still remember when we had weekly meetings, trying to do everything possible to create the system. Although some periods were tough, the fruitful outcomes made everything worthwhile.

Times in Ann Arbor, spent with such very nice friends, have proven a stable foundation to me. The transition of adapting to an unfamiliar culture and environment could have caused great amounts of stress; however, my experiences are remembered with extreme confidence and joy, do to the loving warmth of wonderful friends. Although I cannot enumerate individually (because there are so many), I extend a heartfelt thanks to each and everyone. Jihyang and Jenny came to Ann Arbor last year, and we are as three musketeers. They hold a special place with me, as prior to their arrival I had no female Korean friends in the Ann Arbor. They offered a spice and variety of life, packing my stay here with fun. I cannot imagine how enjoyable it would have been had they arrived earlier.

The support from my parents has been by far the greatest contribution to my life's work. They have always trusted me and offered endless backing. I am so happy that they are healthy, active, positive, and enthusiastic about work and life. Their example of kindness and their wonderful attitudes have been exceptional role models for my life.

The energy of my grandmother, an awesome woman, is unending, and her concern for me is noteworthy. Thank you so much, Grandma! I would also like to thank my two brothers and my sister-in-law as well, who have always expressed concern about my wellness and have desired my success and happiness.

Finally, I want to thank my fiancé, Yong Jin, for his continued love and support.

TABLE OF CONTENTS

LIST OF FIGURES

ABSTRACT

Microfabrication technology has enabled traditional chemical and biological research to be performed at the micrometer scale, but the control of particles suspended in fluids and the fluids themselves remain a significant challenge. This dissertation is aimed at developing simple and versatile control systems for fluids and small entities (e.g., particles and molecules) in fluids. Accordingly, three methods have been explored using electric and fluidic micromanipulation, as well as physical deposition.

First, dielectrophoretic DNA positioning and elongation in a microchannel have been examined with modified surface chemistry and electrode conditions. Less hydrophilic surfaces provided more controllable stretching, presumably due to the decreased non-specific adsorption of DNA on these surfaces compared to their more hydrophilic counterparts. Smoothed electrode edges allowed more controlled stretching, and, moreover, thin electrodes (50 nm) provided dense electric field and gave ~90% success rate of DNA stretching.

Second, a microstencil method has been developed to pattern thermally and chemically sensitive materials. The microstencil has a bi-layer structure comprised of two polymeric films (i.e., parylene and SU8). The parylene layer enables the microstencil to be mechanically peeled from hydrophilic substrates and SU8 provides height to control the amount of material deposited. The amount is also controlled externally by performing multiple spin or dip coating processes. As an initial demonstration of the method, a wide

range of chemically and thermally labile materials has been patterned: wax, cells, and proteins.

Third, a continuous synthesis system for anisotropic microparticles with different shapes and sequences has been developed. The anisotropic particles are configured by exploiting a combination of geometrical confinement and microfluidics to pack particles into a narrow, terminal channel, and the packed particles are then bonded by thermal fusing. The width and length of the channels reproducibly specify the configuration of the anisotropic particles that will be produced. Complex sequences are obtained by coupling the sequential actuation of metering lines with the input flow of different particles. By using the process, linear and triangular homogeneous (A) and heterogeneous (A-B and A-B-A) particle chains have been synthesized.

CHAPTER 1
INTRODUCTION

Motivation

With the recent advances of microfabrication technology, allowing rapid novel technology development and dramatic cost reduction, Lab-on-a-chip (LOC) devices have been realized to perform microscale chemical or biological researches[1, 2]. LOC devices are mostly constructed with microfluidic channels and microfabricated electrodes, and include microfluidic components such as valve, pump, reactor, separator, and detector to conduct sequential steps in a single device. The early stage of LOC devices provided tools for genetic analysis such as DNA microarray, polymer chain reaction (PCR), and capillary electrophoresis (CE)[1, 2]. Strong advantages of LOC devices (i.e., rapid process, high throughput, automation, and nano-liter amount sample) have led to the development of other microfluidic devices such as clinical diagnostic devices, protein and cell manipulation devices, and immunoassay devices[3-7]. As the devices advance, the control techniques have also improved to control flow, mass transport, and heat transfer in the microsystems.

The primary control methods widely conducted in LOC devices are electrokinetic and fluidic control as well as control via surface modification. These controls are aimed to manipulate either fluid in microchannels or particles (or molecules) in fluid. The

major constituent of LOC devices are liquid in the microfluidic channel; thus, precise manipulation of the microfluidic process has been one actual key to the operation and performance of LOC. Liquid flow in the microchannel is controlled either by external pressure sources, external mechanical pumps, integrated micropumps (i.e., pressure-driven flow control)[8-12] or by electrokinetic force (i.e., electroosmotic flow control)[13, 14]. Electrokinetic forces are also utilized to control individual molecules or particles in the fluid by employing electrical properties of particles and fluid (e.g., Capillary Electrophoresis)[1, 15]. Due to the very large surface to volume ratio of microchannels, significant influence of the liquid-channel wall interface is expected. Therefore, surface modification has been another important factor in controlling microfluidics. Among these, three specific controls are selected and investigated for this dissertation: Dielectrophoretic DNA stretching, microstencil for patterning, and anisotropic particle synthesis using microfluidic control.

Dielectrophoretic DNA stretching

Recently, single DNA molecule based research has advanced considerably, as the information obtained from single molecule manipulation is more specific and accurate compared to that obtained from conventional methods, which generally average many molecules. DNA stretching is an excellent method to perform single molecule manipulation, and the molecule can be stretched by electrostatic, hydrodynamic, or magnetic forces[16-23]. Dielectrophoretic stretching is one of the most common methods using electrostatic force[7, 17, 24]. This method is possible as the DNA molecule is polarized under a non-uniform electric field constructed of geometrically different electrodes. The

DNA molecules between the two electrodes are stretched along the electric field line under the influence of a strong alternating electric field (10^6 V/m, 1MHz). The strong advantage of this stretching method is that further researches such as DNA-protein interaction and enzymatic cutting of DNA molecules can be conducted easily on the same system. Moreover, the method can be incorporated readily into the more complex integrated device to perform complete DNA analysis using single molecule manipulation.

The fundamental DEP DNA stretching system is optimized in this work by regulating electric and surface system properties. A set containing one pointed-shape electrode and one flat electrode is used to generate a non-uniform electric field required for DEP. Noteworthy is the fact that variances of electrode gap, shape, and thickness generate different electric field gradients, yielding a recognizable effect on DNA stretching. Surface modification has improved the controllability of the electrokinetic control performed in the system. Surfaces treated with higher silane concentrations have performed more optimally due to the decreased nonspecific adsorption of DNA on these surfaces, compared to their more hydrophilic counterparts.

Microstencils for patterning non-traditional materials

The patterning of non-traditional materials may contribute significantly to the application areas using microsystems. Traditional photolithographic patterning typically involves cyclic processing steps such as photoresist coating, thermal treatment, UV exposure, chemical development, and wet/dry etching[25]. As MEMS technology is harnessed for newer applications particularly related to biology, some classes of materials and surfaces need to be used that are incompatible with the chemical or thermal process

steps associated with standard microfabrication. Shadow masking and imprinting have been recently developed for the non-traditional materials[26, 27]. However, greater impact would be generated if a developed method could be combined with traditional microfabrication technology to achieve precise alignment, creating a traditional-nontraditional hybrid system.

Microstencil, developed in this work, employs photolithographically patterned parylene-SU8 bilayer, and the stencil layer is easily peeled off from the surface mechanically without the use of chemical solvents. As the stencil is prepared by traditional microfabrication technology, precise alignment of deposited material is achieved straightforwardly. The height of the stencil layer depends on the thickness of the SU8 layer, which may determine the amount of material deposited internally. External control processes such as multiple spin-coatings and multiple dip-coatings also control the amount of patterning materials. As an initial demonstration, we have patterned wax, cells, proteins, sol, and CYTOP^{TM}.

Anisotropic particle synthesis by using microfluidic control

Fluidic manipulation of materials in micro channels has been the indispensable control method in a microfluidic system, and it can be utilized to achieve many novel applications such as anisotropic particle synthesis. To date, spherical shaped microparticles are primarily employed in microparticle research and very few techniques have been developed to synthesize non-spherical anisotropic particles. Microcontact printing is one technique that has been successfully used for fabricating non-spherical particles, which uses non-wetting substrates and molds to confine liquid precursors inside

the features of the mold, allowing for the generation of isolated particles[28]. Continuous flow lithography, a second technique, utilizes microscope-projection photolithography to polymerize mask-defined regions in microchannel contained monomer flows[29]. The use of a liquid precursor in these two methods, to synthesize particles, has the advantage of speed, without shape limitations. However, the technique's disadvantage is a limit on the type of materials that can be used, greatly reducing the functionality of the synthesized particles. Particle synthesis, via microfluidic control and complex channel geometry, would be a good solution for the issues produced by current techniques. As particles are transported by pressure-driven flow, different particles can be transported through the system by the same method. Moreover, different particles may possess their own properties and chemistry, which require different reaction methods to link them. Furthermore, microfabricated systems, constructed with silicon and glass, have excellent adaptability, and thus are easily modified for each case.

In our system, the sequences and shapes of the anisotropic particles are determined by employing a combination of geometrical confinements and microfluidics to pack precursor colloids into a narrow, terminal channel. The width and length of the channel define shape of the anisotropic particle that will be produced. The precursor spheres packed in the production zone are then permanently bonded into particles via thermal fusing. The flow in the production zone is reversed to release the particles for collection and use. Particles produced have linear chain structures with precisely configured, repeatable bond angles. With software programmable microfluidics, sequence and shape anisotropy are combined to yield synthesized homogeneous (type

"A"), surfactant-like (type "A-B") or tri-block (type "A-B-A") internal sequences in a single device.

Organization of this dissertation

The theme of this dissertation is to investigate and develop electric and microfluidic control components to manipulate molecules and particles in microfabricated devices. As previously mentioned, three distinct works are studied by executing electric and microfluidic control and as well surface modification. Dielectrophoretic (DEP) DNA stretching and its optimization are presented in Chapter 2 as an electric control component. A novel surface patterning technique called "Microstencil" is described in Chapter 3. The method for anisotropic particle synthesis is developed by exploiting fluidic control in complex microchannel geometry, and is introduced in Chapter 4. The presented method employs the combination of continuous microfluidic control and sintering of polymeric particles. Therefore, Chapter 5 describes in greater detail the fluidic control used in the synthesis method, and Chapter 6 reports the characteristics of sintering methods and sintered particles.

Through the methods presented in this dissertation, useful means have been provided to manipulate molecules and particles in microfabricated devices, and conclusions and future works are stated in Chapter 7. Although each developed method possesses its own goal and purpose, all works can be unified by the concept of providing robust systems to manipulate small entities in microchannels. By optimizing conditions for DEP DNA stretching, more controllable and reliable electric field control is achieved,

resulting in a robust DNA stretching system. The novel patterning technique developed here has provided an extremely simple and versatile way of surface modification, which can be applied to many different applications, which involve electric and fluidic control. The fluidic control system developed for particle synthesis is very flexible, facilitating its utilization for other applications such as cell-manipulation devices and synthesis, via other reaction schemes.

References

1.   Lagally, E. T.; Emrich, C. A.; Mathies, R. A., Fully integrated PCR-capillary electrophoresis microsystem for DNA analysis. *Lab chip* **2001,** 1, 102-107.

2.   Pal, R.; Yang, M.; Lin, R.; Johnson, B. N.; Srivastava, N.; Razzacki, S. Z.; Chomistek, K. J.; Heldsinger, D. C.; Haque, R. M.; Ugaz, V. M.; Thwar, P. K.; Chen, Z.; Alfano, K.; Yim, M. B.; Krishnan, M.; Fuller, A. O.; Larson, R. G.; Burke, D. T.; Burns, M. A., An Integrated Microfluidic Devices for Influenza and Other Genetic Analyses. *Lab chip* **2005,** 5, (10), 1024-1032.

3.   Carlo, D. D.; Wu, L. Y.; Lee, L. P., Dynamic single cell culture array. *Lab chip* **2006,** 6, 1445-1449.

4.   Voldman, J., Electrical Forces For Microscale Cell Manipulation. *Annu. Rev. Biomed. Eng.* **2006,** 8, 425-454.

5.   Pregibon, D. C.; Toner, M.; Doyle, P. S., Multifunctional Encoded Particles for High-Throughput Biomolecular Analysis. *Sience* **2007,** 315, 1393-1396.

6.   Han, J.; Craighead, H., *Analytical Chemistry* **2002,** 74, 394-401.

7.   Namasivayan, V.; Larson, R.; Burke, D.; Burns, M., *Analytical Chemistry* **2002,** 74, 3378-3385.

8.   Eddington, D. T.; Beebe, D. J., Flow control with hydrogels. *Advanced Drug Delivery Reviews* **2004,** 56, 199-210.

9.   Liu, D.; Maxey, M.; Karniadakis, G. E., A fast method for particulate microflows. *Journal of Microelectromechanical systems* **2002,** 11, (6), 691-702.

10.   Nath, P.; Roy, S.; Conlisk, T.; Fleischman, A. J., A System for Micro/Nano Fluidic Flow Diagnostics. *Biomedical Microdevices* **2005,** 7, (3), 169-177.

11.   Pal, R.; Yang, M.; Johnson, B. N.; Burke, D. T.; Burns, M. A., Phase Change Microvalve for Integrated Devices. *Anal. Chem.* **2004,** 76, 3740-3746.

12.   Santiago, J. G.; Wereley, S. T.; Meinhart, C. D.; Beebe, D. J.; Adrian, R. J., A particle image velocimetry system for microfluidics. *Experiments in Fluids* **1998,** 25, 316-319.

13.   Bazant, M. Z.; Squires, T. M., Induced-Charge Electrokinetic Phenomena: Theory and Microfluidic Applications. *Physical Review Letters* **2004,** 92, (6), 066101.

14. Wouden, E. J. v. d.; Heuser, T.; Hermes, D. C.; Oosterbroek, R. E.; Gardeniers, J. G. E.; Berg, A. v. d., Field-effect control of electro-osmotic flow in microfluidic networks. *Colloids and Surfaces A: Physicochem. Eng. Aspects* **2005,** 267, 110-116.

15. Morgan, H.; Green, N. G., *AC Electrokinetics: Colloids and nanoparticles.* Research Studies Press: Philadelphia, 2003.

16. Gosse, C.; Croquette, V., *Biophysics Journal* **2002**, 3314-3329.

17. Washizu, M.; Kurosawa, O., *IEEE Transcations on Industry Applications* **1990,** 26, 1165-1172.

18. Washizu, M.; Kurosawa, O.; Arai, I.; Suzuki, S.; Shimamoto, N., *IEEE Transcations on Industry Applications* **1995,** 31, 447-456.

19. Washizu, M.; Nikaido, Y.; Kurosawa, O.; Kabata, H., *Journal of Electrostatics* **2003,** 57, 395-405.

20. Turner, S.; Cabodi, M.; Craighead, H., *Physical Review Letters* **2002,** 88.

21. Allemand, J.; Bensimon, D.; Jullien, L.; Bensimon, A.; Croquette, V., *Biophysical Journal* **1997,** 73, 2064-2070.

22. Bakajin, O.; Duke, T.; chou, C.; Chan, S.; Austin, R.; Cox, E., *Physical Review Letters* **1998,** 80, 2737-2740.

23. Bensimon, D.; Simon, A.; Croquette, V.; Bensimon, A., *Physical Review Letters* **1995,** 74, 4754-4757.

24. Herbert, A. P., *Dielectrophoresis.* Cambridge University Press: Cambridge, 1978.

25. Madow, M., *Fundamentals of Microfabrication.* CRC Press LLC: 1997.

26. Guo, L. J., *J. Phys. D: Appl. Phys.* **2004,** 37, (11), R123-R141.

27. Jackman, R. J.; Duffy, D. C.; Cheriniavskaya, O.; Whitesides, G. M., *Langmuir* **1999,** 15, 2973-2984.

28. Rolland, J. P.; Maynor, B. W.; Euliss, L. E.; Exner, A. E.; Denison, G. M.; DeSimon, J. M., *Journal of American Chemical Society* **2005,** 127, 10096-10100.

29. Dendukuri, D.; Pregibon, D. C.; Collins, J.; Hatton, T. A.; Doyle, P. S., Continuous-flow lithography for high-throughput microparticle synthesis. *Nature Material* **2006,** 5, 365-369.

CHAPTER 2

OPTIMIZATION OF DIELECTROPHORETIC DNA STRETCHING

IN MICROFABRICATED DEVICES

Introduction

Manipulation of single biomolecules such as DNA, RNA, and proteins facilitated significant advances in biology. For example, an optical trap produced by highly focused laser light can be used to grab and move a molecule as well as exert measurable forces on biomolecules.[1, 2] These manipulations can be used to determine molecular properties such as elasticity both in a natural state and under tensional or torsional stress. Another example is the study of molecular motors by single molecule manipulation.[3] By using optical tweezers to follow the progression of a single kinesin molecule on a microtubule rail, it has been found that the two-headed kinesin molecule progresses in steps of 8 nm for each ATP consumed.

Technological advances in micro/nano technology and high resolution visualizing systems facilitate single molecule manipulation. The trapping[4, 5] and stretching[6, 7] of DNA molecules, one of the most widely used molecules in single-molecule experiments, has been achieved using microdevices. Through high-resolution fluorescence microscopy, real-time restriction[8] and replication[9] of a single DNA molecule has been observed and,

moreover, the transport properties of a single DNA molecule were obtained.[10] In addition, the use of atomic force microscopy (AFM)[11] have affected considerable progress in the arrangement and manipulation of single molecules.

DNA molecules can be stretched by various means including electrostatic, hydrodynamic, or magnetic forces. Washizu used dielectrophoresis and electroosmotic flow to stretch DNA molecules.[6, 7, 12, 13] Entropic constriction has also been employed to stretch DNA by electrostatic forces.[14] In order to use a magnetic force, magnetic tweezer[15] that use magnetic fields and beads are necessary. Stretching by hydrodynamic force was performed either with free molecular ends or with one end immobilized to a solid surface.[16-18] In practice, anchoring methods tend to give more consistent stretching than free-end methods. Thus most DNA stretching involves anchoring one end of the DNA molecules onto an electrode, bead, or other solid surface, and stretching the molecule using some type of force.

Dielectrophoretic stretching is one of the most common methods in DNA manipulation.[6, 7] Dielectrophoresis is a non-contact manipulation technique that enables positioning and orientating DNA molecules in micro and nano devices.[19] A Dielectrophoretic force results from the interaction between an induced dipole on the molecule and a non-uniform electric field, and is a function of frequency, electric field and dielectric properties of the molecule and medium. Depending on the conditions, the molecule moves either toward (positive dielectrophoresis) or away from (negative dielectrophoresis) the region of high electric field gradients. If the molecule is more polarizable than its medium, positive dielectrophoresis is observed; conversely negative dielectrophoresis will occur if the molecule is less polarizable. In order to stretch DNA

molecules, high frequency (>1MHz) and high voltage (~1 MV/m) AC electric fields are typically used and result in negative dielectrophoresis.

In this work, we have studied the parameters affecting dielectrophoretic stretching of DNA in a microfabricated device and found the stretching is a function of the surface, microelectrode, and bulk solution properties. We have optimized those parameters and been able to achieve more constant DNA stretching.

Materials and Methods

Device fabrication

The device for DNA electrostretching was made by bonding two separate sides: channel and electrode (Figure 2.1). Fluidic channels are made on thick glass (500μm thickness, 100-mm diameter, Dow corning Pyrex 7740 in Midland, MI) by hydrofluoric acid etching. 50nm thick chrome and 300nm gold layers were deposited on bare glass surface and photoresist (PR 1827, Shipley company in Newton, MA) was spun, patterned by channel mask layer and developed in MF 319 solution (Rohm and haas electronic materials in Spartanburg, SC). Metal layers on developed area were removed by commercial etchants (Gold etchant, Gold etch-type TFA, Transene Company, Inc. in Danvers, MA; Chrome etchant, CR-14 chromium photomask etchant, Cyantek Corporation in Fremont, CA). The channel shaped glass region was then etched by hydrofluoric acid (J.T. Baker in phillipsburg, NJ). After obtaining the desired depth (20μm), the remaining photoresist and metal layers over glass surface were striped by photoresist removal solution (PRS 2000) and prospective etchants. The wafer was rinsed

in DI water, dried by air, and diced into each pieces. Holes were drilled on both ends of channel by electrochemical discharge drilling to inject sample into channel.
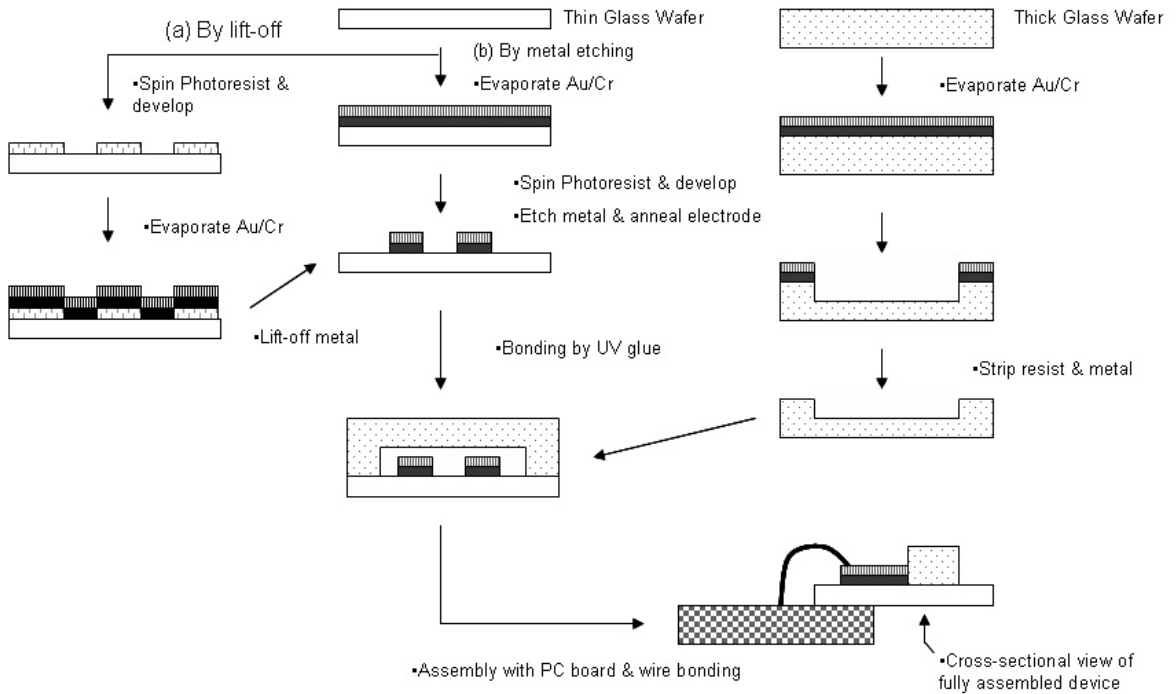
Figure 2. 1. Schematic process of microfabricated electrostretching device; (a) Lift-off, (b) metal etching for electrode fabrication.

Electrodes were fabricated on thin glass wafer (100μm thickness, 100-mm diameter, Precision Glass & Optics D263 in Santa Ana, CA). Two different methods were used in this work: Lift-off and Metal etching. For lift-off methods, photoresist was spun, patterned and developed on bare glass wafers. 15~50nm chrome layer and 50~300nm gold layer were deposited over developed photoresist. Then the wafer was immersed in acetone solution (J.T Baker) to lift-off unwanted parts of the metal and was rinsed in DI water and dried. For metal etching, 50~300nm gold layer and 15~50nm chrome layer were deposited on bare glass wafer and photoresist was spun, patterned and developed. Metal layers were etched (Gold etchant, Gold etch-type TFA, Transene

13

Company, Inc.; Chrome etchant, CR-14 chromium photomask etchant, Cyantek Corporation) and then the remained photoresist was stripped in PRS 2000 solution. The wafer was rinsed, dried and diced by diamond tip glass cutter (Glass cutter diamond, Fisher Scientific). For each process, some wafers were annealed at around 450°C for 10 min to improve the edge of electrode.

The obtained glass channel and electrode sides were bonded by optical adhesive (Type SK-9 Lens bond, Summers optics in Hatfield, PA). The bonded device was wired to printed circuit board (PCB) by gold or aluminum wire bonding for electrical contact. The backside of channel remained opened for accessibility during viewing in an inverted microscope.

Surface treatment

Four different surfaces were prepared in this work: clean glass, piranha cleaned surface, sigma-cote coated surface, and tetramethylchlorosilane (TMCS) coated surface. For the clean glass surface, both channel and electrode pieces were cleaned sequentially with acetone, isopropyl alcohol (2-Propanol, J.T. Baker) and DI water and bonded by UV curing. Piranha cleaned surface was made by soaking in piranha solution (1:3 v/v of hydrogen peroxide (Hydrogen peroxide 30%, J.T. Baker) and sulfuric acid (J.T. Baker)) for 40 min. The glass pieces were washed sequentially with water, warm acetone (120°C), warm isopropyl alcohol (IPA) (120°C) and water, and then dried.

For sigma-cote coated surface, sigma-cote solution (Sigma-Cote, Sigma Aldrich) was injected into channel and left to be dried. To get more lasting surface, it was placed in a 100°C oven for 30 min. To treat surfaces with TMCS (Chlorotrimethylsilane, Sigma

Aldrich), the inside of the channel was incubated for 1 hr by TMCS mixture (1:5 v/v solution of TMCS in tetrachloroethane (1,1,2,2-Tetrachloroethane, Sigma Aldrich) solution) and the channel was washed three times with tetrachloroethane (TCE), IPA and DI water, and then air-dried.

To measure surface contact angles, 2 µl of water was dropped on the treated surface and the drop image was captured horizontally. The image was then analyzed by Image J software (NIH) to measure the angle between the baseline of the drop and the tangent at the drop boundary.

DNA sample preparation

Plain λ-phage DNA and thiol-labled λ-phage DNA were prepared in this work. For thiol-labled λ-DNA, λ-phage DNA (New England Bio Lab in Ipswich, MA) with a 12 base-long single stranded "overhang" on each end was obtained and oligonucleotides for "overhang" sequence were synthesized. 5'-termini of λ-DNA was dephosphorylated by shrimp alkaline phosphate. A ligation reaction was done by T4 ligase enzyme and the concentration of thiol-labled λ-DNA was measured using a spectrometer. The thiol-labled DNA was labeled again with fluorescent marker YOYO-1 (Molecular Probes in Carlsbad, CA) at a dye-to-base-pair ratio of 1:5.

DI water (pH 8, conductivity 2µS/cm) plus 20% β-mercaptoethanol to prevent photobleaching was used as sample buffer and was mixed with 4 wt% of linear polyacrylamide (CEQ Separation gel LPA-1, Beckman Coulter in Fullerton, CA) to enhance molecule stretching. A high concentration of β-mercaptoethanol (20%) was used in this work similar to that used in the work by Namasivayan et al. in 2002 but lower

concentrations (4%) have also been used successfully.[20] Labeled DNA molecules were mixed with that sample solution to make final concentration of DNA sample as 50 pg/μl. After mixing, the DNA sample was degassed under the vacuum for 30 min.

Electric field application

Alternating current (AC) voltage was generated from a function generator (MX-9300A, Elenco). The frequency was regulated from 1Hz to 2.3 MHz and the amplitude was ranged from 2 Vp-p to 25 Vp-p. Waveforms were monitored by an oscilloscope (TDS 3014B, Tektronix).

Fluorescence microscope

An Inverted fluorescence microscope (TE-200, Nikon) was used to observe the motion of single DNA molecules. High magnification (x100) oil immersion objective was used to get high resolution and an electronic shutter was used to prevent photobleaching. The molecular behavior was visualized using a digital CCD camera (Photometrics Cascade 512B Cooled CCD 16Bit Back Thinned Camera, Roper in Tucson, AZ) and data analysis was done by Metaview software. A 100-W mercury lamp with FITC filter was used as an excitation source. Time-sequenced images were taken with 50~100 ms exposure time per image to obtain time-dependent behavior.

Results and Discussion

Fundamental DNA stretching system

The device we constructed for DNA stretching uses dielectrophoresis to capture and elongate DNA molecules. By using a non-uniform electric field generated by a pointed electrode (high field gradient) and a straight electrode (low field gradient), we can control the movement and extent of stretching, as shown in Figure 2. 2. Generally, DNA molecules are attracted to the higher field gradient region at low frequency (~1 KHz) and stretched by negative dielectrophoresis at high frequency (~1MHz).[19] For immobilization, a thiol-and-gold method was incorporated as described previously.[21]
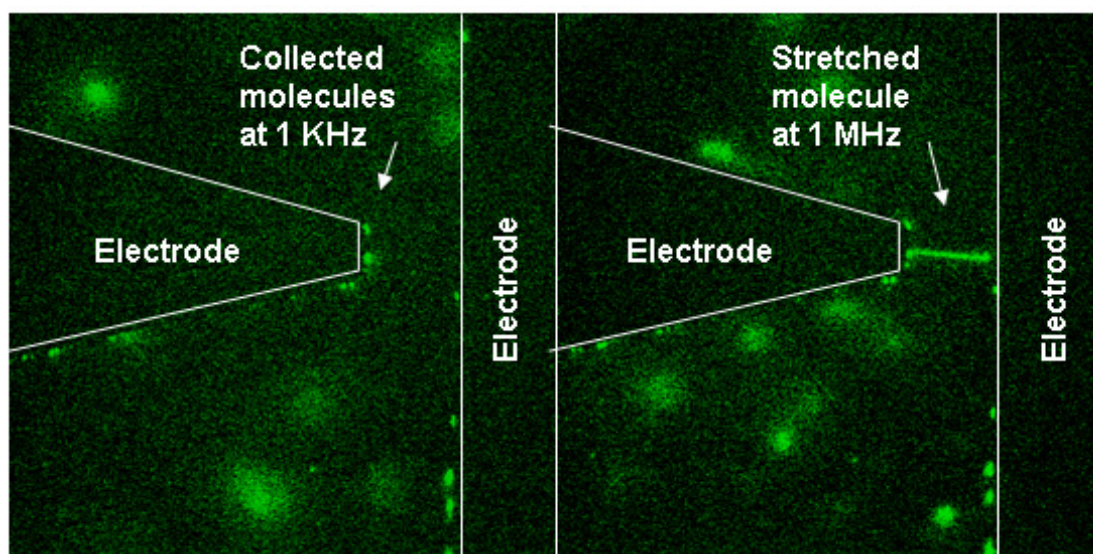
Figure 2. 2. Dielectrophoretic stretching of DNA. A non-uniform electric field is generated by a pointed electrode and a straight electrode, and one end of molecule is immobilized at the electrode edge by thiol-and-gold linking. Molecules are attracted at 1KHz, 7 V

The directional movement of the molecules is frequency dependent in accordance with their dielectric properties. That is, the transition frequency at which the

dielectrophoretic force reverses from positive to negative will depend on the molecule's dielectric properties. In our system, we applied low frequencies of 500 Hz to 100 kHz, and observed that most molecules moved toward a higher electric field gradient region. Molecules were repelled from high field-gradient regions if frequencies higher than 700 kHz were used. There was a combination of positive and negative dielectrophoresis in the frequency range of 100 kHz to 700 kHz (i.e., some molecules moved toward gradients and some molecules moved in the opposite direction).
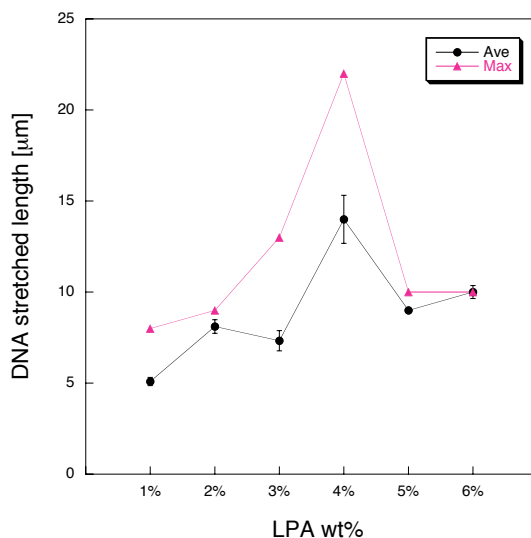
Figure 2. 3. Effect of LPA concentration to DNA stretching, Approximately 4 wt% of LPA gave the longest stretched DNA length.

DNA elongation is a strong function of solution conditions such as polymer concentration, conductivity, and pH values. Figure 2. 3 shows the effect of polymer concentration on DNA stretching. The highest average (15 μm) and maximum (22 μm) stretched length we observed in this polymer-assisted system was with 4 wt% LPA solution. This result strongly supports the previously reported result that approximately 5 times the critical entanglement concentration of this polymer is optimal for stretching.[20]

A low conductivity, pH 8 buffer is optimal for DNA stretching. Stretching experiments were performed with solutions of pH 4, 8 and 10, but elongation of DNA could only be obtained in the pH 8 solution indicating that dielectrophoretic stretching occurs best near physiological pH values. Low conductivity solutions are also best for dielectrophoretic stretching. High conductivity solutions produce a large amount of joule heating, and resulting molecular movement depends on the temperature increase in the fluid and not on the dielectric force. Moreover, a high level of bubble generation was observed that disrupted the stretching process.

 Molecular motion can also be induced by convection. Stretching of DNA molecules and circulation of peripheral molecules occurs at the same time during the dielectrophoresis process when the frequency is higher than 700 kHz. The molecules attracted to the region between the pointed and straight electrodes move linearly, and the molecules immobilized on the pointed electrode are stretched along the field lines. Those molecules that exist outside the gap move in a circular fashion (Figure 2. 4). Minerick et al.[22] have reported a similar observation during the manipulation of red blood cell in an AC field. They measured both dielectrophoresis linear velocity (either toward or away from high field density region) as a function of AC frequency and angular velocity of electrorotation as a function of frequency. We measured the velocity of negative dielectrophoresis by particle tracking and the value obtained at 2 MHz (~ 2.7 μm/sec) is in the range of previously reported negative dielectrophoretic velocities. We also observed that the velocity of DNA increased with the increasing frequency, a result consistent with the work of Minerick et al.

(a)

(b)
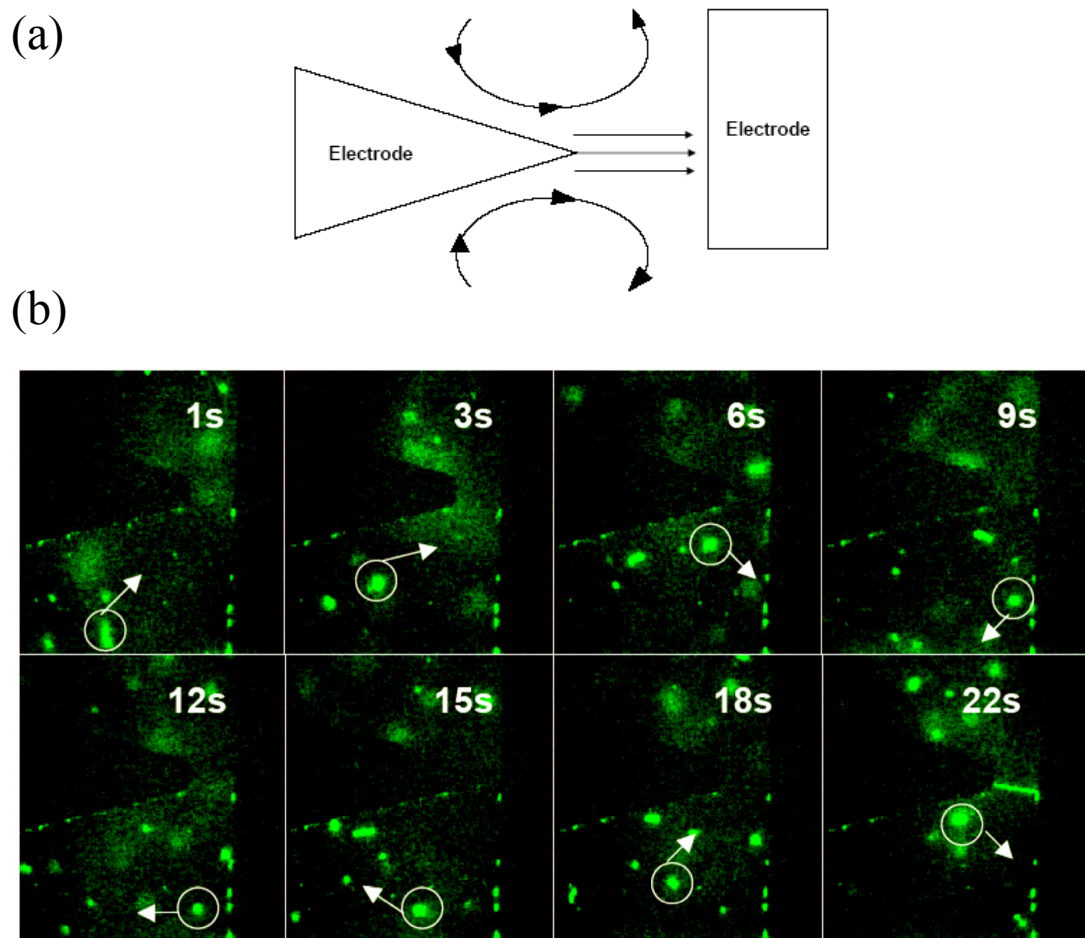
Figure 2. 4. (a) Direction of DNA movement under negative dielectrophoresis condition. Molecules between the electrode gap move linearly and are stretched, and molecules outside of the gap have the motion of co-field rotation. (b) Time sequence of DNA movement under negative dielectrophoresis condition.

Microfabricated electrode characterization

Electrode edge smoothness plays an important role in attracting DNA molecules to the intended stretching area. Rough electrode edges provide many small points along the electrode's edge that generate high electric field gradients resulting in molecular movement. Figure 2. 5(a) shows how DNA molecules are attracted to the rough edges of the electrode, particularly on the straight electrode (vertical white trace on electrode

edge), while Figure 2. 5(b) shows how the DNA molecules are attracted to the smooth pointed electrode area only. Pixel intensity measurements of a horizontal line that includes both edges of the electrodes (Figure 2. 5(c,d)) confirm this observation by showing similar intensities on both edges when rough electrodes are used but only one high peak on the pointed electrode side for smooth electrode edges.
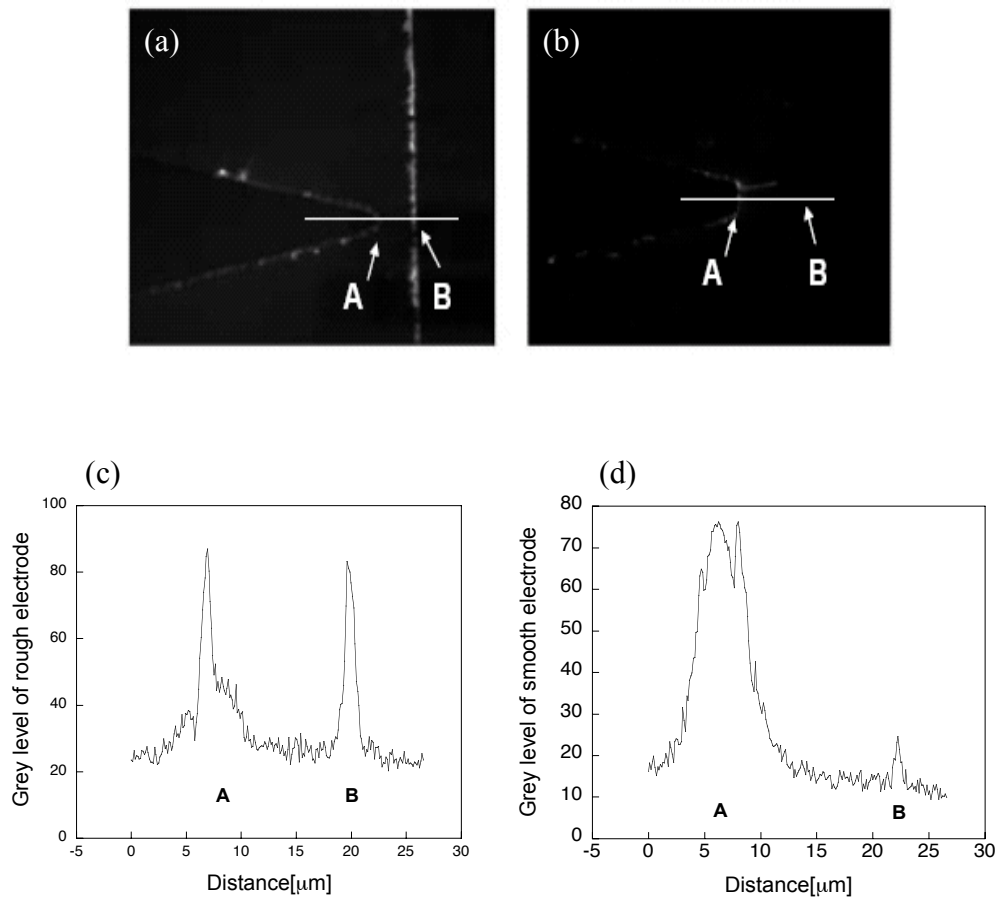
Figure 2. 5. DNA stretching using (a) a rough electrode edge and (b) a smooth electrode edge. Many molecules were attracted to the random peaks of the rough electrode edge while DNA molecules are only gathered around the pointed electrode area in (b); (c), (d) Gray levels obtained through horizontal lines that includes both electrode edges (higher value represents brighter point). Similar degree of gray level was obtained on both electrode edges when rough electrode edge was used (c) while only one high peak was obtained at the pointed tip electrode side when smooth electrode edge was used (d). These graphs were obtained by averaging 6 different lines from different figures.

We are able to obtain this smooth electrode edge by performing electrode annealing following metal etching. Figure 2. 6 shows scanning electron microscopy (SEM) images of the top and cross-sectional views of a gold electrode after fabrication by lift-off and etching. As seen in the figure, both methods lack a highly smooth and straight edge. Annealing of the 300 nm gold layer at 450°C for 10 min was then performed and the resulting electrode had a smooth edge (Figure 2. 7).

(a) Top (lift-off)   (b) cross-section (lift-off)

(c) Top (etching)   (d) Cross-section (etching)
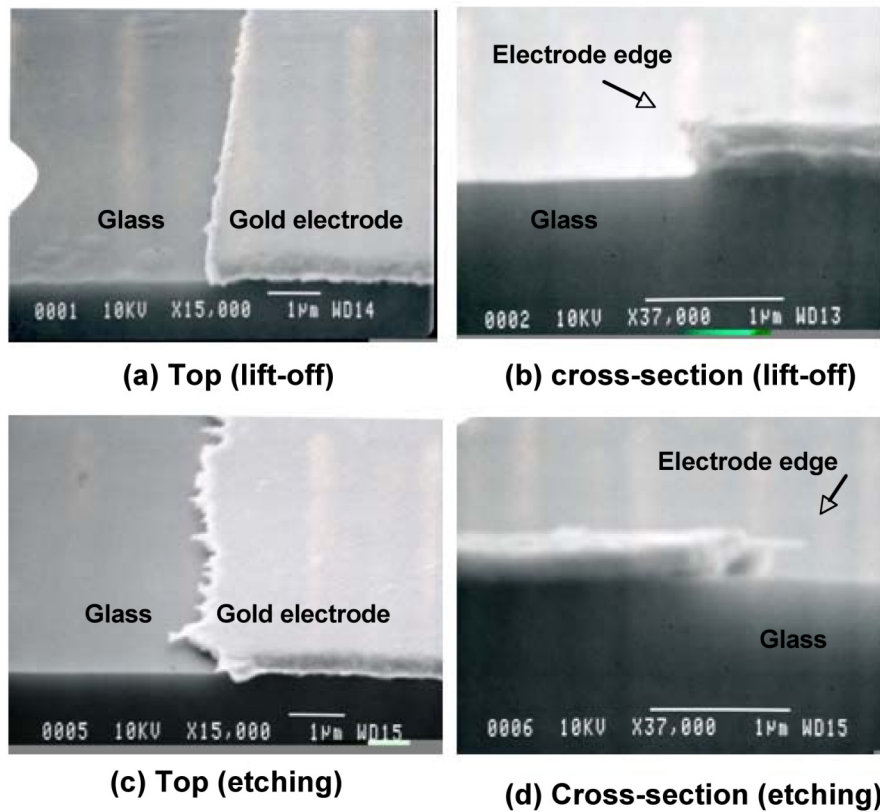
Figure 2. 6. Scanning electron microscopy (SEM) images of the top and cross sectional view of gold electrode after fabrication by lift-off (a, b) and metal etching (c, d).
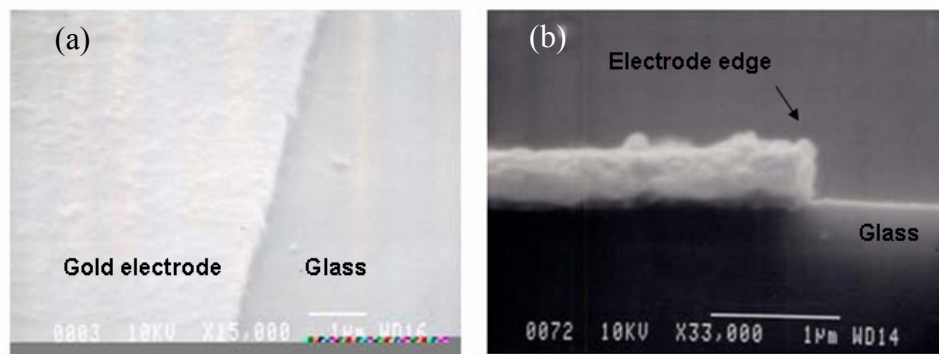
Figure 2. 7. SEM image of electrode after annealing at 450℃ for 10 min. Annealing was performed after metal etching to make smooth electrode edge. (a) Top view, (b) cross-sectional view
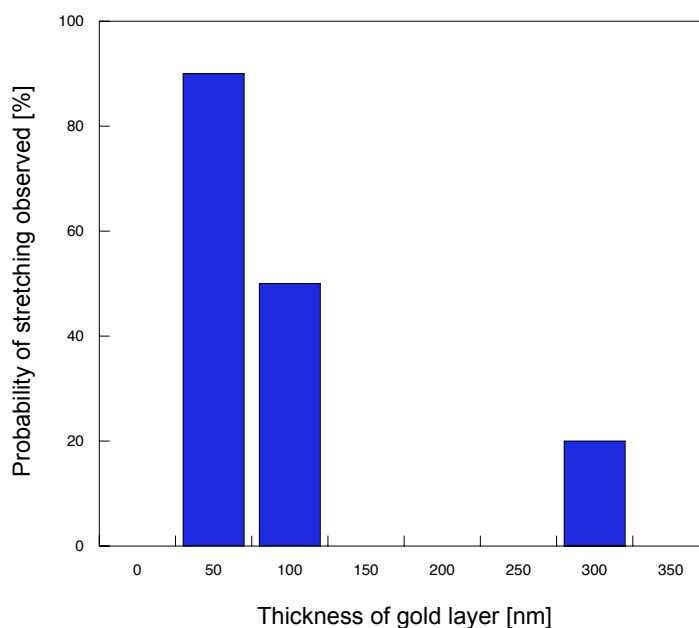
Figure 2. 8. Effect of electrode thickness on DNA stretching. Substantial increase in the probability of observing DNA stretching was achieved with a 50 nm thick gold layer.

The thickness of the electrode also affects DNA stretching with thinner metal electrodes giving a higher probability of stretching than thicker electrodes. The

probability includes both completely and partly stretched molecules (there were always molecules in the gap both in free solution and attached to the surface that did not stretch). Three different thicknesses (350, 135, 65 nm) were used to evaluate the success rate of the stretching. Substantial increase in the probability of observing DNA stretching is obtained when using a thinner metal layer (Figure 2. 8). The cause of this phenomenon is most likely due to the higher vertical field gradient obtained with the thinner electrode.
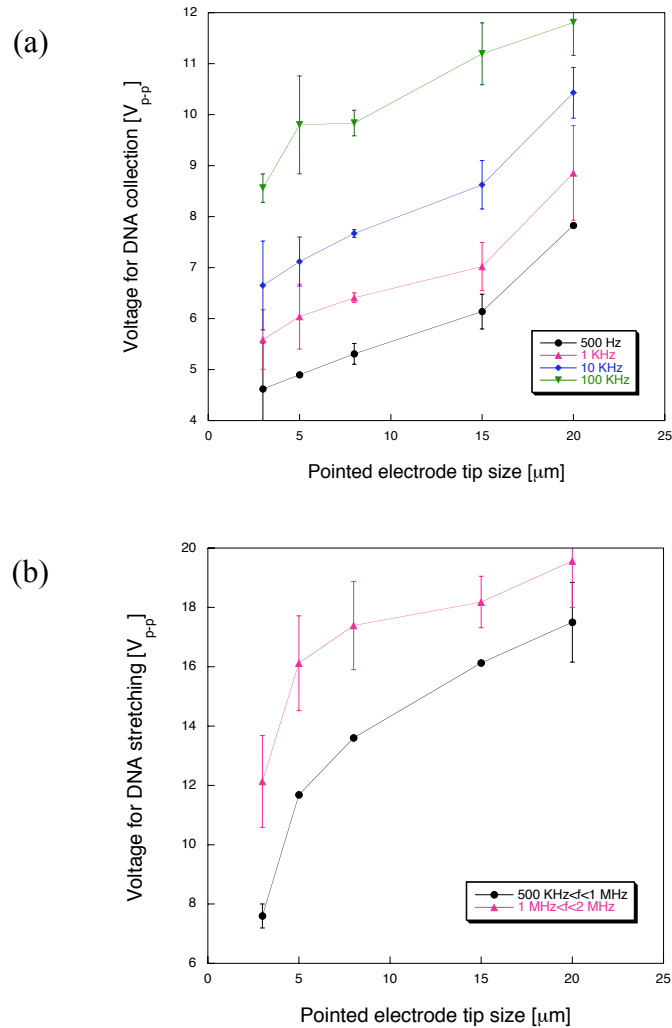
Figure 2. 9. Voltage required initiating DNA attraction to the pointed tip electrode region (a) and voltage required initiating DNA repulsion from the pointed tip electrode region (b). In both cases, smaller voltages are required to cause molecule movement when sharper electrodes are used.

The electric field properties such as the field gradient, strength, and frequency are adjustable parameters in dielectrophoretic DNA stretching. The tip size of the pointed electrode was varied to investigate how it affects DNA stretching. Figure 2. 9(a) shows the voltage value required to cause positive dielectrophoresis of DNA molecules (i.e., attraction to the high field gradient region). As can be seen from the figure, a smaller voltage value is required to initiate positive dielectrophoresis movement when a sharp electrode tip is used than with a more rounded electrode. A similar phenomenon was observed when higher frequencies were applied to repel DNA from high field-gradient regions (negative dielectrophoresis). As seen in Figure 2. 9(b), the required voltage for a 20 μm electrode tip is approximately 2 times higher than the voltage for a 3 μm electrode tip. The lower voltage for sharper electrodes is a result of the higher electric field gradient generated compared to blunter electrodes at the same voltage.

Changing the gap between the pointed and straight electrodes can also influence DNA stretching. As seen in Figure 2. 10, the effect is more noticeable when the sharp tip is used but negligible with blunt tips. The gap width also affects the formation of DNA "bridges" between electrodes. The average stretched length of λ-DNA in most cases was 15 μm, and DNA bridges were quite often observed when the gap width was narrower than 15 μm. When a gap of 10 μm was used, both ends of the DNA molecule are attracted to the surface of the metal electrodes. When this occurred, the DNA molecule did not shrink after the electric field was turned off.
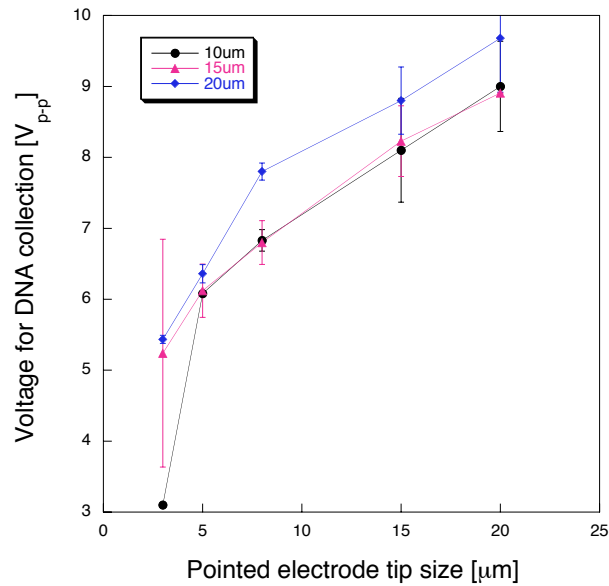
Figure 2. 10. Effect of different gap sizes on stretching. The effect is more noticeable when a sharp tip is used but negligible with a blunt tip.

Electric field properties

DNA molecules can be stretched in our system at frequencies higher than 500 kHz, but steady, stable stretching could not be obtained below 2 MHz. At 700 kHz, the stretched DNA would move away from the electrodes immediately after stretching and would not remain in the gap. Those DNA molecules that were stretched in the fluid flow and failed to remain stationary. At 1 MHz, one end of the DNA molecule would easily attach to the pointed electrode and remain stretched. However, the molecule did not maintain its stretched form for more than 2 seconds, and would recoil back to the pointed electrode. At 2 MHz, the stretched DNA was stable meaning that it did not fluctuate or collapse as long as the field was applied.

Bubble generation occurs easily at low frequencies due to electrolysis. Higher frequencies reduced this reaction with virtually no bubbles generated at frequencies

26

higher than 100 kHz. As seen in Figure 2. 11, bubbles are generated at low voltages when a sharp electrode and low frequency are applied. Moreover, the voltage for bubble generation is quite close to that for molecular attraction, especially in case of a sharp electrode.
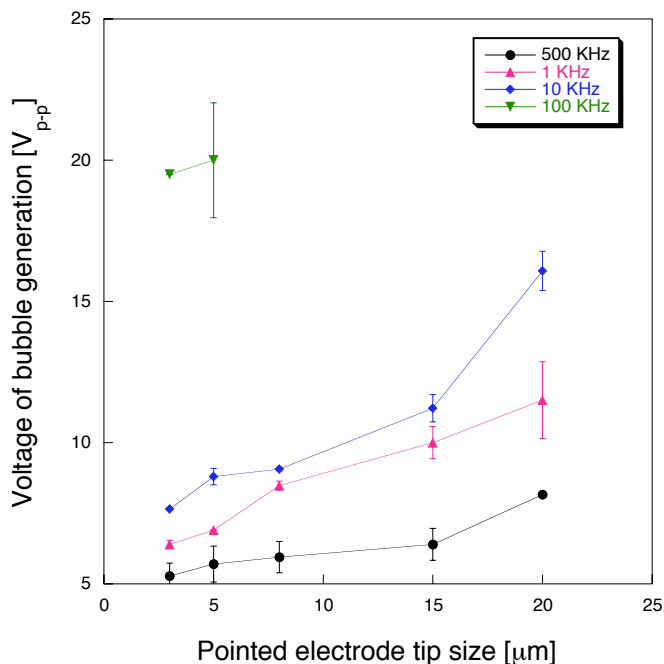
Figure 2. 11. Bubble generation. Bubbles are generated at low voltage when a sharp electrode and low frequency are applied.

Surface properties

The length of stretched DNA molecules is longer on surfaces with a high contact angle than those with a low contact angle. We performed DNA stretching on surfaces with two different contact angles: an untreated glass surface ($\theta=40°$) and a silane coated surface ($\theta=80°$). Figure 2. 12 shows that more than 70% of the molecules on the 80° surface are longer than 15 µm compared to only ~30% on the 40° surface. The fact that a

longer stretch length is obtained on more hydrophobic surfaces is consistent with literature data on other stretching techniques.[18]
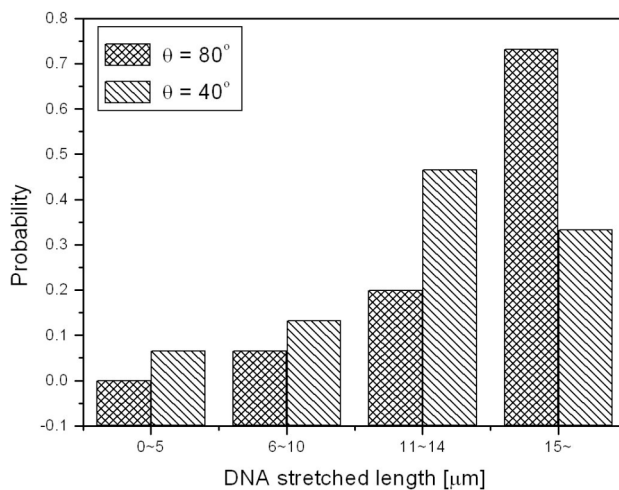
Figure 2. 12. The stretched length distribution on both higher contact angle surface (80°) and lower contact angle surface (40°); longer stretched length is obtained on more hydrophobic surface.

To further investigate the effect of surface hydrophobicity, the surface contact angle was modified by changing the dilution ratio of TMCS in TCE. Figure 2. 13(a) shows the dilution ratio of TMCS in TCE as well as the contact angle of each surface. Figure 2. 13(b) shows the average stretched length of a DNA molecule over the silane-coated surface of several silane concentrations. As seen in these two figures, an increase in TMCS concentration produces a higher contact angle and results in a longer stretched length. The maximum length of the averaged values (15.7 μm) is obtained at the 1:5 ratio of TMCS to TCE, and the longest stretched length of DNA at that point is 25 μm, a length appreciable longer than the fully stretched length of λ-DNA. The stretched length decreases above the 1:5 ratio with the length at high TMCS concentration being shorter

28

than on a clean glass surface with no silane. This result suggests that a surface contact angle of 85° may be optimum for DNA stretching although additional experiments with other surface treatment agents need to be performed to confirm this hypothesis.

(a)

(b)
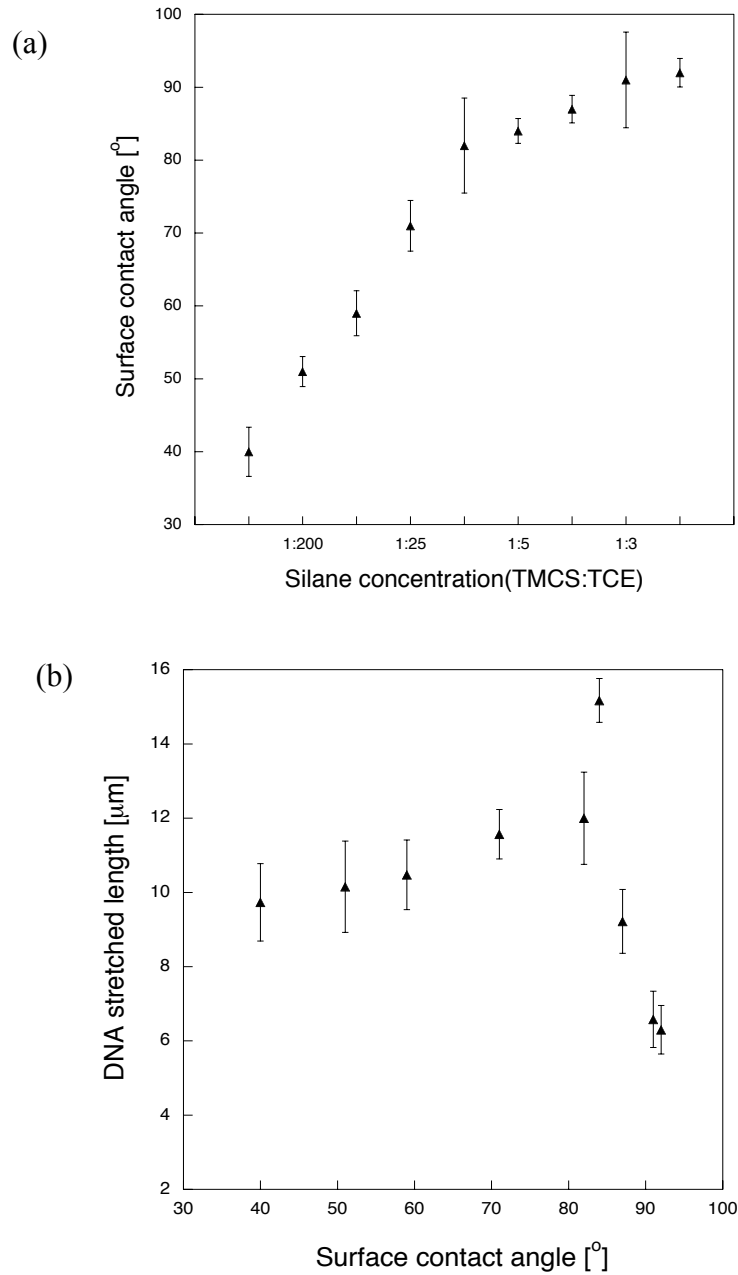
Figure 2. 13. Surface contact angles over coated surfaces with different silane concentration (a), and averaged stretched length of DNA molecules over the silane-coated surface of different surface contact angles (b). Higher silane concentration produces higher surface contact angle and longer DNA stretched length.

Surfaces with high surface contact angles inhibit the molecules' nonspecific adsorption. Figure 2. 14 shows sequential images of DNA stretching (a) over a clean glass surface and (b) over a silanated surface. In Figure 2. 14(a), stretched molecules are observed sticking to the glass surface even after the electric field is turned off. In addition, several coiled DNA molecules stick randomly on the more hydrophilic glass surface. However, the stretched molecules on the hydrophobic surface recoil easily when the electric field is turned off (Figure 2. 14(b)). Nonspecific adsorption of other DNA molecules was not observed on this surface in any significant degree. In comparing the two, the rate of nonspecific adsorption is almost 4 times lower on silane-coated surfaces than on untreated glass. We have counted the number of DNA molecules in 10 minutes that adhere to a 60 μm^2 surface and found that approximately 11 molecules stick to the silane-coated surface while 40 molecules stick to the clean glass surface.
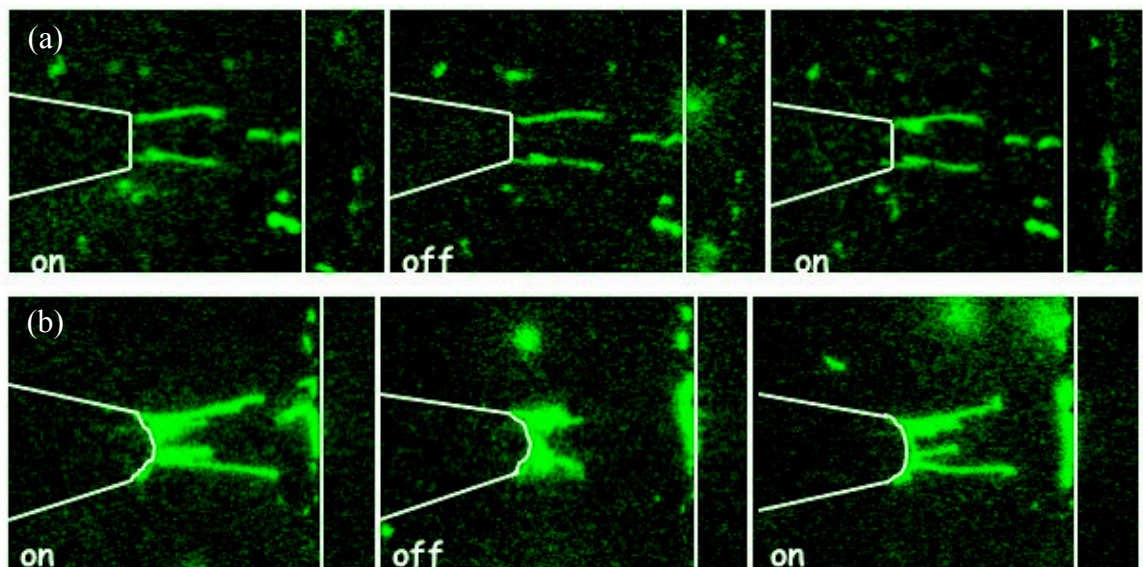
Figure 2. 14. Sequential image of stretched DNA over (a) clean glass surface and (b) silane-coated surface. Stretched molecules over silane-coated surface did not adhere to the surface and were free in the solution.

Conclusions

In this work, we have investigated the optimum conditions for robust and controllable DNA electrostretching. By optimizing the solutions conditions, electric field strength and shape, and the surface properties, success of DNA stretching can approach 90%. Also, stretched molecules on more hydrophobic surfaces are less adherent and may be more amenable for additional interactions. For example, certain proteins that bind to DNA may be somewhat inhibited from binding if a stretched molecule is adhered to the surface at a large number of locations.

Molecular manipulation by dielectrophoresis is a relatively common technique but there are still unexplored topics in this area. Additional studies are needed to investigate other parameters such as temperature, surface property and buffer-ion dependence on stretching. With the design of more reliable microfabricated DNA stretching devices, integrated systems may be possible that perform multiple analysis operations on a single DNA molecule extracted from a single cell or other minute samples.

References

1. Bustamante, C.; Bryant, Z.; Smith, S. B., *Nature* **2003,** 421, 423-427.

2. Wang, M. D., *Current Opinion in Biotechnology* **1999,** 10, 81-86.

3. Maier, B.; Strick, T. R.; Croquette, V.; Bensimon, D., *Single Molecules* **2000,** 2, 145-151.

4. Han, J.; Craighead, H., *Analytical Chemistry* **2002,** 74, 394-401.

5. Han, J.; Turner, S.; Craighead, H., *Physical Review Letters* **2001,** 86, 1394.

6. Washizu, M.; Kurosawa, O., *IEEE Transcations on Industry Applications* **1990,** 26, 1165-1172.

7. Washizu, M.; Kurosawa, O.; Arai, I.; Suzuki, S.; Shimamoto, N., *IEEE Transcations on Industry Applications* **1995,** 31, 447-456.

8. Schafer, B.; Gemerihardt, H.; Uhl, V.; Greulich, K. O., *Single Molecules* **2000,** 1, 33-40.

9. Maier, B.; Bensimon, D.; Croquette, V., *PNAS* **2000,** 97, 12002-12007.

10. Wirtz, D., *Physical Review Letters* **1995,** 75, 2436-2439.

11. Hu, J.; Zhang, Y.; Gao, H. B.; Hartman, B. L. U.; Li, M. Q., *China-EU forum on nanosized technology* **2002**, 262-267.

12. Yamamoto, T.; Kurosawa, O.; kabata, H.; Shimamoto, N.; Washizu, M., *IEEE Transcations on Industry Applications* **2000,** 36, 1010-1017.

13. Washizu, M.; Nikaido, Y.; Kurosawa, O.; Kabata, H., *Journal of Electrostatics* **2003,** 57, 395-405.

14. Turner, S.; Cabodi, M.; Craighead, H., *Physical Review Letters* **2002,** 88.

15. Gosse, C.; Croquette, V., *Biophysics Journal* **2002**, 3314-3329.

16. Allemand, J.; Bensimon, D.; Jullien, L.; Bensimon, A.; Croquette, V., *Biophysical Journal* **1997,** 73, 2064-2070.

17. Bakajin, O.; Duke, T.; chou, C.; Chan, S.; Austin, R.; Cox, E., *Physical Review Letters* **1998,** 80, 2737-2740.

18. Bensimon, D.; Simon, A.; Croquette, V.; Bensimon, A., *Physical Review Letters* **1995,** 74, 4754-4757.

19. Herbert, A. P., *Dielectrophoresis*. Cambridge University Press: Cambridge, 1978.

20. Namasivayan, V.; Larson, R.; Burke, D.; Burns, M., *Analytical Chemistry* **2002,** 74, 3378-3385.

21. Ulman, A., *An Introduction to Ultrathin Organic Films from Langmuir-blodgett to Self-Assembly*. Academic Press: New York, 1991.

22. Minerick, A.; Zhou, R.; Takhistov, P.; Chang, H., *Electrophoresis* **2003,** 24, 3703-3717.

CHAPTER 3
MICROSTENCILS FOR PATTERNING NON-TRADITIONAL MATERIALS

Introduction

MEMS devices have relied on photolithography and thin film processing techniques optimized by the semiconductor industry to form micro- and nano-structures. This photolithographic patterning of structures typically involves cyclic processing steps such as photoresist coating, thermal treatment, UV exposure, chemical development, and wet/dry etching.[1] As MEMS technology is harnessed for newer applications, particularly related to biology, some classes of materials and surfaces used may be incompatible with the chemical or thermal process steps associated with standard microfabrication. In response to this increasing need to pattern non-traditional materials several novel microfabrication techniques have been developed the most prominent of which are imprinting and shadow masking.

Imprinting is a pattern transfer technique that has been successfully used for patterning non-traditional materials.[2] The imprinting process uses a mold with the desired pattern made by standard lithography. Recently, poly-dimethylsiloxane (PDMS) molds made using soft lithography have also been used. This mold is then brought in contact with the material that needs to be patterned. The wetted mold is then contacted to another

substrate to transfer the material onto that substrate. Adjusting the surface properties can control the wetting and de-wetting of the mold and the substrate. The imprinting modes have been used to pattern a variety of materials and substrates including 3-dimensional multi-layer patterning.

An alternative to imprinting is the use of a shadow or dry mask. The term "dry" is used because no solvents are required to deposit the patterned mask onto the substrate.[3-5] The earliest shadow masks were rigid silicon wafers that were etched through. These silicon shadow masks can be cleaned and re-used making their use relatively low-cost. However, the problem with this method is that an air gap always exists between the mask and the substrate, giving rise to features larger than the mask openings due to lateral leakage and oblique deposition.

Patterned polymeric films provide better adhesion to the substrates to be patterned and hence are good candidates for shadow masks. Jackman et. al used a patterned PDMS layer as a shadow mask.[6] The technique involved spinning a layer of PDMS on a substrate previously patterned with SU8 structures. The PDMS membrane was then peeled off and spread on the substrate to be patterned. Although this method was used to pattern a variety of materials including gels and biological molecules, the handling and the alignment of the thin membrane is not straightforward. More recently parylene films patterned with standard lithography and reactive ion etching have been used as shadow masks.[7] These masks have the advantage that parylene can be mechanically peeled from hydrophilic substrates after patterning. Parylene can also be patterned by non-lithographic methods.[8]

We present a photo-lithographically patterned parylene-SU8 bi-layer microstencil that can be used for micropatterning. The parylene layer enables mechanical peeling of the hybrid film from a hydrophilic substrate and eliminates the use of harsh chemicals typically required for releasing the resist. The SU8 layer is photo-lithographically patterned ensuring alignment with existing features. The role of the SU8 layer is to provide a mask for parylene etching as well as provide height to the microstencil for controlling the amount of material patterned. Alternatively, the amount of material patterned can be externally controlled using a variety of techniques including spin coating and thin film deposition. The microstencils were defined on silicon, glass, and polymer substrates, and then used to pattern chemically and thermally sensitive compounds including cells, wax, sol, and CYTOP^{TM}.

Material and Methods

Microstencil fabrication

As shown in Figure 3.1 the fabrication begins by depositing a 2 μm parylene film on the wafer (PDS 2010 LABCOTER$^®$ 2; Specialty Coating Systems, Indianapolis, IN). Silicon wafers (<100>, 500 μm thick, 10 cm diameter), borofloat glass wafer (500 μm thick, 10 cm diameter), and cyclic olefin copolymer plaques (2 mm thick, Zeon Chemicals) were used in this study. SU8 (MicroChem Corp., Newton, MA) was then spin coated on the wafer. The wafer was baked at 65°C and 95°C on a hot plate. The desired pattern was then exposed on the wafer using a mask aligner (Cannon PLA 501FA, 405nm wavelength, 550 light integral). A post bake was performed at 65°C and 95°C after

which the wafer was developed in SU8 developer (MicroChem Corp., Newton, MA). The spin speed, baking time, and developing times varies with the grade of SU8 and the target thickness. The conditions can be obtained directly from the suppliers. The parylene film was then etched using oxygen plasma reactive ion etching (RIE 2000; South Bay Technologies, 100watts and 100mT oxygen plasma). The desired material was then deposited onto the exposed substrate with the SU8-parylene hybrid layer serving as a shadow mask.

Starting substrate

CVD paylene film

SU8 lithography for patterning

Etch parylene

Deposit

Peel stencil
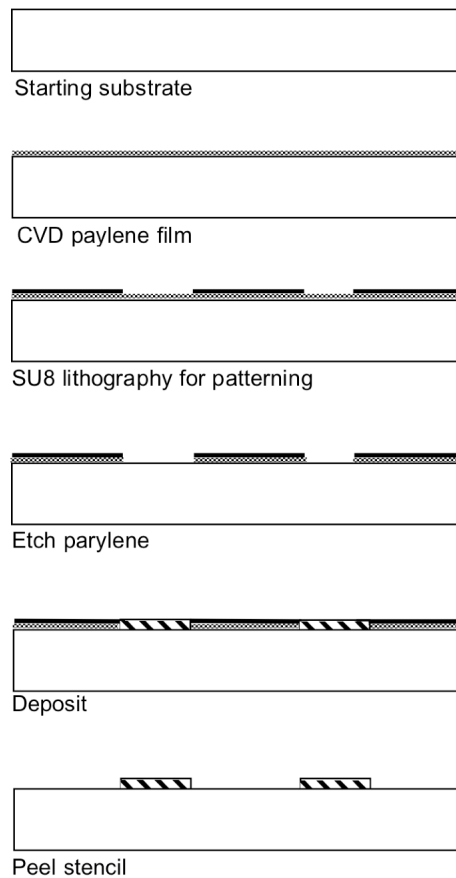
Figure 3. 1. Process flow for the microstencil process.

Cell preparation and patterning

C2C12 cells were maintained in Dulbecco's modified Eagle's medium (DMEM) supplemented with 15% fetal bovine serum (FBS), 100 unit/ml penicillin, 100 μg/ml streptomycin, and 0.29 mg/ml L-glutamine in a humidified 5% CO_2 /95% air incubator at 37°C. C2C12 myoblasts were grown to approximately 80% confluence before being washed (with phosphate-buffered saline solution), trypsinized, and seeded onto the glass substrate. The cells were then cultured in a CO_2 incubator for 1 hr. Subsequently the cells were fixed and examined on an inverted microscope (Nikon TE-300) with a 10X objective. Black and white images were captured with a CCD camera (Hamamatsu ORCA-E100). Cell culture reagents were obtained from Invitrogen (Carlsbad, CA) unless otherwise mentioned.

Sol preparation and patterning

The preparation of 1% Pt/Al_2O_3 sol begins by heating 38 ml of deionized water to 85 $^{\circ}$C in a conical flask. 3.968 g of Aluminum Isopropoxide (AIP) was added to the heated water under vigorous stirring. The conical flask was then connected to a total reflux condenser and the slurry was stirred at 85°C for 1 h. 233 μl of HNO_3 acid (70% wt) was added to the mixture and the refluxing condenser was closed. This mixture was stirred for 1 h again at 85°C. 0.0796 g of Platinum was added to 6.705 g of 1,3 butanediol in a separate beaker and stirred to dissolve the Pt completely. The 1,3 butanediol-Pt solution was added to the sol (at 85°C) and stirred for 1 h. The heater was then switched off and the solution was stirred for 24 h. The patterned device was immersed vertically into the sol solution at 3 cm/s, left immersed for 5 min, and then withdrawn at 3 cm/s.

38

Excess sol was removed from the edges of the device and the device was dried at 120^OC for 30 min. Additional coatings of the sol were then applied to the device which was dried after every coating. Finally the pattern was peeled and the device was calcined at 550^OC for 15 min.

Bond strength testing

The strength of the bond between two the two layers of a hybrid device was tested mechanically using an MTS Alliance RT30 electromechanical test frame (MTS Systems Corp., MN). The two sides of the hybrid device were bonded to two steel platens using a steel weld epoxy (ITW Performance Polymers, Riviera Beach, FL). The assembly was then fixed into the bond tester and pulled apart at a rate of ~60 μm/min. TestWorks4 software (MTS Systems Corp., MN) was used to collect and analyze data during tensile testing. Load and displacement data were recorded. Bond yield strength was calculated using the bonded area and the failure load.

Results and Discussion

Basic Process

The basic process flow for patterning materials using microstencils is shown in Figures 3.1 and 3.2. A parylene film is deposited on a hydrophilic substrate from which it can be mechanically peeled. A SU8 film is spun on top of the parylene and the desired pattern is photo-lithographically transferred to the SU8 film. The SU8 pattern provides the mask to etch the parylene film in the desired areas to expose the substrate. If required,

the SU8 layer can also provide the desired height in the vertical direction for controlling the amount of material deposited. The parylene-SU8 microstencil can be mechanically peeled off using tweezers.
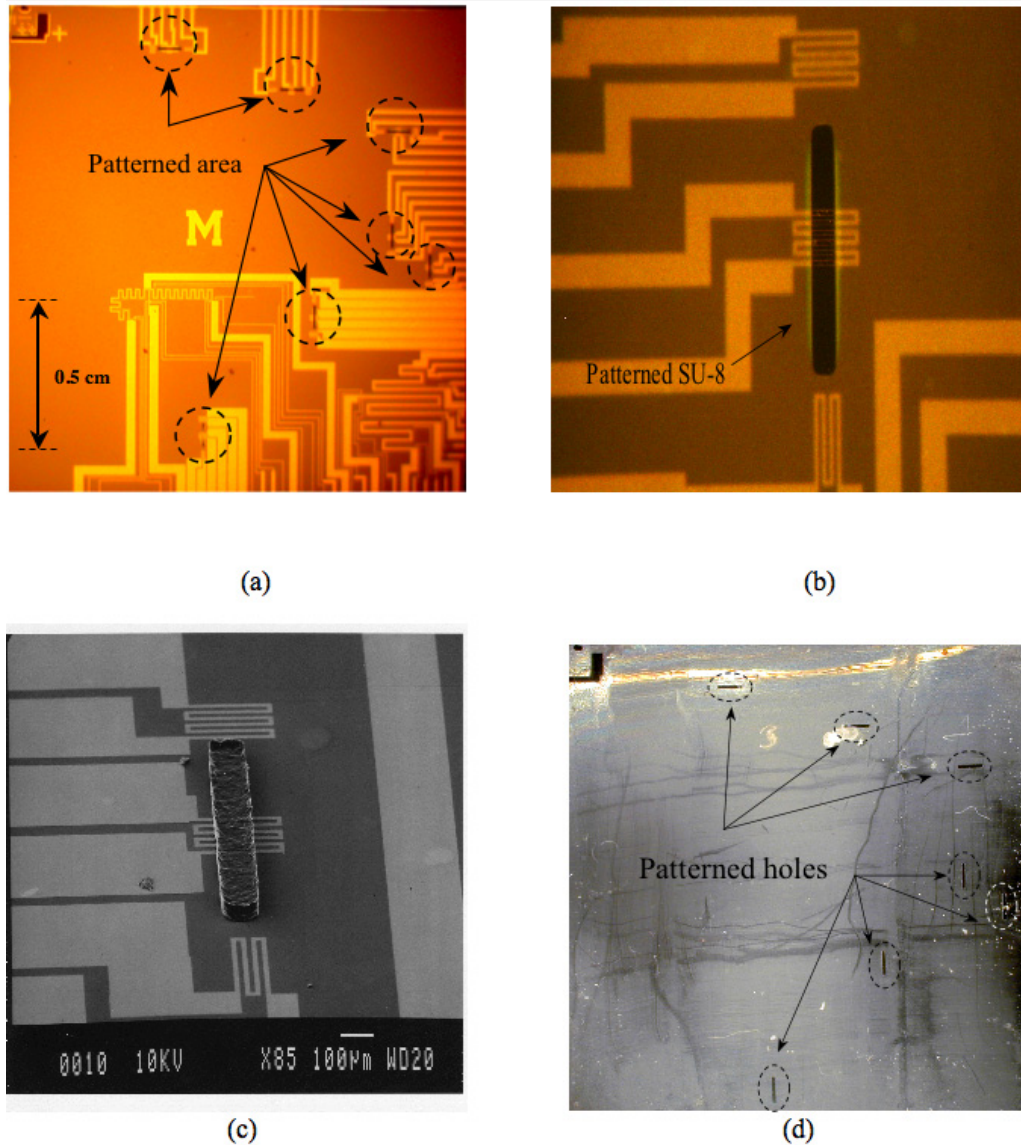
Figure 3. 2. Patterning using microstencils: a) Patterned microstencil. b) Close view of one window. c) SEM image of patterned wax on the surface. d) Peeled off parylene/SU8 microstencil.

This microfabrication process does not require any wet chemicals and can be used on different substrates (Table 3.1). We have used cyclic olefin copolymer (COC) for the initial demonstration of this process and have patterned approximately 20 µm high structures on both glass and COC using the 2015 grade of SU8 (2000 rpm spin rate). The final heights of the microstencil were 19.9 µm and 19.8 µm for glass and COC respectively. In all cases, a 2 µm parylene layer was used and ensured successful peel-off from all substrates. This microstenciling technique is also versatile with regard to the broad range of materials that can be patterned, particularly those that are too sensitive to be patterned by traditional mechanisms.

Substrate	SU8 grade	Viscosity (cSt)	Intended thickness of SU8 (µm)	Final thickness of microstencil (µm)
Silicon	5	290	5	3.9
Silicon	2015	1250	21	20.6
Silicon	2075	22000	110	109
Glass	2015	1250	21	19.9
COC	2015	1250	21	19.8

Table 3. 1. Microstencil thickness for different cases.

The amount of the material deposited by this technique can be controlled either externally or through self-regulation. External control mechanisms such as spin coating and self assembly based on surface energies can also be obtained using traditional resists. Microstencils offer to extend these techniques to chemically and biologically sensitive materials. Additionally the microstencil process also offers the ability to control the

amount of material deposited based on the height of the microstencil. The height of the SU8 structures can be controlled easily from 1-100 μm using different SU8 grades and processing conditions. We have used this technique to pattern three different heights of approximately 4 μm, 20 μm, and 110 μm, all with a parylene layer of approximately 2 μm (Fig. 3.3). The conditions used for these are listed in Table 3.1. We have been able to control the height of the microstencil to within a few microns of the designed height, and the accuracy can be further improved by optimizing the process conditions (e.g., spin rate, plasma characteristics). The height of the patterned SU8 for all three conditions is approximately equal to the final height of the parylene-SU8 hybrid film, suggesting that the etch rates of the SU8 and the parylene are approximately equal for the etching conditions used.
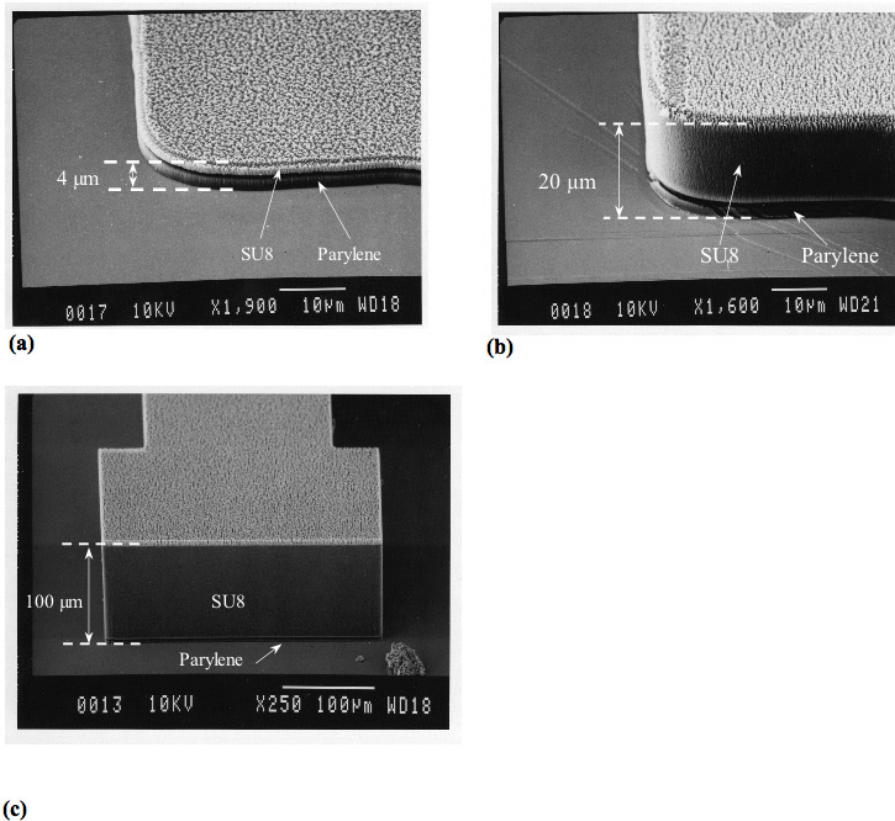
Figure 3. 3. SEM images of SU-8 pattern with different heights.

External control

We have used different external mechanisms for controlling the thicknesses of the deposited material including regulated dip coating and spinning. Dip coating is a standard procedure for deposition of sol materials on substrates with the height of the final structure controlled by the coating parameters and the number of coats applied. A silicon substrate patterned with a ~ 21 μm thick parylene/SU8-2015 microstencil was dip coated with a sol solution (described earlier). The parylene/SU8 microstencil was then peeled off and the device was calcined at 500^OC for 30 minutes. Three different heights of 0.5 μm, 1 μm, and 1.5 μm for the final film were obtained by performing 1, 2, and 3 repetitions of the dip process respectively (Fig. 3.4a). As seen from the Figure 3.4b the microstencil process resulted in a very uniform layer with no cracks even for a relatively thick layer. The bump on the edge of the coated sol is most likely due to the capillary effect between the patterned SU8 walls and the liquid sol. Surface treatment to suppress this effect could be used if this non-uniformity needs to be avoided.

Another example where the height is externally controlled and where it is advantageous to avoid harsh chemicals is the patterning of CYTOP^{TM}. CYTOP^{TM} is a Teflon-like coating used for bonding. The traditional process involves spinning CYTOP^{TM} on the device, spinning and patterning resist, plasma etching the CYTOP^{TM}, and finally stripping away the resist. The use of chemicals affects the properties of the CYTOP^{TM} and subsequently the bond strength. An alternative is to use the microstencil as shown in Figure 3.5. Here a 3.9 μm parylene-SU8 microstencil is patterned to match the channel area. CYTOP^{TM} is then spun at 1000 rpm and baked at ~100^OC on a hot plate

for 15 min to yield a height of ~2 μm. The channel is then gently peeled off to leave the clear channel areas (Fig. 3.5a-c). Bonding is performed in a hot press at a pressure of ~1000 psi and temperature of 100° C. Subsequent fluidic tests with a FITC-labeled Bovine Serum Albumin (BSA) show that there is no leakage or clogging of the microchannel (Fig. 3.5d). The bond strength was measured using the procedure described earlier and was found to be approximately 4 times higher than those that were bonded using traditional patterning techniques.

The microstencil process was also used to pattern thin films deposited with a conventional e-beam evaporator. Microstencils were formed on a silicon substrate having 2000 Å of thermal oxide for electrical isolation. 1000 Å of platinum thin films with 300 Å of titanium as an adhesion layer were deposited through the micostencil pattern of heater lines. For the two lines patterned by this technique, resistances of 165 Ω and 420 Ω were obtained, close to the designed resistances of ~190 Ω and ~400 Ω respectively. It should be noted that the exact resistances cannot be predicted even with a traditional patterning process due to the variations in the deposition for different runs as well as variations across a single wafer. The externally controlled patterning of metal demonstrates the feasibility of using the microstencil as an alternative resist, while the sol and cytop patterning demonstrate its applicability to non-traditional materials.

(a)

1.5 μm

0006   10KV   X8,000   1μm WD44
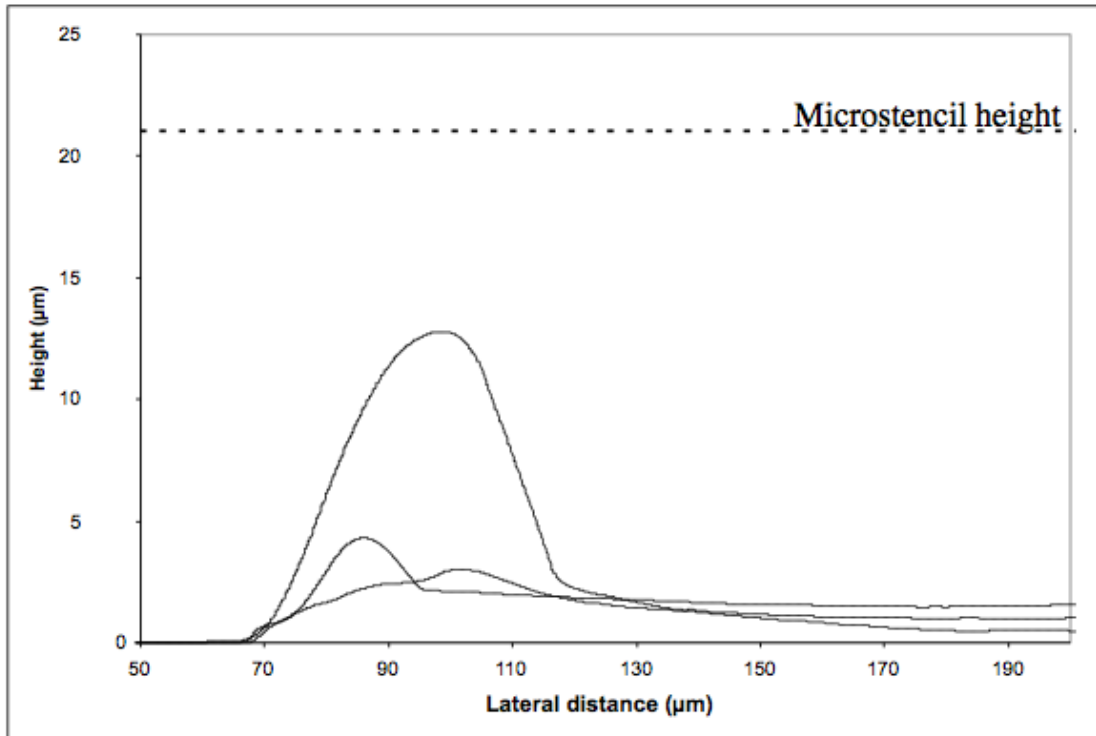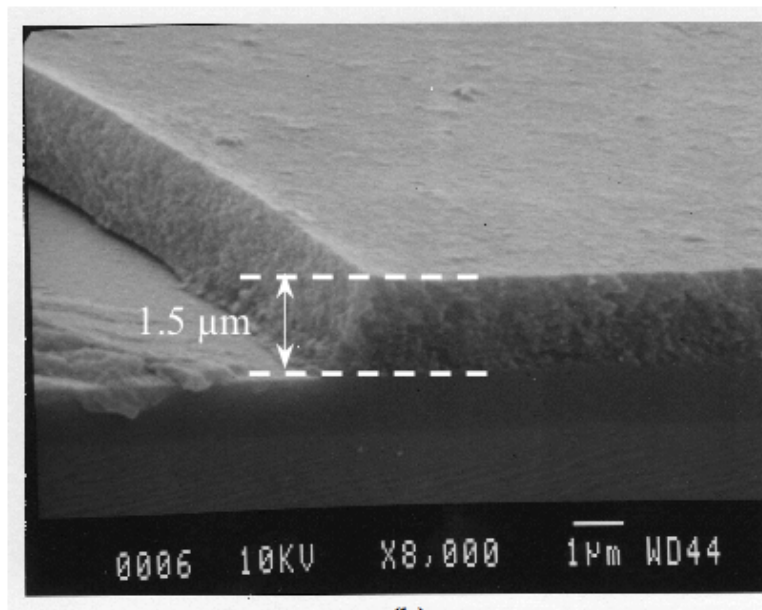
(b)

Figure 3. 4. Sol patterning. (a). Surface profiles of different thicknesses of the calcined sol patterned using the microstencils. The three different heights were obtained by changing the number of dip coatings. The bump near the edge is probably due to the capillary effects near the microstencil wall. (b). SEM image of a calcined sol structure on a silicon substrate. Note that the layer was broken in the center; the edge bump is not visible.
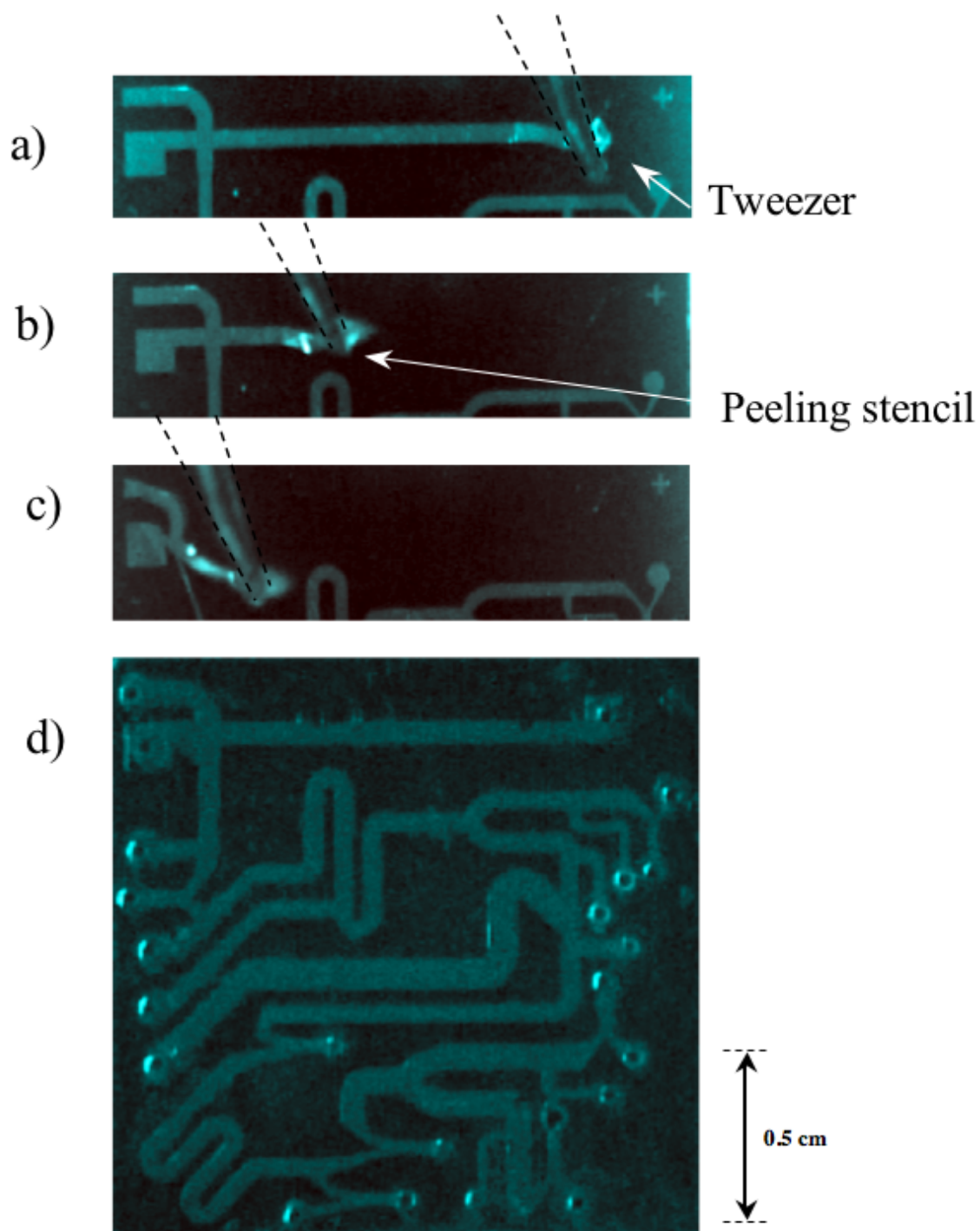
Figure 3. 5.Cytop patterning. a). – c). Peeling the parylene-SU8 membrane with a tweezer from the channel area after spinning CYTOP. d). Optical image of a bonded device that is filled with a fluorescent solution.

Self-regulated patterning

The amount of the material deposited can also be controlled internally by the material-microstencil interaction and material substrate interaction. This type of internally controlled or self-regulated patterning using microstencils eliminates the requirement for an external mechanism for controlling the amount of material deposited. The first scheme for self-regulation involves using the height of the microstencil to squeegee materials that are in liquid or paste-like forms with the resulting height of the deposited material being approximately equal to the height of the microstencil.
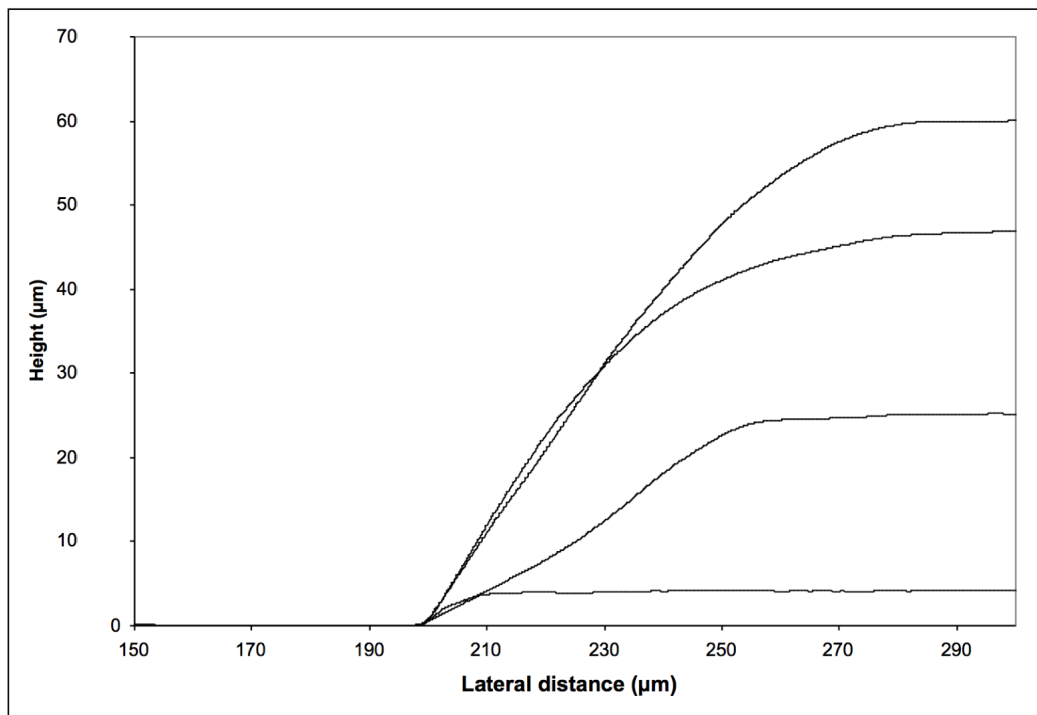
Figure 3. 6. Wax patterning: Surface profiles of different thicknesses of wax patterned using the microstencils.

An example of this technique is the patterning of wax. After the microstencil was patterned on a device (Figs. 3.2a and 3.2b) the temperature of the device was raised using a heating chuck connected to an oil bath. Excess Logitech wax was then applied over the

patterned substrate using a squeegee. The device was removed from the heating chuck and allowed to cool to room temperature. The microstencil was then peeled off to define the wax structures (Fig. 3.2c, d). Different microstencil heights were used to deposit 4 μm, 25 μm, 47 μm, and 60 μm high wax structure (Fig. 3.6). It should be noted that due to the volume contraction associated with phase change the final height of the wax column was slightly less than the height of the microstencil. If the height of the wax column is critical the microstencil height can be designed to compensate for this contraction. An added advantage of this technique is the photolithographic alignment of the patterned wax (via the openings in the microstencil) with the underlying features on a previously patterned substrate (Fig. 3.2c).
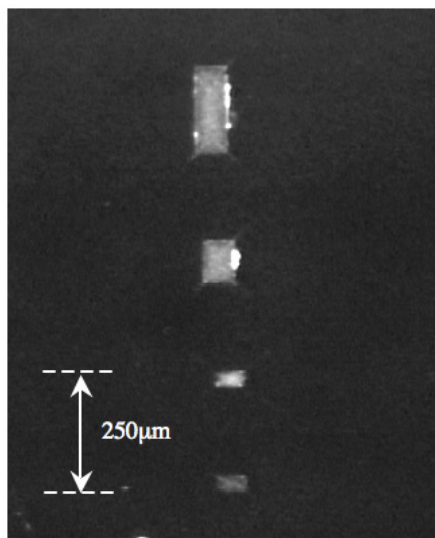
Figure 3. 7. Protein patterning: Patterns of fluorescently labeled BSA protein with different length and widths.

The second scheme for self-regulation is self-assembly of sensitive biological and chemical materials on a substrate. The surface charges on proteins and cells enable them to adhere spontaneously to the substrate. Figure 3.7 shows an optical micrograph of FITC

labeled Bovine Serum Albumin (BSA) protein on a silicon substrate using an approximately 20 μm microstencil as the mask. The device was flushed with 0.5 g/L solution of the BSA and the solvent was allowed to evaporate at room temperature after which the microstencil was peeled off. Patches as small as 100 μm by 60 μm were patterned by this method.
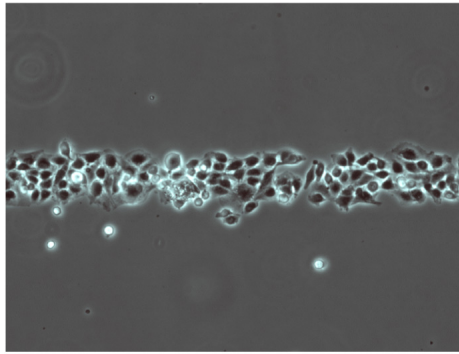
Figure 3. 8. Cell patterning: Line of C2C12 cells seeded on glass substrate.

Another example of self-assembly using microstencils is the patterning of cells. C2C12 myoblasts were patterned on a glass substrate using an approximately 20 μm thick parylene/SU8-2015 layer. In this process the microstencils were automatically released by the cell culture medium and were then rinsed off from the patterned area. The deposition of the cells is governed by the interaction of the cells and the glass substrate alone resulting in a monolayer of the patterned cells (Fig 3.8). The microstencils enable the self-assembled patterning of these biological molecules by eliminating the requirement for chemical release of the masking layer.

Conclusions

The use of MEMS technologies for applications involving chemically and thermally sensitive biochemical compounds has placed a demand for the development of new microfabrication techniques. The micro-patterning procedure presented in this work uses no harsh chemicals and enables intrinsic control over the amount of material deposited by adjusting the height of the patterned structures. This technique is very versatile as it can be used on a large variety of substrates. These micropatterns were used to define cells and proteins that can be used in biological applications. Photo-lithographically aligned wax columns can be used for various applications that require patterned paraffins such as phase-change valves[9]. Externally controlled films of CYTOP patterned in the absence of harsh chemicals have been shown to yield higher bond strength, and the sol patterned by this method can be used to define catalyst for applications like micro-fuel cells. Thus this microstencil technique will help integrate non-traditional materials with traditional microfabricated devices.

References

1. Madow, M., *Fundamentals of Microfabrication*. CRC Press LLC: 1997.

2. Guo, L. J., *J. Phys. D: Appl. Phys.* **2004,** 37, (11), R123-R141.

3. Tixier, A.; Mita, Y.; Gouy, J. P.; Fujita, H. J., *J. Micromech. Microeng.* **2000,** 10, 157-162.

4. Brugger, J.; Berenschot, J. W.; Kuiper, S.; Nijdam, W.; Otter, B.; Elwenspoek, M., *Microelectronic Engineering* **2000,** 53, 403-405.

5. Graff, M.; Mohanty, S. K.; Moss, E.; Frazier, A. B., *J. Microelectromechanical systems* **2004,** 13, 956-962.

6. Jackman, R. J.; Duffy, D. C.; Cheriniavskaya, O.; Whitesides, G. M., *Langmuir* **1999,** 15, 2973-2984.

7. Atsuta, K.; Suzuki, H.; Takeuchi, S. In International conference on Miniaturized Systems for Chemistry and Life sciences, Malmo, Sweden, September 26-30, 2004; Malmo, Sweden, 2004.

8. Vaeth, K. M.; Jackman, R. J.; Black, A. J.; Whitesides, G. M.; Jensen, K. F., *Langmuir* **2000,** 16, 8495-8500.

9. Pal, R.; Yang, M.; Johnson, B. N.; Burke, D. T.; Burns, M. A., Phase Change Microvalve for Integrated Devices. *Anal. Chem.* **2004,** 76, 3740-3746.

CHAPTER 4
PROGRAMMABLE FLUIDIC SYNTHESIS OF MICROPARTICLES WITH CONFIGURABLE ANISOTROPY

Introduction

Demand for particles with shape and interaction anisotropy is fueled by applications in self-assembly[1, 2], drug delivery carrier design[3] and barcoding[4]. Subtle changes in particle anisotropy produce surprising effects. For example, transforming a rod from a spherocylinder to an ellipsoid eliminates its smectic phase and the transition pressure of the liquid crystal cubatic phase is linked to cube roughness[5, 6]. In addition, particle shape is a determinant of the efficacy of macrophage phagocytosis[3]. The richness of applications for anisotropic particles has driven research in new particle synthesis techniques. Batch syntheses have yielded a broad array of faceted, branched and patterned particles[1] including colloidal molecules[7, 8] as well as patchy[9] and Janus[10] particles. Electrical, optical, magnetic and deformation fields have also been applied to produce anisotropic colloidal particles[11].

Uniformity of anisotropic particle shape and internal structure is critical to self-assemble complex structures and arrays for end-use applications such as photonic band gap materials[12]. Among the explosion of recent synthetic methods, two classes – those based on confinement effects and those based on microfluidics – yield exceptional uniformity. First, Xia and coworkers have formed colloidal molecules and chains by

confinement of particles in patterned surfaces and channels[8, 13] while Wu and coworkers[14] have formed non-closed packed lattices by self-assembly of millimeter scale beads confined in packed columns. Second, microfluidic methods have introduced the possibility of continuous synthesis. For example, two-phase flow through a microfabricated nozzle or T-junction yields droplets of controlled size that can be subsequently solidified into particles[15]. Alternatively, local regions of a monomer solution have been polymerized by flow-through photolithography[16].

To date, confinement-based synthetic methods lack the continuous processing capability of microfluidics including the potential for programmable operation. Meanwhile, the microfluidics methods, all based on the solidification of liquid precursors, lack the means to flexibly introduce complex internal shape and material anisotropy. Combining the attributes of confinement and microfluidics in a single synthesis method would yield the ability to simultaneously program highly uniform shape and material sequences into the particles. Such a flexible method could be applied to continuously produce particles with classes of anisotropy that are not available through either approach, or by any other method.

Here we introduce such a continuous synthesis technique based on the principles of confinement, microfluidic processing and permanent bonding to yield particles with novel and configurable forms of shape and material anisotropy. In addition to possessing global shape anisotropy, these particles also incorporate new forms of local anisotropy, including repeated bond angles, concavity and uniform roughness. With software programmable microfluidics, the material anisotropy of linear chains can be designed to yield homogeneous (type "A"), surfactant-like (type "A-B") or tri-block (type "A-B-A")

internal sequences – all produced in a single device. Moreover, the continuous fluid processing method makes only minimal constraints on the input precursor particles. Thus, although here we use latex beads with different optical signatures to distinguish between "A" and "B" type, the rich array of materials and chemistries that have been previously incorporated into microparticles are equally well compatible with the method. Because of the method's programmability and the unique way in which shape and material anisotropy are combined in the synthesis products, anisotropic particles produced by it will be applicable to areas of the chemical sciences such as barcoding[17], self-assembly[18] and drug delivery carrier design[3].

Material and Methods

Materials

Polystyrene microspheres were used as precursors. The manufacturer reported diameter of the large and small spheres is 21.14 ± 0.04 μm and 9.91 ± 0.73 μm, respectively. The small particles contain a dye to distinguish themThe carrier solvent dimethyl sulfoxide (DMSO, Sigma-Aldrich) was selected because of its high boiling temperature (189 °C) and its non-swelling interaction with polystyrene ($c_{PS/DMSO}$ = 1.36 at 25°C and 1.20 at 80°C)[28].

Microfabricated device

Fluidic channels and metal heater were fabricated on opposite sides of a polished Silicon oxide wafer (450 μm thickness, 100mm diameter, 5000Å thermal oxide layer). For channel etching, photoresist (PR 1827) was spun, patterned and developed in MF 319 solution. The oxide layer of the developed region was etched in buffered hydrofluoric acid solution. Channels were etched in a STS Deep reactive ion etcher. After etching, the oxide layer on the channel side was again stripped. Metal heaters were fabricated on the backside by lift-off of a Ti/Pt (300Å/1000Å) layer in acetone solution. Ports for sample injection and fluidic control were made by electrochemical discharge drilling of a glass wafer (Pyrex 7740, 100mm diameter, 700 μm) that had been cleaned in hydrogen peroxide-sulfuric acid mixture (1:3 v/v). The resulting glass and silicon wafers were aligned, anodically bonded, diced and wired to a printed circuit board.

Fluidic control

A software configured pressure, vacuum, or neutral load was applied through syringes connected to each port. To rapidly switch ($t_{switch} \sim 5$ ms) between the three states during a synthesis cycle, syringes were connected to a set of 2-way and 3-way solenoid valves (Numatech) that were operated by computer control (Labview 7.1, National Instruments).

Particle fusing

Fusing is accomplished at a temperature set by controlling a Ti/Pt heater fabricated on the back of the chip. The resistance value of the metal heater is ~0.39 KΩ.

Fusing is accomplished by raising the temperature to a set point that can be varied between T = 65 – 85 °C. At the condition of 50 VDC (T = 80°C) fusing is achieved in less than 300 ms. After heating, the particle is cooled by convective flow and then released into the collection chamber.

Image acquisition and processing

In situ imaging of the particles in device was accomplished with a stereoscope (Olympus SZX-12) and digital camera (Nikon Coolpix 4500). High-resolution particle images were acquired with 10x, 40x and 60x objectives on upright (Zeiss Axioscope) or inverted (Nikon Eclipse TE2000-U) microscopes. Bond angles between the fused particles were measured in the following way: The edge detection tool of image analysis software (ImageJ 1.34s, National Institute of Health) was used to find particle boundaries. Particle centroids were determined from particle boundaries. The bond angle relative to the particles central axis was determined from the centroid locations.

Results and Discussion

Synthesis Concept, Design and Operation

In our approach (Fig 4.1A), programmable fluid flow is used to sequentially transport precursor particles through a series of narrow (i.e., approximately one particle diameter in width and depth) channels. A constriction or weir in the channel collects the particle sequence with programmed anisotropy in the production zone. A variety of techniques can be used to bond the anisotropic assembly including sintering, UV-initiated

photopolymerization, carboxyl-amine chemistry, DNA hybridization or receptor-ligand binding. After bonding, the flow is reversed to release the manufactured particle for collection and use. A key feature of this scheme is that metering lines located along the production zone allow the internal (material) sequence of the particle chain to be specified by means of a series of software programmed pressure actuation steps. For example, each of the material sequences (products) shown at Fig. 4.1A right can be made by means of the two-metering line device.

Fig 4.1B reports the steps of a typical synthesis cycle. The particle produced is a linear chain of homogeneous sequence with regular, alternating bond angles. The geometry of the production zone fixes both the length (N = 11) and bond angle (angle relative to particle centerline, a = $29.3° \pm 2.3°$). Continuous flow (Q ~ 3.5 μl/min) through the production zone compresses the sequence. An on-chip resistive heater raises the local temperature to near the glass transition point to fuse the particles into a permanently bonded chain. The minimum time for fusing is 300 ms. The high-resolution optical micrograph shows that the alternating structure created by the fluidic processing is conserved during the fusing step.
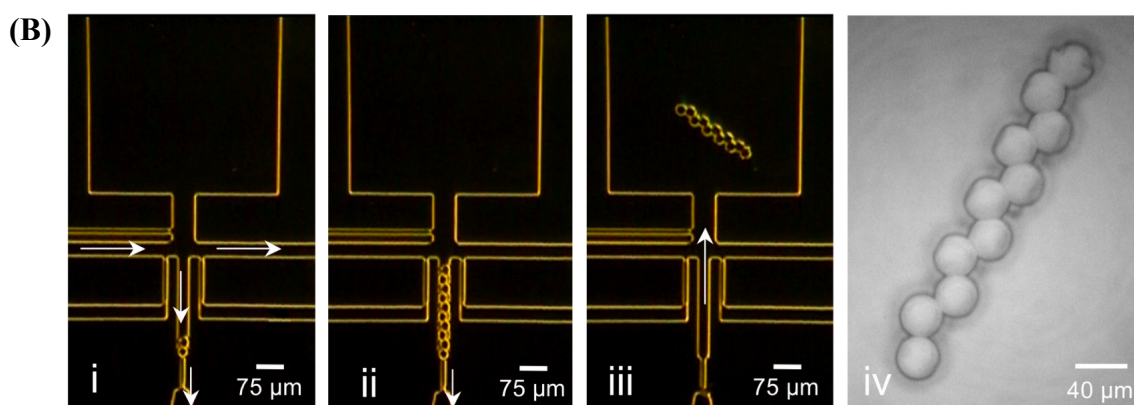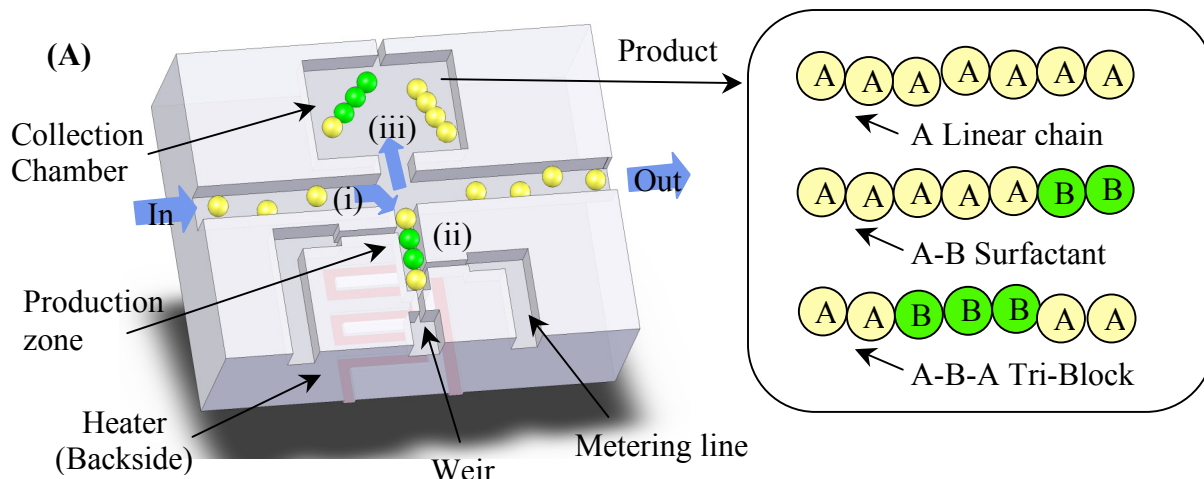
Figure 4. 1 (A) Schematic diagram of the continuous synthesis process. Particles (0.05 wt%) flow single-file in DMSO to the production zone (i) where they undergo reaction (ii) and collection (iii). The length and width of the zone and the actuation of input and metering lines control the sequence synthesized. Depending on actuation, each of three kinds of chains shown can be synthesized. (B) Image sequence shows the operational steps involved in the synthesis of a particle chain by thermal fusing. The sequence is loaded (i), fused (ii) and released (iii). Arrows show direction of flow. The input particles are 21.1 μm polystyrene beads. Fusing is accomplished at T = 80 °C by operating a Ti/Pt heater fabricated on the back of the chip. After heating, the particle is cooled by convective flow and then released into the collection chamber. (iv) High-resolution optical microscopy image of the particle chain synthesized. The tail of the particle has been imprinted with the geometry of the flow constriction at the end of the production zone. The sphericity of the particles in the chain is a function of the fusing temperature.

One unexpected effect of applying vacuum pressure to the weir during the thermal profile, as shown in the Fig 4.1B micrograph, is that the shape of the weir is imprinted on the tail of the synthesized chain. This imprint uniquely identifies a particle's head and tail, thereby approximately doubling the amount of information that could be encoded in their anisotropic structure for applications such as colloidal barcoding[3]. If desired, actuating the weir pressure profile during the production step removes the shape effect (as shown, e.g., for chains in Fig 4.4).

ii	Inject	Wash	Heat	Eject
1	P	N	N	N
2	N	P	N	P
3	V	V	V	P
4	N	N	N	P
5	N	V	N	N
6	P	P	P	N
7	N	N	N	V
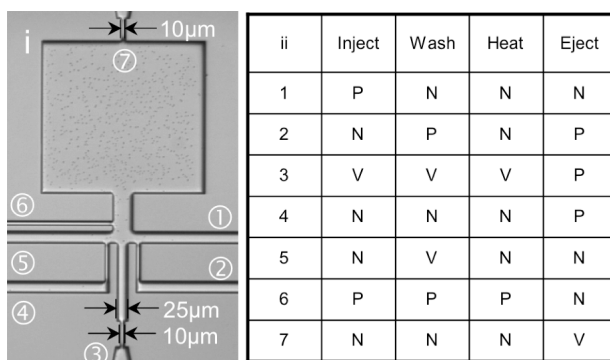
- P : Pressure ($\approx$ 8 psi)
- N : Neutral
- V : Vacuum ($\approx$ 10 inHgVac)

Figure 4. 2. Typical operation cycle to produce the anisotropic particle shown in Fig. 4.1. Seven channels (numbered as in left panel) are actuated among three states (positive pressure, positive vacuum, neutral) to load precursor spheres, wash/meter the sequence of particles packed at the weir, fuse the packed sequence, and eject it into the product reservoir.

Figure 4.2 describes how pressure inputs to the device are used to control the loading, washing, fusing and release steps in each synthesis cycle. Pressure is actuated among three states including high-, neutral-, and low-pressure settings at seven channels. We note that the wash step is included in every synthesis cycle to avoid or remove defective assemblies prior to the fusion step.

Angle : 31.1 ± 3.4

Length : 210 μm

Temp. : 65 °C

Angle : 40.3 ± 3.8

Length : 167 μm

Temp. : 85 °C
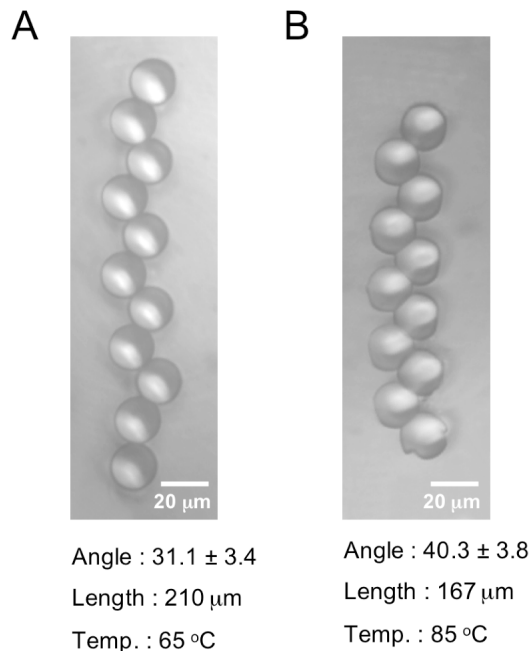
Figure 4. 3. Effect of fusing temperature on the sphericity of particles configured into anisotropic chains. As the fusing temperature is increased from 65°C (A) to 85° (B) particles in the chain increasingly soften and distort along the microchannel wall of the production zone. The sphericity of the particles is greater at the lower set point fusing temperature than at the higher set point.

Synthesis uniformity

An effect of the thermal profile is to flatten the sides of the particles that comprise the chain, as shown in Fig 4.1B (iv). This flattening is due to slight distortion of the particles by the microchannel walls as they are softened during fusing. While this non-sphericity may be desirable for some applications, the amount of distortion can be controlled or eliminated by adjusting the fusion temperature. Figure 4.3 reports the effect of the fusion temperature on the sphericity of the particles that are incorporated into the particle chains. We find that during fusing the particles may flatten against the microchannel walls. The degree of distortion is principally controlled by the fusing temperature. At low fusing temperatures (T = 65°C), the particles soften to only a small

60

degree. In this case, the distortion effects are minimal and the sphericity of the particles of the chain is very high (Fig 4.3A). At high fusing temperatures (T = 85°C), the particles are more non-spherical (Fig 4.3B). Thus, the sphericity of the particles in the chains can be controlled by adjusting the fusing temperature.

(A)

i	ii	iii
L/2R = 1.23	L/2R = 1.54	L/2R = 1.80
15.5 ± 3.8	31.7 ± 3.0	57.0 ± 1.8

(B)

$$\sin\alpha = \frac{L}{2R} - 1$$

(C)

L/2R = 1.96

α_1 : 49.3 ± 2.6

α_2 : 77.7 ± 3.7
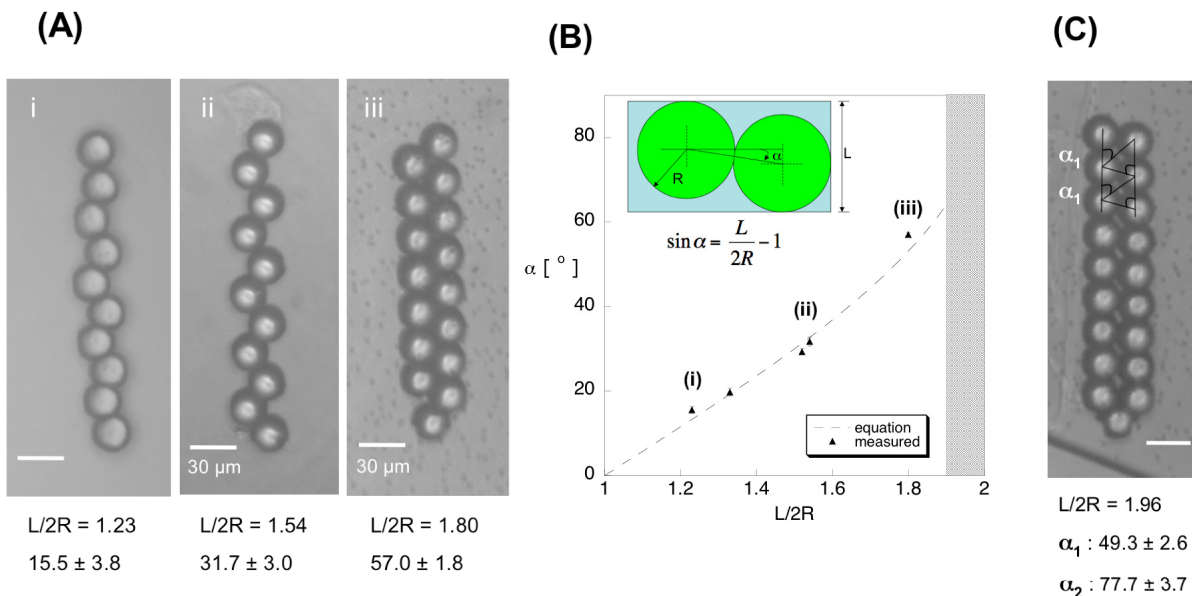
Figure 4. 4. Effect of channel geometry on chain bond angle. (A) Image of synthesized particles chains with different bond angles. The interior bond angles of the permanent chains from image processing are shown. The number of monomers in each chain is consistent with the production zone geometry (i.e. width and length) used to produce it. (B) Comparison of experimental and theoretical bond angles. Error bars (standard error of the mean) are comparable to the size of the datum points. A regime in which chains with irregular bond angles are formed is shaded at the right of the plot. (C) Chain with irregular bond angles formed in a microchannel of dimensionless width L/2R = 1.96. The two (alternating) bond angles are 49.3 ± 2.5° and 77.7 ± 3.7°.

To evaluate the uniformity of the synthesis from particle to particle, we performed the following experiment and analysis: In a particular synthesis run, a series of twenty-six chains, each 5 particles in length, was sequentially synthesized (i.e. yield = 100%). Of the chains, eight were randomly selected for high-resolution microscopy and bond angle

analysis (c.f. Material and Methods). The chains are highly uniform: the measured mean bond angle a = 32.4° with standard deviation, s = 1.5°. In addition, the silicon devices did not fail due to jamming, clogging or fouling during the loading, fusing or release phases of the production cycle. For example, to date, multiple devices have been exercised for hundreds of production cycles without observing such effects. Thus, the process reproducibly yields highly uniform particles with a low failure rate. Design features that contribute to performance include: (i) dilute concentration of input particles (~ 0.05 wt%) to eliminate jamming; (ii) silicon substrate to minimize device/particle adhesion; (iii) metering (wash) lines to achieve additional fluidic flexibility and control. In particular, we use a wash step in every synthesis cycle (c.f. Figure 4.2) to remove excess particles from the top of the production zone and thereby avoid fusing defective assemblies.

Design and Control of Anisotropic Particle Internal Structure

This method is a powerful means to configure the shape and sequence of anisotropic particles. Because the ratio of channel width to particle diameter controls the bond and torsional angles between precursor particles, chain structure is reminiscent of polymers and can be varied from linear to alternating to helical[19, 20]. Such corrugated chains also have local concavity potentially beneficial to drug delivery carrier design[3]. In the size range of interest here, a simple 2D model for the stacking of individual particles of radius R in a channel of width L is $\sin\alpha = \dfrac{L}{2R} - 1$, where a is the angle of a segment connecting the centroids of two adjacent particles relative to the centerline of the chain[19]. As shown in Fig 4.4A, we varied the ratio L/R to produce chains with a varying from

$15.5 \pm 3.8°$ to $57.0 \pm 1.8°$. Here the error is the standard deviation, s, of all interior bond angles of the chain. The agreement between the bond angle model and the measured average is good, as shown in Fig 4.4B. As the bond angle is increased above $\sim 60°$, synthesized chains transition from a regular structure with a unique bond angle to an irregular one characterized by two bond angles (Fig. 4.4C), again in good agreement with previous studies of sphere packings[19]. These results show that the precise control of chain structure yielded by microfabrication and fluidic processing propagates through the fusing step to the finished products of the synthesis.

We note that the interior bonds angles of the chains are very precise – the typical standard deviation of angles in a chain is less than 10% of the mean value, particularly for particles that are fused such that their sphericity is preserved (c.f. Figure 4.3). In this case, the principle determinants of the variability in bond angles are the size polydispersity of the precusor spheres (s = 3.5%) and the variation in the width of the microchannel production zone (s = 0.6%).

Combining material and shape anisotropy

In Fig 4.5 we show that the method's combination of local shape control and configurable sequence can be applied to synthesize permanently bonded particles with new kinds of anisotropy. As an example of programmed fluidic synthesis, the top image sequence reports particles produced in a production zone configured with two metering lines. By coupling the sequential actuation of these lines with the input flow of either A or B particles, we produce A-B (Fig 4.5B) and A-B-A (Fig 4.5C) type sequence anisotropy. The particles are reminiscent of molecular agents for assembly such as

surfactants, associative thickeners and block copolymers. These microscale materials however display structural rigidity that is absent from their molecular analogues. Also in Figure 4.5, at bottom, we find that shape and material anisotropy can be combined to form particles with well-defined patchiness[1]. To form triangular prisms[21], we taper the geometry of the production zone. The particles formed, shown in Fig. 4.5E, display uniform roughness useful for tuning liquid crystal phase boundaries[6]. In Fig. 4.5F, we controllably introduce patchiness by labeling one vertex of the prism with a type A particle. The remainder of the prism, populated with ~ 10 μm particles, shows roughness that differs from the particle formed from the ~ 20 μm spheres.
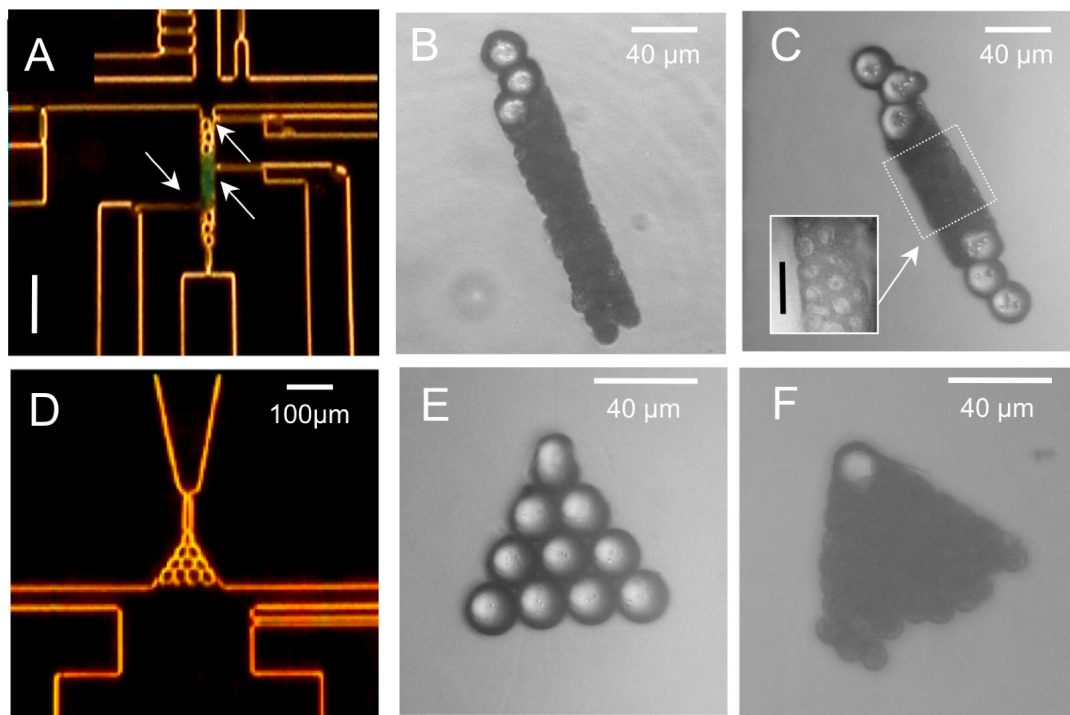
Figure 4. 5. Material and shape anisotropy produced by the method. (A) Image of the production zone of a device configured with two metering lines for sequence control. The scale bar is 100 μm. The arrows indicate metering lines. The device can be used to produce type A, A-B and A-B-A chains. The large (type-A) and small (type-B) polystyrene particle sizes are 21.1 μm and 9.9 μm, respectively. The small particles contain a blue dye to distinguish them. The A-B-A particle sequence shown is formed by repetition of the following cycle at each metering location: First, particles of appropriate type (A or B) are packed into the channel. Second, excess particles are expelled by actuation of the metering line. From this single device design, chains with the material sequence heterogeneity of B and C are produced. The inset of Fig. 3C is high-resolution image showing that the internal structure of the small particles persists after fusing. The scale bar is 20 μm. The tapered channel production zone of D can be packed to form homogeneous triangular prisms with uniform roughness (E). Combining type A and B particles results in both shape anisotropy and patchiness (F). The size scalability of the method is shown in G. FITC labeled spheres of 3.0 μm diameter are packed in a production zone of depth 8.5 μm. The fused chain after release from the production zone is shown in (H). The variable fluorescence records the alternating bond angles that result from vertical packing in the production zone microchannel.

65

Conclusion

A powerful attribute of the method presented is that the particle's sequence can be dynamically controlled through fluidic processing. For instance, mixtures of type A, A-B, and A-B-A structures could all be made in a single linear channel device with the final composition of the mixture controlled solely by software. Parallelization of the channels in a single device offers further possibilities for enhanced synthetic flexibility and throughput. For example, the 1.08 x 0.66 mm^2 single channel device of Fig. 1B operates at 0.25 Hz for the synthesis of corrugated chains, implying an unoptimized production rate of $>10^5$ particles/hour/cm^2. This estimate implies the simultaneous operation of 10-100 channels in a single device. For monolithic channels, this degree of parallelization is consistent with current microfluidic technology[27]. Thus, quantities necessary for applications such as 3D visualization of self-assembly or cell population barcoding are accessible by means of this technique.

References

(1)   Glotzer; S. C.; Solomon; M. J. *Nature Materials* **2007**, *6*, 557-562.

(2)   Glotzer; S. C.; Solomon; M. J.; Kotov; N. A. *AIChE Journal* **2004**, *50*, 2978-2985.

(3)   Champion; J. A.; Mitragotri; S. *Proc National Academy Sciences* **2006**, *103*, 4930-4934.

(4)   Pregibon; D. C.; Toner; M.; Doyle; P. S. *Science* **2007**, *315*, 1393-1396.

(5)   John; B. S.; Stroock; A.; Escobedo; F. A. *J. Chem Phys.* **2004**, *120*, 9383-9389.

(6)   John; B. S.; Escobedo; F. A. *J. Phys. Chem B* **2005**, *109*, 23008-23015.

(7)   Valignat; M. P.; Theodoly; O.; Crocker; J. C.; Russel; W. B.; Chaikin; P. M. *Proc. Nat. Acad. Sci.* **2005**, *102*, 4225-4229.; Lu; Y.; Xiong; H.; Jiang; X. C.; Xia; Y. N.; Prentiss; M.; Whitesides; G. M. *Journal of the American Chemical Society* **2003**, *125*, 12724-12725.; Rolland; J. P.; Maynor; B. W.; Euliss; L. E.; Exner; A. E.; Denison; G. M.; DeSimone; J. M. *Journal American Chemical Society* **2005**, *127*, 10096-10100.; Manoharan; V. N.; Elsesser; M. T.; Pine; D. J. *Science* **2003**, *301*, 483-487.; Cho; Y. S.; Yi; G. R.; Lim; J. M.; Kim; S. H.; Manoharan; V. N.; Pine; D. J.; Yang; S. M. *Journal of the American Chemical Society* **2005**, *127*, 15968-15975.

(8)   Yin; Y.; Lu; Y.; Gates; B.; Xia; Y. *J. Am. Chem. Soc.* **2001**, *2001*, 8718-8729.

(9)   Zhang; G.; Wang; D. Y.; Mohwald; H. *Angew. Chem. -Int. Edit.* **2005**, *44*, 7767-7770.

(10) Cayre; O.; Paunov; V. N.; Velev; O. D. *J. Mater. Chem.* **2003**, *13*, 2445-2450.

(11) Furst; E. M.; Suzuki; C.; Fermigier; M.; Gast; A. P. *Langmuir* **1998**, *14*, 7334-7336.; Terray; A.; Oakey; J.; Marr; D. W. M. *Applied Physics Letters* **2002**, *81*, 1555-1557.; Roh; K. H.; Martin; D. C.; Lahann; J. *Nature Materials* **2005**, *4*, 759-763.; Roh; K. H.; Martin; D. C.; Lahann; J. *Journal of the American Chemical Society* **2006**, *128*, 6796-6797.; Champion; J. A.; Katare; Y. K.; Mitragotri; S. *Proc National Academy Sciences* **2007**, *104*, 11901-11904.; Mohraz; A.; Solomon; M. J. *Langmuir* **2005**, *21*, 5298-5306.

(12) Ozin; G. *Chem Comm.* **2003**, 2639-2643.; Colvin; V. L. *Mrs Bulletin MRS Bull.* **2001**, *26*, 637-641.

(13) Xia; Y.; Yin; Y.; Lu; Y.; McLellan; J. *Adv. Func. Mater.* **2003**, *13*, 907-918.; Yin; Y.; Xia; Y. *Journal of the American Chemical Society* **2003**, *125*, 2048-2049.

(14) Wu; H. K.; Thalladi; V. R.; Whitesides; S.; Whitesides; G. M. *Journal of the American Chemical Society* **2002**, *124*, 14495-14502.

(15) Nie; Z. H.; Xu; S. Q.; Seo; M.; Lewis; P. C.; Kumacheva; E. *Journal of the American Chemical Society* **2005**, *127*, 8058-8063.; Nisisako; T.; Torii; T.; Higuchi; T. *Chem Eng J.* **2004**, *101*, 23-29.; Fernandez-Nieves; A.; Cristobal; G.; Garces-Chavez; V.; Spalding; G. C.; Dholakia; K.; Weitz; D. A. *Advanced Materials* **2005**, *17*, 680.; Shepherd; R. F.; Conrad; J. C.; Rhodes; S. K.; Link; D. R.; Marquez; M.; Weitz; D. A.; Lewis; J. A. *Langmuir* **2006**, *22*, 8618-8622.; Dendukuri; D.; Tsoi; K.; Hatton; T. A.; Doyle; P. S. *Langmuir* **2005**, *21*, 2113-2116.

(16) Dendukuri; D.; Pregibon; D. C.; Collins; J.; Hatton; T. A.; Doyle; P. S. *Nature Materials* **2006**, *5*, 365-369.

(17)   Braeckmans; K.; De Smedt; S. C.; Leblans; M.; Pauwels; R.; Demeester; J. *Nature Reviews. Drug Discovery* **2002**, *1*, 447-456.

(18)   Anderson; V. J.; Lekkerkerker; H. N. W. *Nature* **2002**, *416*, 811-815.; Ozin; G. A.; Arsenault; A. C. *Nanochemistry A Chemical Approach to Nanomaterials*; RSC Publishing: Cambridge, 2005;

(19)   Kumacheva; E.; Garstecki; P.; Wu; H.; Whitesides; G. M. *Phy Rev Lett* **2003**, *91*, 128301.

(20)   Pickett; G. T.; Gross; M.; Okuyama; H. *Phys Rev Lett* **2000**, *85*, 3652-3655.

(21)   Malikova; N.; Pastoriza-Santos; I.; Schierhorn; M.; Kotov; N. A.; Liz-Marzan; L. M. *Langmuir* **2002**, *18*, 3694-3697.

(22)   Mazur; S.; Beckerbauer; R.; Buckholz; J. *Langmuir* **1997**, *13*, 4287-4294.

(23)   Dendukuri; D.; Hatton; T. A.; Doyle; P. S. *Langmuir* **2007**, *23*, 4669-4674.

(24)   Hodges; C. S.; Cleaver; J. A. S.; Ghadiri; M.; Jones; R.; Pollock; H. M. *Langmuir* **2002**, *18*, 5741-5748.

(25)   Kwok; D. Y.; Lam; C. N. C.; Li; A.; Zhu; K.; Wu; R.; Newmann; A. W. *Polymer Engineering and Science* **1998**, *38*, 1675-1684.

(26)   Dreyfus; R.; Baudry; J.; Roper; M. L.; Fermigier; M.; Stone; H. A.; Bibette; J. *Nature* **2005**, *437*, 862-865.

(27)   Thorsen; T.; Maerki; S. J.; Quake; S. R. *Science* **2002**, *298*, 580-584.

(28)   Cong; Y.; Zhang; Z.; Fu; J.; Li; J.; Han; Y. *Polymer* **2005**, *46*, 5377-5384.

CHAPTER 5

MICROFLUIDIC PARTICLE MOTION IN MICROCHANNELS
USING PRESSURE CONTROL

Introduction

The use of particle-containing fluid in microchannels has expanded significantly due to its excellent visualization power and capability of particle manipulation. Microparticles work as tracer particles, facilitating visualization of complex microflow such as eletrokinetic and thermal fluid motions[1-4]. In addition, they are traceable to measure microflow velocity[5] if the particles are the appropriate size and shape to follow the flow without disrupting the flow field. Microparticles have also proven excellent test-materials for biomolecules such as DNA, cell, and protein to predict the biomolecules' motions in complicated local conditions such as the electric field gradient and geometrical changes[4, 6-8]. This is due to the fact that similar-sized particles are obtainable, closely matching those of the biomolecules, which can be easily modified if needed. Moreover, assemblies of microparticles are attained through the particle-containing fluid manipulation in particular geometries[9-12]. The manipulation of the particle-containing fluid in microchannels is one advantageous means of controlling microparticles as various kinds of particles may be controlled simply by the same

method. In this process, particle manipulation is achieved spontaneously along with fluid manipulation.

Either electrokinetic or pressure-driven forces primarily manipulate the particle-containing fluid in the microchannels. Especially, the former allows both direct particle manipulation and indirect particle manipulation through carrier-fluid control. Dielectrophoresis (DEP) and Electrophoresis (EP) are two common methods employing electrokinetic force to manipulate charged or induced charged particles directly in the surrounding medium. DEP uses non-uniform AC electric fields in the 10kHz to 100 MHz range to position cells or particles on or between electrodes[4, 8, 13-17], while EP employs a DC electric field to move and separate charged molecules and particles[4, 6, 17]. Electroosmotic flow control is a representative method to control microflows electrokinetically and can be applied to control a particle-containing fluid. Electroosmosis (EO) controls the motion of ionized liquid in microchannels, relative to stationary liquid, by an electric field[1, 4, 18, 19]. For instance, if the channel wall is negatively charged (e.g., a glass channel), the counter ions in the electrical double layer are positive ions, which move toward the negative electrode, generating an EO flow in that direction. This fluid transportation is referred to as EO pumping and it is widely used in microfluidic systems.

Control via pressure-driven flow in microchannels is another method of manipulating particle-containing fluid. One advantage of pressure-driven control is that both charged and uncharged particles are transportable without specific separation. Additionally, complicated fabrication steps such as microelectrode fabrication are unnecessary if a simple, pressure-control is achieved through only a few different

71

external pressure settings. For laminar flow in a microchannel, many forces such as gravitational and inertial are negligible and, especially, thermal motion is imperceptible for micro-scale particles[18, 20]. Therefore, particles can flow easily from high to low pressure points if there is moderate fluidic resistance. The fluidic resistance in microchannels is proportional to fluid viscosity and channel length and reciprocal to a channel's cross-sectional area and a square of the hydraulic diameter[18]. As a pressure difference is volumetric flow rate multiplied by fluidic resistance, the pressure gradient is controlled by changing channel geometries (i.e., channel length and a cross-sectional area) when other values (i.e., viscosity and volumetric flow rate) remain the same. This control is simple and easy; however, it may provide higher-quality controls if such components as a confinement or a valve are employed in a system[21, 22].

Presented here is a new method to manipulate particles in a microchannel, primarily via controlling particle-containing fluid. The flow control is achieved by performing a simple three-point pressure control (i.e., neutral, low, high-pressure settings) combined with the use of a geometric complex (i.e., a branched-channel network). A microchannel with flow restriction, called a weir, is prepared to capture a specific number of particles in a channel. The width of the weir is narrower than the diameter of a particle and the shape of the microchannel is varied to generate different particle-assembly shapes, (i.e., a linear chain, triangle, and M shapes). Additional particle-free control lines are utilized to obtain specific sequence structures (i.e., A-B and A-B-A). Although only polymeric particles are tested in the paper, this system is very applicable to biological molecules as well as metallic particles for many novel demands.

72

Moreover, the assembled structures possess great potential for various applications such as cell labeling, microbarcodes, and novel crystals consisting of different particles.

Materials and Methods

Silicon device fabrication

The device fabrication includes four different processes: silicon channel etching, glass drilling, and anodic bonding of silicon and glass sides. The fluidic channels and metal heaters are fabricated and aligned on either side of the polished Silicon oxide wafer (450 μm thickness, 100mm diameter, 5000Å thermal oxide layer). For silicon channel etching, photoresist (PR 1827) is spun, patterned by a channel mask layer, and developed in the MF 319 solution. The oxide layer of the developed area is etched in buffered hydrofluoric acid solution. After these lithography steps are performed, the wafer is transferred into the STS Deep Reactive Ion Etcher for channel etching. After etching is completed, the oxide layer on the channel side is stripped by utilizing buffered hydrofluoric acid.

Electrochemical discharge drilling is accomplished on the glass wafer (Pyrex 7740, 100mm diameter, 700 μm) to obtain holes for sample injections and fluid control. The glass wafer is cleaned in Piranha Clean Solution, which is a mixture of hydrogen peroxide solution and sulfuric acid solution (1:3 v/v). The obtained glass and Silicon wafers are aligned and bonded by anodic bonding. The bonded wafer is subsequently diced employing a dicing saw, and wired to a printed circuit board by gold ball wire bonding to obtain electrical connection. The Silicon channel side remains open to build a

fluid interconnection system, to be observed by stereoscope. Glass pillars are bonded over each hole on the glass by UV glue for syringe connection.

Preparation of a silicon mold for a PDMS channel

The silicon mold is prepared for this work in order to control channel dimension precisely. Positive photoresist (PR 1827; Shipley Co., Newton, MA) was spun on a Hexamethyldisilazane (HMDS; J.T. Baker, phillipsburg, NJ) coated silicon wafer (<100>, 450 μm thick, 100 mm diameter). The wafer is soft-baked at 90 °C for 1 min, patterned by a mask layer (i.e., clear field mask), developed in the MF 319 solution (Rohm and Hass Electronic Materials, Spartanburg, SC) for 50 sec and hard-baked at 110 °C for 10 min in a convection oven. After these lithography steps are accomplished, the wafer is transferred into the STS Deep Reactive Ion Etcher (Surface Technology System, Newport, UK), which uses alternating passivation (C_4F_8) and etching steps (SF_6 and O_2). After the etching step is completed, the remaining photoresist was stripped in the PRS 2000 solution (J.T. Baker, Phillipsburg, NJ). The wafer is rinsed in DI water and air-dried.

PDMS channel fabrication

The fluidic channel was prepared by curing at 80°C for 1 hour using a 10:1 ratio mixture of PDMS prepolymer and curing agent (Sylgard 184, Dow Corning, Midland, MI). Individual fluidic channel devices were then cut using a scalpel, holes were punched, and the channel devices were then sealed to glass cover slips using UV ozone (UVO cleaner, Jelight, Irvine, CA).

Particle sample preparation

Two different polystyrene particles, Megabead NIST Traceable Particle Size Standard 20.0 μm (Polysciences, Inc.) and Polybead Dyed Blue 10.0 μm microsphere (Polysciences, Inc.) are utilized as precursor particles. Particles are mixed in DI water, and the concentration of the sample is 0.05 wt% for both particles.

Pressure control

Fluid control is performed by applying pressure, vacuum, or neutral states at each hole. Pressure is applied by delivering carrier fluid into the system. Every hole is connected with syringes (3cc Disposable Reservoir System and Barrel Adapter Assembly, EFD) containing DI water and fluid is pushed by pressure and pulled by vacuum. In order to switch those three states easily, a set of 2-way and 3-way valves (Numatech) is prepared and connected to the syringes. These solenoid valves are computer controlled (Labview 7.1, National Instruments). A pressure controller (VSO-EP, Parker Pneutronics) is connected at the pressure source to regulate pressure application.

Image processing

All experiments have been performed under stereoscope (Olympus SZX-12) with a digital camera (Nikon Coolpix 4500) for imaging. The camera output is recorded and digitized. High-resolution particle images are taken by Upright Microscope (Zeiss Axioscope) with 10x and 40x objectives.

Results and Discussion

A simple three-point control (STP) in complex channel geometry is beneficial to particle-containing fluid manipulation in a microsystem. It does not require any other microfluidic control components (e.g., microvalve and electrode). Moreover, pressure gradient (i.e., the driving force of this fluid control) is spontaneously generated by both pressure-setting values from the external pressure source and pressure drop caused by channel resistance. Another merit of this method is that the control process does not depend on the particles' properties, thus it brings excellent flexibility to the system. Many previous researches on cells and particles require their capture and transport, which is typically carried out by either using electrokinetic force such as dielectrophoresis[14, 15, 23] or using geometric confinements[10, 11, 24, 25]. Accordingly, we combine the STP control and geometric confinement to build an all-purpose control system.

Particle flows and capture

The flow of uncharged microparticles (i.e., larger than 2-3 μm in diameter) in a narrow microchannel is dominated by a drag force caused by fluid flow around the particles. The displacement of free particles, due to thermal (Brownian) motion, are significant if the diameter of the particles is less than 2-3 μm. Inertial forces and gravitational force are both negligible; the former results from the laminar flow nature, while the latter is attributed to the density similarity between particle and fluid. Therefore, the drag force parallel to the direction of translation for a rigid particle is defined by Stokes drag law, $F_D = -6\pi\mu a U$, where μ is fluid viscosity, a is particle

diameter, and U is fluid velocity (Figure 5.1(i)).   Consequently, particles tend to flow toward the lowest pressure point (i.e., the direction of fluid) in a system.

Channel restrictions, whose width is narrower than a particle diameter, stop the particles' flow, only allowing fluid flow through the restriction.   This geometric confinement allows fluid flow between a particle and a channel wall and the flow plays important roles in reducing non-specific adhesion of particles to the channel wall, and in delivering chemical reagents to a particle stack, if needed (Figure 5.1 (ii)). The width (a) and depth (b) of a microchannel in this work are nearly identical to the diameter of the particles (i.e., (a) and (b) are both 25 μm for the use of a 20 μm sized particle), facilitating the entrance of one particle at a time.   When many particles create a stack within a channel, each particle tends to follow the path of least fluidic resistance, always producing a zigzag-shaped chain[10, 11, 26].   As a result, configurational entropy increases and porosity is minimized.
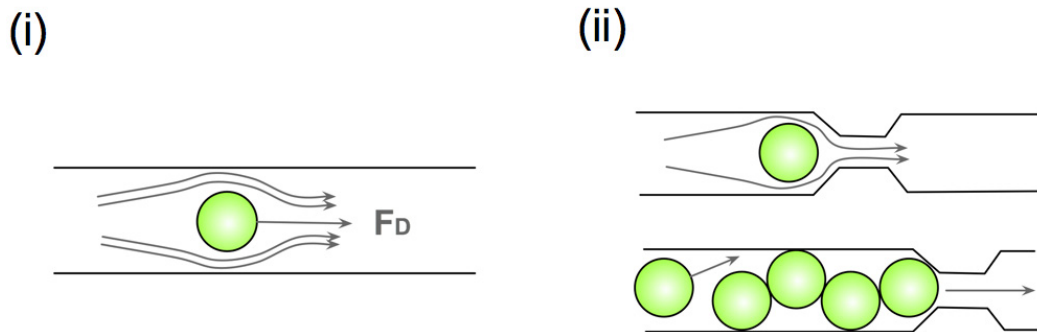
Figure 5. 1. Schematic illustration of particle flow in a microchannel. (i) Particle flow in a confinement-free microchannel. F$_D$ is Stoke's drag force and the arrows indicate streamlines. (ii) Particle flow in a microchannel with confinement (Top). The particle stops at the restriction but there is still some fluid flow around a particle and through the restriction. Stacking of particles in a channel (Bottom). Particles form a zigzag-shaped chain because they tend to follow the path with least fluidic resistance (arrow direction).

The capture of particles by a channel restriction and fluid flow through a particle stack are examined in the fabricated silicon microchannel (Figure 5.2). 20 μm Polystyrene particles are injected and dragged into a confined microchannel by vacuum force. The depth and width of the microchannel are 25 μm and the width of the weir is 10 μm. A wash line (b) is employed to clear all particles above the line (more information in section III). Subsequently, a fluorescent solution is injected after this process to confirm fluid flow through a particle stack. As can be seen from Figure 5.2(ii), there is sufficient fluid flow through the particle stack and the weir.
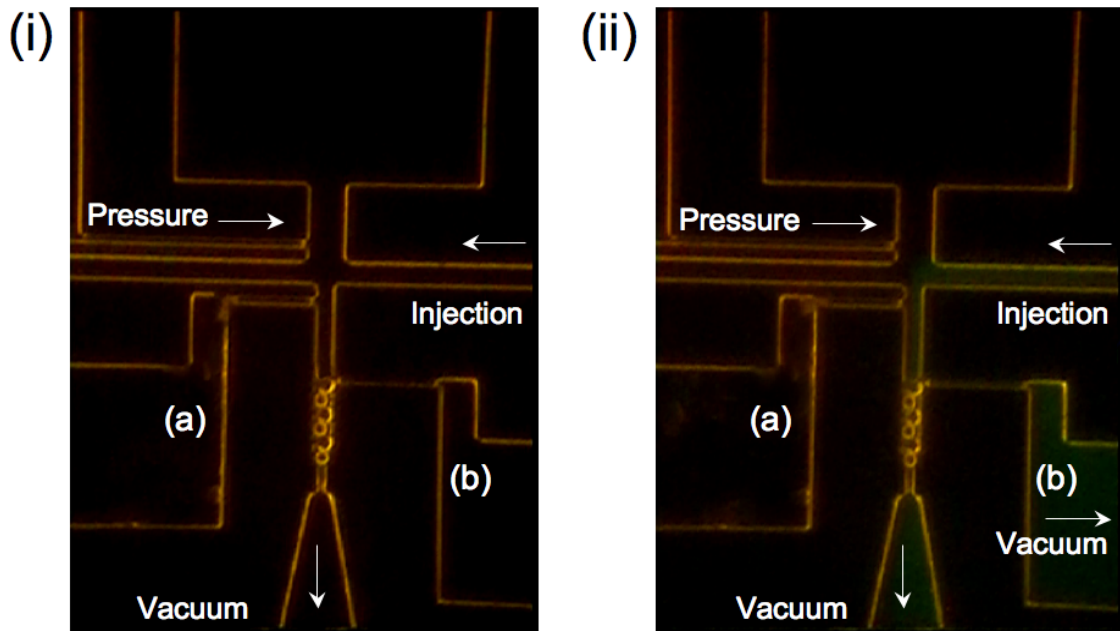
Figure 5. 2. Capture of particles and confirmation of fluid flow. The width and depth of the particle-collection channel is nearly the same as the diameter of the particles. Particles are injected by vacuum and some particles above line (b) are washed away by flow from the line (i). Fluorescent solution is injected by vacuum to verify fluid flow through a particle stack (ii).

The design of a confined channel is varied based on specific interests. For example, it can be rectangular (Figure 5.3 (i), (iv)), triangular (Figure 5.3 (ii), (v)), or

have a complex geometry such as an "M" (Figure 5.3 (iii), (vi)). After the particle injection step, washing follows to clear out all particles above the confinement channel to create a precise shape of particle structure. Figure 5.3 (vi) shows non-uniform roughness at the junction, differing from the configurations in Figure (iv) and (v). This imperfection is caused by the wide opening of the confined channel, a specific property resulting from the "M" structure. In order to meter out particles at the junction, the fluid force must overcome the force caused from particle-particle interaction. At the wide opening pictured in Figure 5.3 (vi), particles aggregate more; thus, they possess greater interaction force than particles at the smaller opening evidenced in Figure (iv) and (v), generating non-uniform roughness.
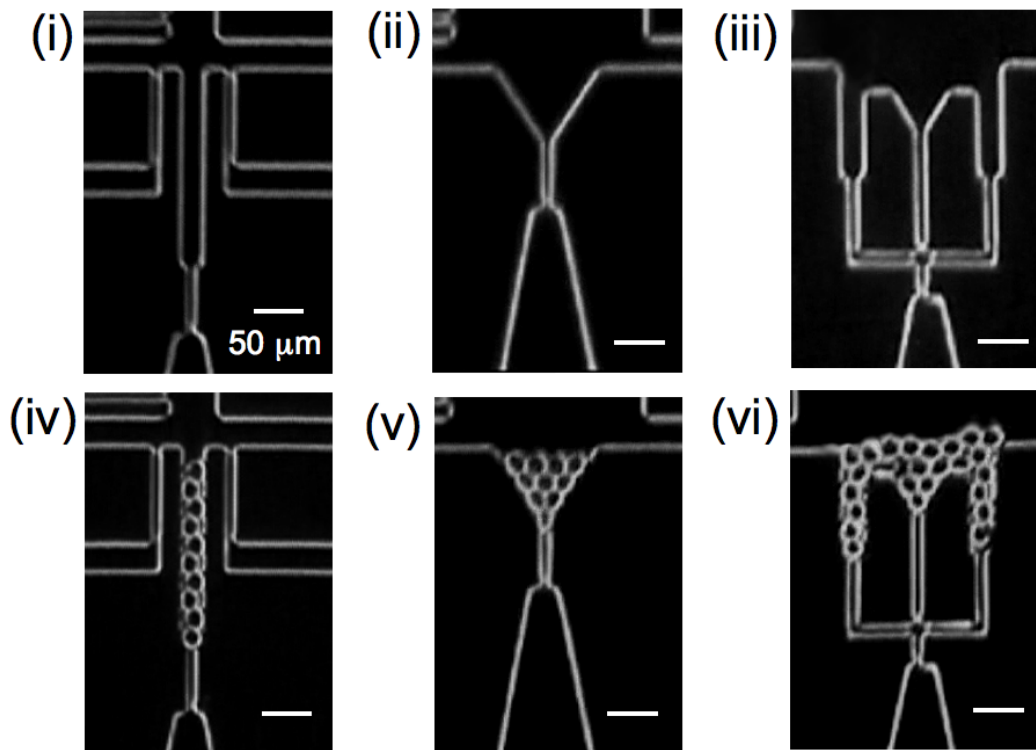
Figure 5. 3. Different designs of a channel confinement. (i) rectangular channel; (ii) triangular channel; (iii) M-shape channel; (iv) linear chain-shaped stack; (v) triangular shaped stack; (vi) M-shaped stack.

Complex particle arrangement

The STP control is used to direct microparticles to different locations in a branched-channel network. The complex channel geometry is designed and each port is connected to a pressure source, controlled independently by a computer (Labview 7.1). As previously mentioned, particles are carried by fluid in a microchannel, so fluid flow control is the main key for this particle transfer. In the system, particles are captured first in a confined channel and then transferred by changing pressure inputs at each port. As evidenced in Figure 5.4, the injection port on the right side has high pressure (H) and the capture and waste sites have low pressure (L) in order to capture a particle and wash all remaining particles. The position set at neutral has flow based on the surrounding pressure gradient. After a low-pressure setting captures a particle in a confined channel, the flow is reversed to move the particle to a different location by changing the pressure setting (Figure 5.4(iii)).
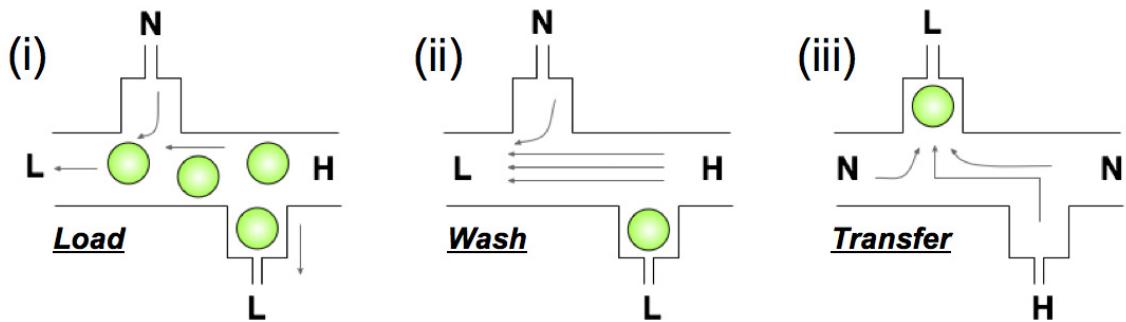
Figure 5. 4. Particle capture and transfer by channel confinement and pressure control. H, N, and L indicate pressure-setting values. H is high pressure, L is low pressure, and N is neutral. Particles always move from a high-pressure setting to a low-pressure setting. Arrows indicate flow directions. The low-pressure setting captures a particle in a confined channel (i), other particles are washed away (ii), and changing pressure settings reverses the flow direction and transfers the captured particle (iii).

Additional visual data regarding fluid flow caused by pressure control shown in Figure 5.4 are presented through velocity field simulation (Figure 5.5). COMSOL (FEMLAB 3.1) simulation is performed using the same geometry and control. For the load and wash step, the same amount of low pressure is applied at both waste (③) and collection points (①), with simulation data depicting flow in both directions. In addition, it is clearly shown that there is outflow from the neutral point (②), as the waste point pressure is lower than neutral. Figure 5.5 (ii) proves a strong streamline from ① to ②, showing that most particles transfer only from point ① to point ②.
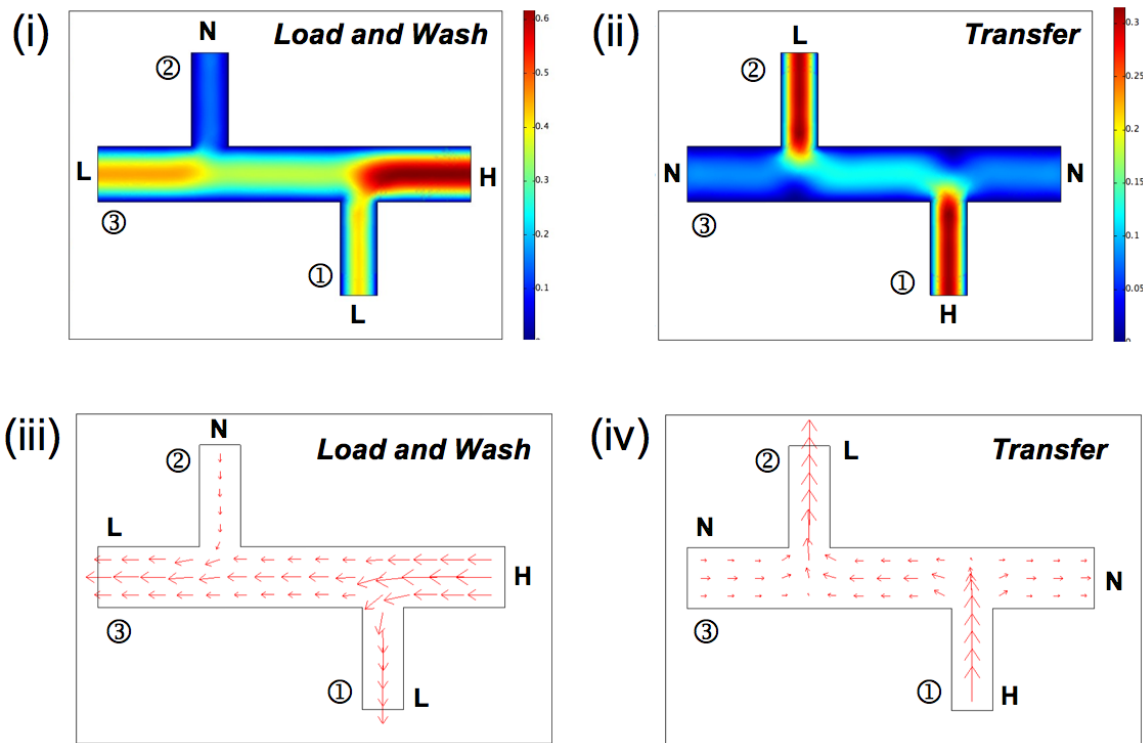
Figure 5. 5. Velocity field simulations for particle load, wash, and transfer steps. (i) and (ii) show the velocity field for each step and the arrows in (iii) and (iv) show flow direction and magnitude.

A heterogeneous structure is prepared by using a combination of capture, meter, and transfer in a branched-channel network (Figure 5.6). First, particles are injected into a confined channel (channel ①) and metered by a washing step. In order to meter a specific number of particles in channel ①, the lengths of the channel should be designed to match the length of a particle chain. In Figure 5.6 the length of channel ① is approximately 220 μm to capture 11 particles (i.e., each particle has a diameter of 20 μm) and the length of channel ② is twice the length of channel ①. Initially, 20 μm particles are injected into channel ① and metered by a washing. Second, the control shown in figure 5.4(iii) is employed to transfer particles from ① to ②, and one particle was accidentally lost during this process. As a final step, smaller particles (i.e., 10 μm in diameter, Blue-dyed polystyrene particle) were injected into channel B. During this step, a 20 μm particle was used as a weir for 10 μm particles. Therefore, restriction can be prepared by a large particle as well as a channel restriction, and this concept is applicable to generate other types of heterogeneous structures.
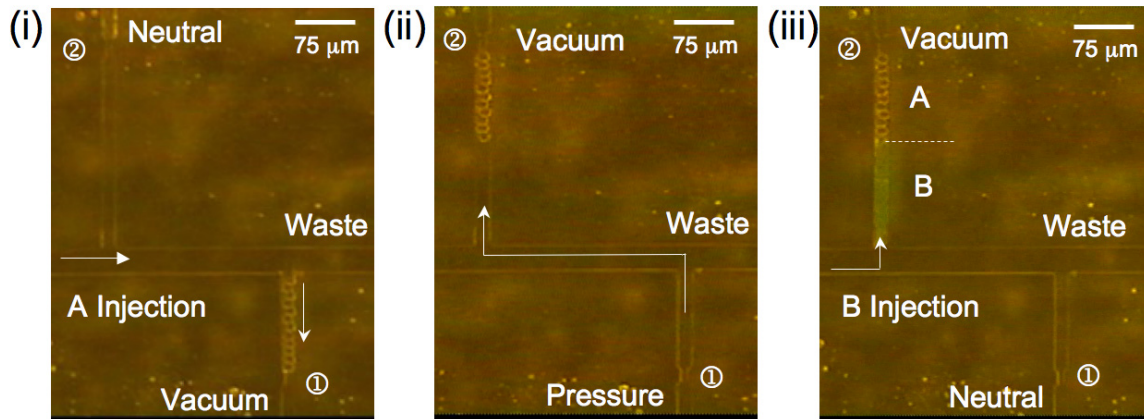
Figure 5. 6. Heterogeneous structure by sequential capture of two different particles. The PDMS channel is fabricated and the depth and width of the confined channel is close to the particle size. The length of channel ① is about 240 μm to capture twelve particles (20 μm in diameter) and that of channel ② is about 480 μm to obtain heterogeneous structures. (i) 20 μm polystyrene particles (N=12) are injected into the channel ① and other particles are washed away. (ii) the captured particles in channel ① are transferred to channel ② by having pressure at ① and vacuum at ②. (iii) 10 μm blue-dyed particles are injected into the channel ② by vacuum and stacked over a 20 μm particle.

The restriction prepared by both a channel restriction and a large particle generates another unique heterogeneous structure such as a Head-Tail structure. Figure 5.7 (i) illustrates how a combination of channel restriction and a variance in particle size are employed for the Head-Tail structure. This device has two separate inlets, one for large particles (i.e., individual large particles are referred to as A) and another for small particles (i.e., individual small particles are termed B), and in the middle of the device, there is a particle-trapping zone. As the first step, A is dragged into place, using two low-pressure lines above the channel restriction. After a washing step, B particles are injected from the second injection port and dragged into the confined channel via the two low-pressure lines. B particles form a stack in the confined channel above A. This process

ends with one final washing step. Figure 5.7 (ii) depicts a silicon device image for 20 μm particles and 10 μm blue dyed particles. 20 μm particles are injected first by vacuum, at a confined channel, and at a waste port to wash away all particles except the two captured in the channel (Figure 5.7 (iii)). As the last step, 10 μm blue particles are injected and stacked over a 20 μm particle, while the flow washes away the remainder.
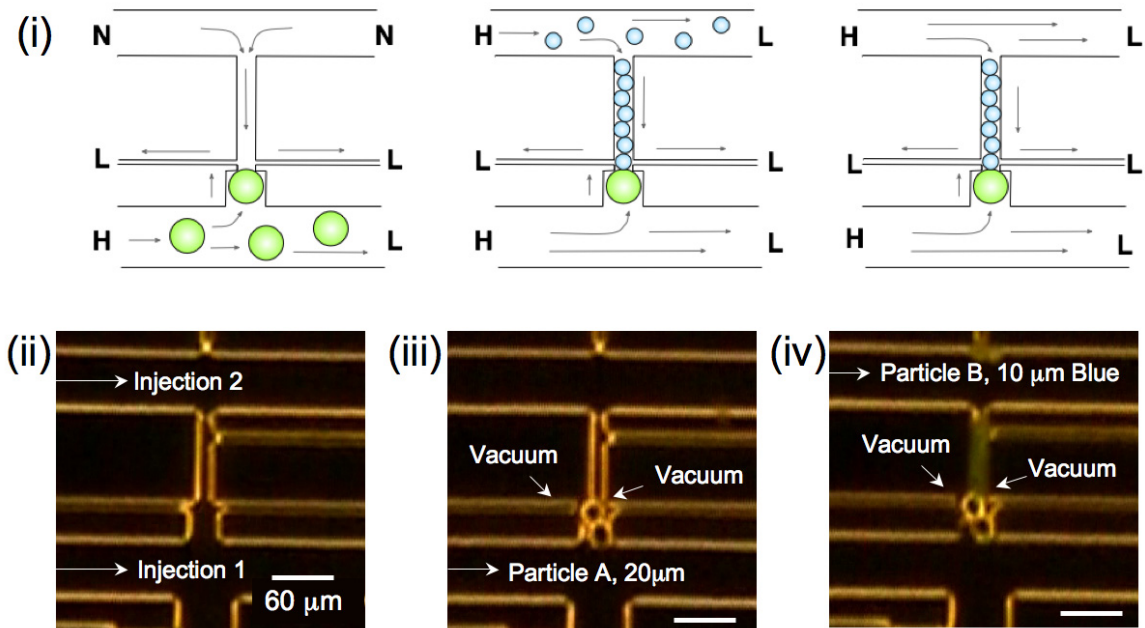
Figure 5. 7. A Head-Tail structure obtained by using a combination of channel restriction and particle restriction. (i) Big particles are injected and a particle is trapped at the confinement channel by two vacuum lines above the restriction. Small particles are injected from the other injection port, dragged into the confinement channel, and stacked over a big particle. (ii) An image of a silicon device showing two separate injection ports and a channel confinement in the middle. (iii) 20 μm polystyrene particles are injected and two of them are trapped. (iii) 10 μm blue-dyed particles are injected and stacked over a 20 μm particle.

Particle-free control line

Employing particle-free control lines in a complex system improves the control process by confining specific sections using out-flow from the line. Particle-free control

lines are additional fluid flow lines in the system, possessing widths narrower than the particle diameter. Previous paragraphs mainly presented the control of particle-containing fluid in complex channel geometry to direct particles to different locations, and to create unique particle structures. In contrast, the use of particle-free control lines do not create any structures but rather enhance the control ability through some fluid outflow, when isolating sections or additional washing is necessitated.

During a process, numerous particles are injected and most remain either in a waste chamber or in an injection chamber. In order to isolate chamber contents, two control lines are placed in close proximity of those two chambers (Figure 5.8 (i)). If those two lines are not actuated, then many contaminant particles enter from the waste and injection chambers during particle transfer (Figure 5.8 (ii)). However, once the control lines are actuated, the outward flow from the lines moves in both directions, blocking particle flow from both chambers at the ends (Figure 5.8 (iii)). Fluid simulation would give more information relative to this control. Refer to Figure 5.8 (ii) and (iii), where Figure 5.9 and 5.10 are introduced to present transfer with and without isolation, respectively.
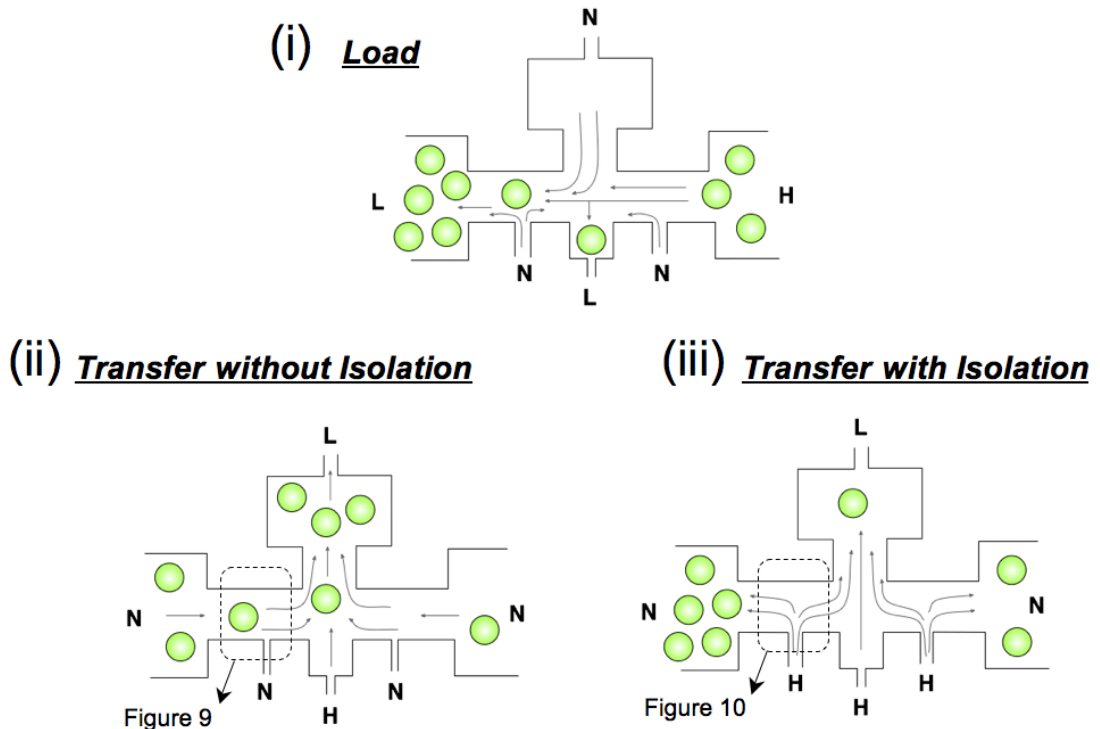
Figure 5. 8. Schematic illustration showing section isolation by particle-free control lines. (i) During a load step, many particles still stay in the injection and waste chambers. (ii) Transfer without section isolation. Some particles are dragged from the waste and injection chamber. (iii) Transfer with section isolation. Two control lines are actuated and they block particle flow from both chambers.

Pressure decreases linearly from the waste chamber (A, neutral setting), to the collection chamber (C, low-pressure setting), if no pressure control line (B) is actuated as shown in Figure 5.9. Under that pressure gradient, fluid always moves from relatively high (waste chamber) to comparatively low (collection chamber) and, consequently, particles also move in the same direction. On the other hand, there is a sharp peak of pressure gradient near the control line if the line (B) is actuated (Figure 5.10 (iii)). As fluid always flow from high to low pressure, the fluid exiting the control line divides and flows in both directions (Figure 5.10 (ii)). Although more streams move toward a

collection chamber, there is still an absence of fluid flowing out from the waste chamber

(A), which sufficiently blocks in-flow from the waste chamber.
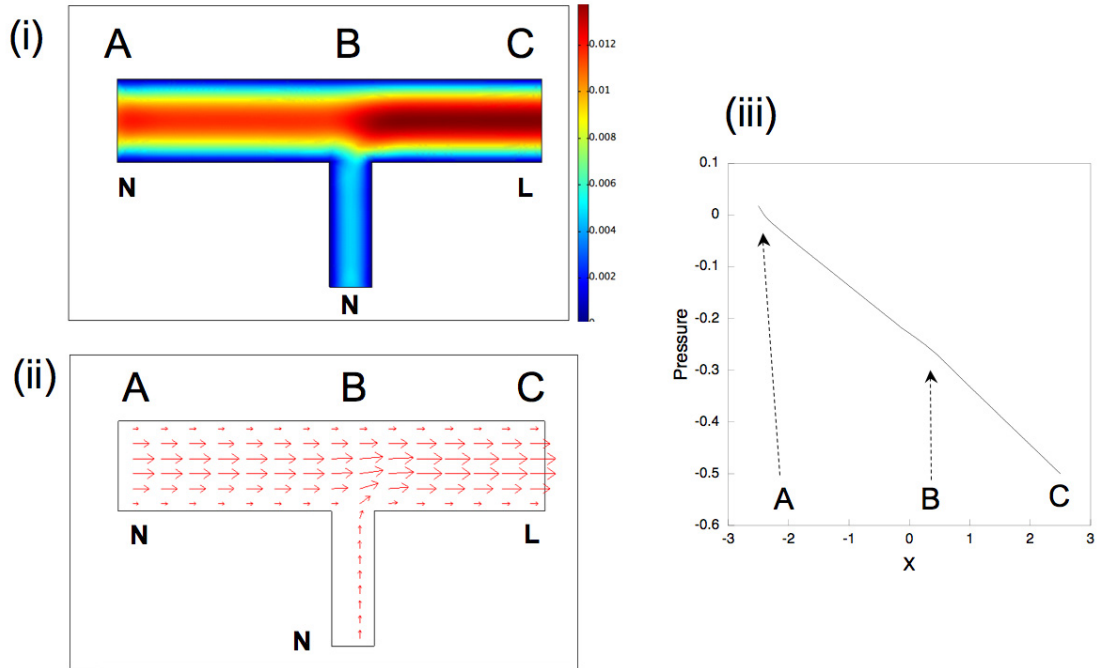
Figure 5. 9. Velocity and pressure field simulation without actuation of a control line. (i) and (ii) show velocity fields and (iii) shows pressure gradient. Arrows indicate flow direction and magnitude. A and B are set at neutral and C is set at low pressure.
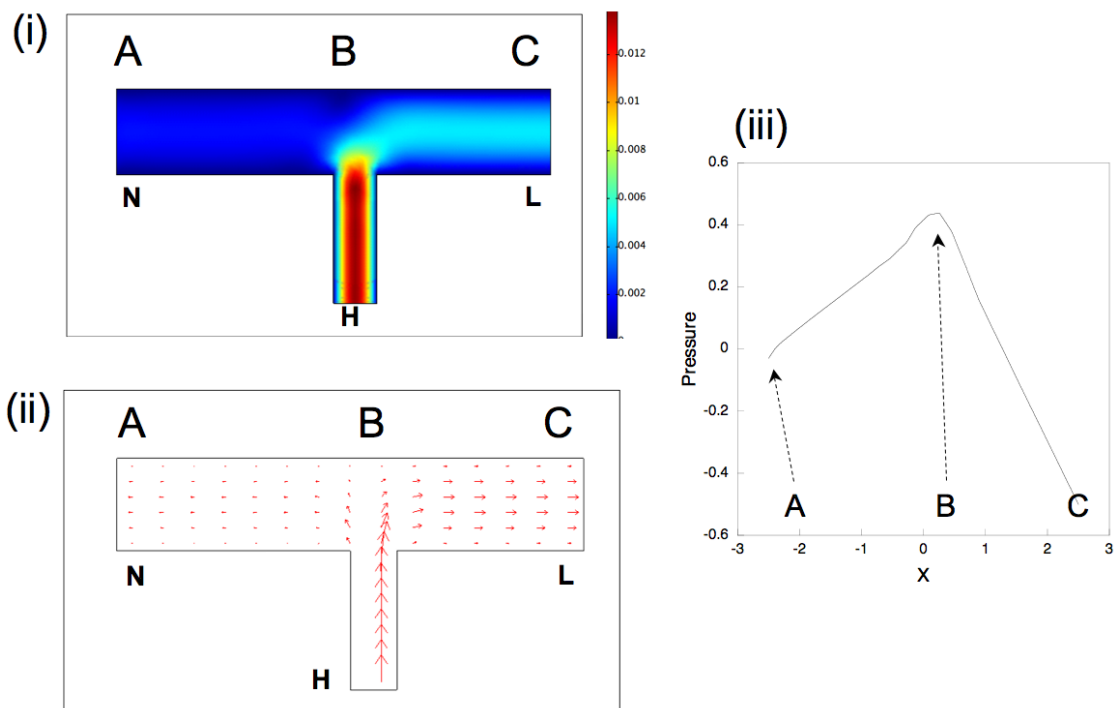
Figure 5. 10. Velocity and pressure field simulation with actuation of a control line. (i) and (ii) show velocity fields and (iii) shows pressure gradient. Arrows indicate flow direction and magnitude. A is neutral, B is set at high pressure, and C is set at low pressure.

The particle-free control line has another usage in metering an exact number of particles in a confined channel. The particles in a restricted channel are metered initially by washing, followed by injection; however, the second measuring is achieved through actuating the control line located at the confined channel. The fluid exiting the control line washes away particles above it (Figure 5.11(i)). Figure 5.11 (ii) illustrates a stack of particles metered by washing flow and (iii) shows a metering step, presenting both isolation of the upper chamber and metering of stacked particles. There is a control line near the upper chamber for section isolation. As the line is actuated during the entire process, there is an absence of particle flow into the chamber, confirmed by the flow of fluorescent solution exiting the control line.
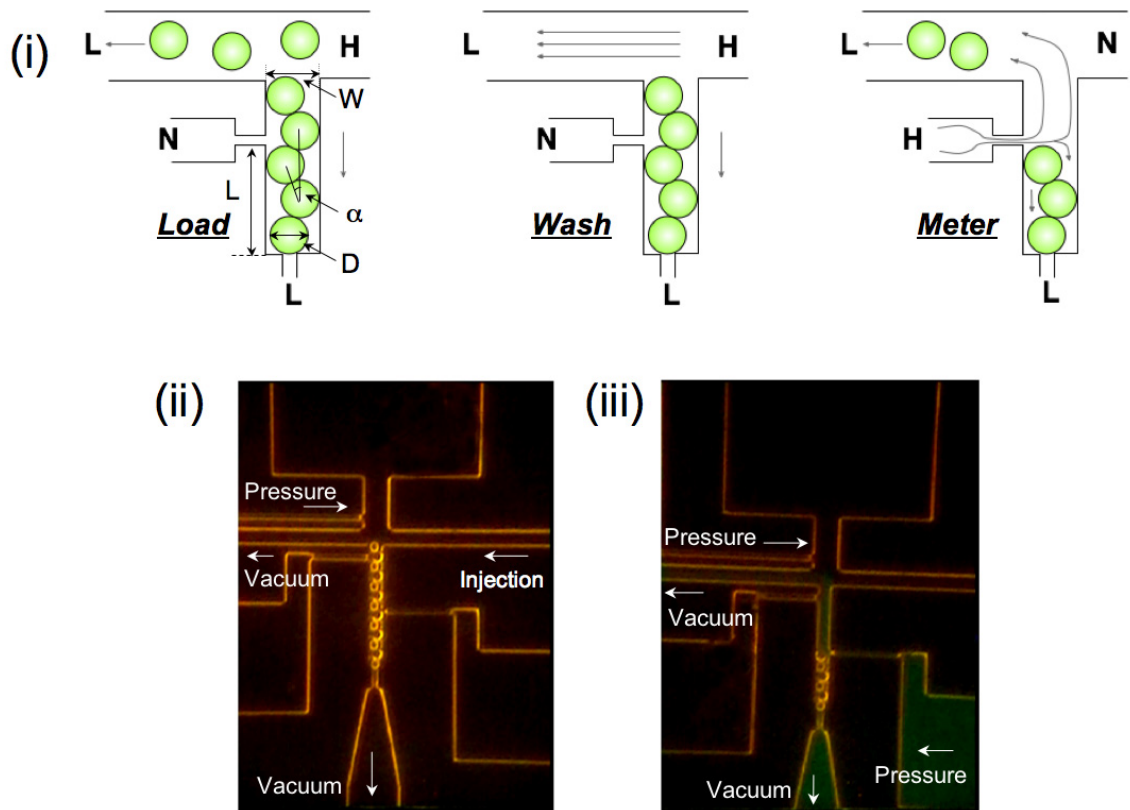
Figure 5. 11. Metering of particles by a particle-free control line. (i) schematic illustration of a metering process. The metering line is set at neutral during load and wash steps and has a high-pressure setting for the metering step to wash away particles above the line. (ii) Full stack of 20 μm particles in a confined channel (N=13). (iii) Metering by control line. Seven particles are washed away and six particles remain. The fluid coming out from the control line contains fluorescent dye to help us visualize the flow direction.

The position of the metering line is important to meter out an exact number of particles. As particles always produce a zigzag shaped chain, the chain length does not correspond to multiples of a particle's diameter. The chain length, L, is

$L \cong D(1 + (n-1)\cos\alpha)$, where D is particle diameter, n is the number of particles, and a is the angle between two adjacent particles (Figure 5.11 (i)). The angle is calculated from

$\sin\alpha = \dfrac{W}{D} - 1$, where W is the width of a channel. The metering line in Figure 5.11 (iii)

is designed to capture only five particles. The metering line is examined 160 times to check reliability and results show the line usually captures five particles (i.e., 124 times out of a total of 160). However, sometimes the line captures four (10 times) or six particles (23 times), having a higher probability of capturing six particles rather than four. Many reasons for this occurrence are possible, however, the metering line position is considered the primary. The position of the metering line in Figure 5.11 (iii), 105 μm, is higher than the chain length, 96.6 μm and the difference between these two is approximately half the diameter of a particle. Therefore, a metering line is best located directly above the end of a particle chain to reduce error.
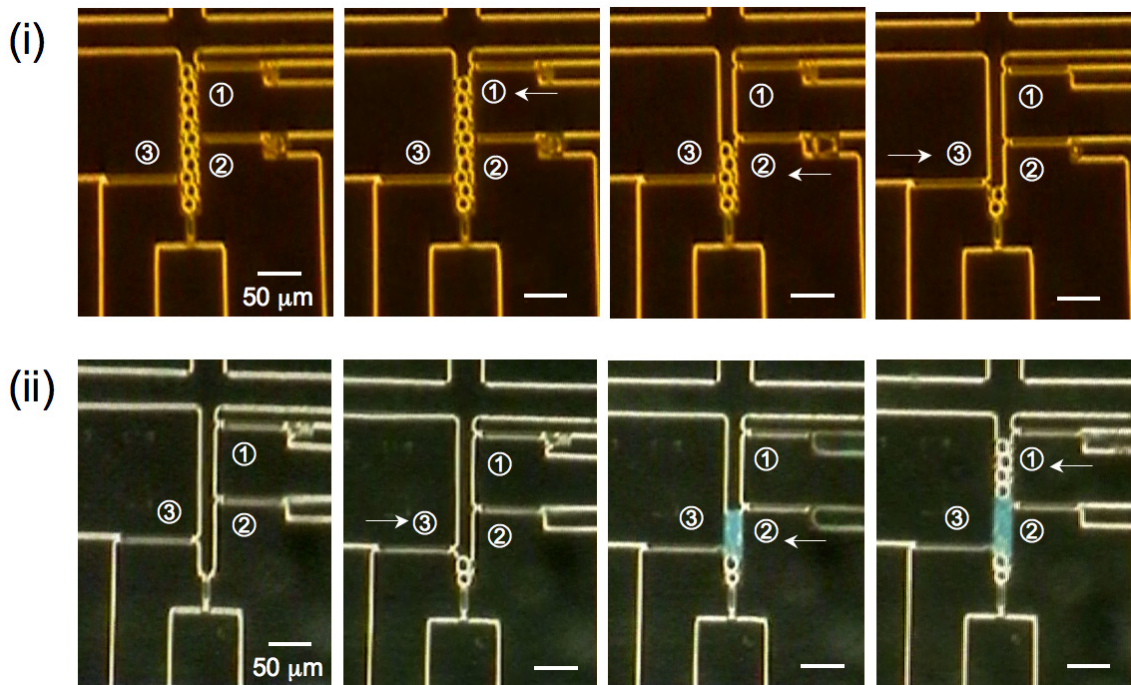
Figure 5. 12. (i) Sequential measuring of particles by multi-control lines. (ii) The process for an A-B-A structure. A is a 20 μm particle and B is a blue-dyed 10 μm particle.

Multiple metering lines, located along a confined channel, enable operation of a sequential metering process and generate a complex structure possessing a specific sequence. Figure 5.12 (i) exemplifies the sequential operation of three metering processes. One particle from the top of the chain is washed out by the actuation of line ①, five particles are captured by the actuation of line ②, and only the last two particles remain in the channel by the actuation of line ③. From the same channel design, a tri-block structure (A-B-A) is obtained. After 20 μm particles injection, line ③ is actuated to retain two particles, and the injection of 10 μm blue-dyed particles follows, metered by line ②. 20 μm particles are injected again and stacked over 10 μm particles, metered by line ① to complete a tri-block structure.

Conclusion

This paper presents a simple, three-point pressure control of particle-containing fluid in complex channel geometry to guide particles' motion toward desired locations. The system includes channel restrictions to confine particles at intended locations and many different geometrical confinements provide particle structure variety. The particle-free control line plays an important role in this system as it generates isolated sections, which allow quality control of movement, and meters a specific number of particles creating unique sequence structures. Particle jamming in a microchannel was not considered a serious problem. Silicon-glass surfaces inherently have less adhesion of particles than polymer surfaces, and experiments had sufficient low sample

concentration, wherein many wash lines in the system assisted in breaking jammed particles.

This particle control system is applicable to many other studies such as particle synthesis and cell biology due to its excellent adaptability. The channel size may be reduced by using traditional micro- and nano- fabrication methods to create structures with smaller particles and, moreover, polymer-based substrate can be used as evidenced in Figure 5.6. In addition, the stacked particles can be fused together to form a unique structure consisting of different particles[27]. Sequence structures may include some information, which can be used as a microbarcode[28] for cell labeling and other innovative applications. It is feasible to employ channel restriction to trap cells, rather than particles, and particle-free control lines can contain specific reagents for cellular assay. As the device materials, silicon and glass, are very common materials in traditional microfabrication, other components (e.g., microvalve and microreactor) can be easily added to construct a more complex integrated device[29, 30].

References

1. Wouden, E. J. v. d.; Heuser, T.; Hermes, D. C.; Oosterbroek, R. E.; Gardeniers, J. G. E.; Berg, A. v. d., Field-effect control of electro-osmotic flow in microfluidic networks. *Colloids and Surfaces A: Physicochem. Eng. Aspects* **2005,** 267, 110-116.

2. Lee, J. S. H.; Barbulovic-nad, I.; Wu, Z.; Xuan, X.; Li, D., Electrokinetic flow in a free surface-guided microchannel. *J.Appl.Phys.* **2006,** 99, 054905.

3. Sniadecki, N. J.; Lee, C. S.; Beamesderfer, M.; DeVoe, D. L. In *Field-Effect Flow Control In Polymer Microchannel Networks*, Transducers, Boston,, June 8-12, 2003; IEEE: Boston,, 2003; pp 682-685.

4. Li, D., *Electrokinetics in Microfluidics*. ELSEVIER: Oxford, UK, 2004; Vol. 2.
5. Santiago, J. G.; Wereley, S. T.; Meinhart, C. D.; Beebe, D. J.; Adrian, R. J., A particle image velocimetry system for microfluidics. *Experiments in Fluids* **1998,** 25, 316-319.

6. Chen, Z.; Burns, M. A., Effect of Buffer Flow on DNA separation in a Microfabricated Electrophoresis System. *Electrophoresis* **2005,** 26, (24), 4718-4728.

7. Kentsch, J.; Dürr, M.; Schnelle, T.; Gradl, G.; Müller, T.; Jäger, M.; Normann, A.; Stelzle, M., Microdevices for separation, accumulation, and analysis of biological micro- and nanoparticles. *IEE Proc.-Nanobiotechol.* **2003,** 150, (2), 82-89.

8. Pohl, H. A., *Dielectrophoresis: The behavior of neutral matter in nonuniform electric fields*. Cambridge University Press: Cambridge, New York, 1978.

9. Robert J. Barsotti, J.; Vahey, M. D.; Wartena, R.; Chiang, Y.-M.; Voldman, J.; Stellacci, F., Assembly of Metal Nanoparticles into Nanogaps. *Small* **2007,** 3, (3), 488-499.

10. Wu, H.; Thalladi, V. R.; Whitesides, S.; Whitesides, G. M., Using Hierarchical Self-Assembly To Form Three-Dimensional Lattices of Spheres. *Journal of American Chemical Society* **2002,** 124, 14495-14502.

11. Kumacheva, E.; Garstecki, P.; Wu, H.; Whitesides, G. M., Two-Dimensional Colloid Crystals obtained by Coupling of Flow and Confinement. *Phys. Rev. Lett* **2003,** 91, (12), 128301.

12.   Xia, Y.; Yin, Y.; Lu, Y.; McLellan, J., Template-Assisted Self-Assembly of spherical Colloids into Complex and Controllable Structures. *Adv. Funct. Mater.* **2003,** 13, (12), 907-918.

13.   Yantzi, J. D.; Yeow, J. T. W.; Abdallah, S. S., Multiphase electrodes for microbead control applications: Integration of DEP and electrokinetics for bio-particle positioning. *Biosensors & Bioelectronics* **2007,** 22, (11), 2539-2545.

14.   Voldman, J., Building with cells. *Nature Material* **2003,** 2, 433-434.

15.   Rosenthal, A.; Voldman, J., Dielectrophoretic Traps for Single-Particle Patterning. *Biophysical Journal* **2005,** 88, 2193-2205.

16.   Morgan, H.; Green, N. G., *AC Electrokinetics: Colloids and nanoparticles.* Research Studies Press: Philadelphia, 2003.

17.   Velev, O. D.; Bhatt, K. H., On-chip micromanipulation and assembly of colloidal particles by electric fields. *Soft Matter* **2006,** 2, 738-750.

18.   Probstein, R. F., *Physicochemical hydrodynamics.* 2nd ed.; John Wiley & Sons, Inc: New York, 1994.

19.   Bazant, M. Z.; Squires, T. M., Induced-Charge Electrokinetic Phenomena: Theory and Microfluidic Applications. *Physical Review Letters* **2004,** 92, (6), 066101-1 - 066101-4.

20.   Liu, D.; Maxey, M.; Karniadakis, G. E., A fast method for particulate microflows. *Journal of Microelectromechanical systems* **2002,** 11, (6), 691-702.

21.   Pal, R.; Yang, M.; Johnson, B. N.; Burke, D. T.; Burns, M. A., Phase Change Microvalve for Integrated Devices. *Anal. Chem.* **2004,** 76, 3740-3746.

22.   Eddington, D. T.; Beebe, D. J., Flow control with hydrogels. *Advanced Drug Delivery Reviews* **2004,** 56, 199-210.

23.   Voldman, J., Electrical Forces For Microscale Cell Manipulation. *Annu. Rev. Biomed. Eng.* **2006,** 8, 425-454.

24.   Carlo, D. D.; Wu, L. Y.; Lee, L. P., Dynamic single cell culture array. *Lab chip* **2006,** 6, 1445-1449.

25.   Rosenthal, A.; Macdonald, A.; Voldman, J., Cell patterning chip for controlling the stem cell microenvironment. *Biomaterials* **2007,** 28, 3208-3216.

26.   Vanapalli, S. A.; iacovella, C. R.; Sung, K. E.; mukhija, D.; Millunchick, J. M.; Burns, M. A.; Solomon, M. J., Assembly and Packing Spheres in Confined Channels for Microfluidic Synthesis of Anisotropic Particles. *Submitted* **2007**.

27.   Sung, K. E.; Vanapalli, S. A.; Mukhija, D.; McKay, H. A.; Millunchick, J. M.; Burns, M. A.; Solomon, M. J., Programmable fluidic synthesis of microparticles with configurable anisotropy. *Submitted* **2007**.

28.   Pregibon, D. C.; Toner, M.; Doyle, P. S., Multifunctional Encoded Particles for High-Throughput Biomolecular Analysis. *Sience* **2007,** 315, 1393-1396.

29.   Lagally, E. T.; Emrich, C. A.; Mathies, R. A., Fully integrated PCR-capillary electrophoresis microsystem for DNA analysis. *Lab chip* **2001,** 1, 102-107.

30.   Pal, R.; Yang, M.; Lin, R.; Johnson, B. N.; Srivastava, N.; Razzacki, S. Z.; Chomistek, K. J.; Heldsinger, D. C.; Haque, R. M.; Ugaz, V. M.; Thwar, P. K.; Chen, Z.; Alfano, K.; Yim, M. B.; Krishnan, M.; Fuller, A. O.; Larson, R. G.; Burke, D. T.; Burns, M. A., An Integrated Microfluidic Devices for Influenza and Other Genetic Analyses. *Lab chip* **2005,** 5, (10), 1024-1032.

CHAPTER 6
SINTERING OF POLYMERIC PARTICLES IN
MICROFABRICATED DEVICES

Introduction

Sintering has been accomplished with metallic, ceramic, and organic powders for many applications such as processing high molecular weight polymer and making metallic filters with very low porosity. Sintered bronze and stainless are used for filtration of steam in food and pharmaceutical applications that require high temperature resistance because metallic particle sintering provides very low porosity, difficult to achieve via other method[1, 2]. High-pressure compaction of polymeric powders, followed by sintering, has been studied for sometime, as this is an efficient process method for polymers difficult to process by conventional methods[3]. Rezaei et al used compaction and sintering to process ultra high molecular weight polyethylene (UHMWPE) because preparing an UHMWPE composite via conventional melt-mixing technologies presents difficulties[4].

Traditional polymeric particle sintering is usually performed in a circulated air oven or a particular hot stage, which shows absence of controllability[2-5]. Particles are placed in a thermal-resistant dish such as a Pyrex glass, sintered in an oven, and the sintered particles are examined under an optical microscope. The main driving force for

sintering of polymeric particles is thermodynamic force to lower their surface energy by reducing their surface area. Most conventional sintering researches are focused on determining particle size limits, applying different materials, and understanding physical and thermal properties of both individual and sintered particles[1, 2, 5]. However, this sintering method has limitations if controlling the shape and producing a unique structure of sintered particles is desired.

Many new technologies have been developed to sinter particles in a more controlled way. Selective laser sintering is one of the growing technologies in particle sintering because of its versatility with regard to metallic, ceramic, and polymeric particles[6-8]. Kathuria produced microstructures by selective laser sintering of metallic powder[7] while Childs et al employed this technique to sinter an amorphous polymer[6]. Moreover, a one-dimensional groove pattern is used to sinter a polymer colloid in specific shapes[9]. In that method, the particles are packed along the grooves by lateral capillary force and sintered in the grooves. Another method, the resistance sintering system, consisted of electric power and metal electrodes to sinter particles, supplying a more effective heating cycle than other conventional heating methods[10].

In this work, a microfabricated on-chip metal heater and microchannel is utilized to sinter polymeric particles into specific shapes. The on-chip heater has been widely used in the semiconductor industry and Bio-MEMS such as gas sensors[11] and micro PCR devices[12, 13]. The use of both microchannel and micro heater enables us to incorporate a particle-sintering component into a complex microfluidic device. In addition, they provide controllable sintering allowing easy controllability of sintering temperature and time through a computer-controlled heating process.

Material and Methods

Device fabrication

The device fabrication includes four different processes: silicon channel etching, lift-off of metal heater, glass drilling, and anodic bonding of silicon and glass sides. Figure 6.1 is an illustrated diagram of the entire fabrication process. The fluidic channels and metal heaters are fabricated and aligned on either side of the polished Silicon oxide wafer (450 μm thickness, 100mm diameter, 5000Å thermal oxide layer). For silicon channel etching, photoresist (PR 1827) is spun, patterned by a channel mask layer, and developed in the MF 319 solution. The oxide layer of the developed area is etched in buffered hydrofluoric acid solution. After these lithography steps are performed, the wafer is transferred into the STS Deep Reactive Ion Etcher for channel etching. After etching is completed, the oxide layer on the channel side is stripped by utilizing buffered hydrofluoric acid.

Metal heaters are fabricated on the backside of the Silicon wafer via metal lift-off. For that step, photoresist (PR 1827) is spun over the oxide layer that performs as an insulation layer for heaters, patterned by a heater mask layer and developed in the MF 319 solution. Ti/Pt (300Å/1000Å) is evaporated over the patterns generated by the lithography process and lifted off in acetone solution. Electrochemical discharge drilling is accomplished on the glass wafer (Pyrex 7740, 100mm diameter, 700 μm) to obtain holes for sample injections and fluid control. The glass wafer is cleaned in Piranha Clean Solution, which is a mixture of hydrogen peroxide solution and sulfuric acid solution (1:3

v/v). The obtained glass and Silicon wafers are aligned and bonded by anodic bonding. The bonded wafer is subsequently diced employing a dicing saw, and wired to a printed circuit board by gold ball wire bonding to obtain electrical connection. The Silicon channel side remains open to build a fluid interconnection system, to be observed by stereoscope. Glass pillars are bonded over each hole on the glass by UV glue for syringe connection.

Figure 6. 1. Schematic diagram of device fabrication. (i) Silicon side fabrication, (ii) drilling of glass side. Silicon and glass side are bonded anodically.

Particle sample preparation

Two different polystyrene particles, Megabead NIST Traceable Particle Size Standard 20.0 μm (Polysciences, Inc.) and Polybead Dyed Blue 10.0 μm microsphere (Polysciences, Inc.), are utilized as precursor particles. Dimethyl Sulfoxide (Sigma-Aldrich) is chosen as the carrier fluid due to its high boiling temperature (189 °C).

Dimethyl Sulfoxide (DMSO) and polystyrene have high polymer-solvent interaction parameters at 25 °C ($\chi_{ps/DMSO}$ = 1.36 > 0.5) and 80 °C ($\chi_{ps/DMSO}$ = 1.20 > 0.5); therefore, polystyrene particles do not swell in DMSO[14]. The concentration of the sample is 0.05 wt% for both particles.

Sintering condition

Polystyrene microparticles are fused physically employing device temperature control. A microfabricated on-chip heater is used to pulse device temperatures up to the softening temperature of the microparticles. The device temperature is increased up to 80 °C, which is slightly lower than the actual glass transition temperature of polystyrene (T_g = 100 °C). The resistance value of the metal heater, approximately 0.39 KΩ and 50 $V_{DC,}$ is applied to achieve a fast heating cycle. Thermal Fusing occurs immediately after the temperature reaches around 80 °C.

Pressure control

Fluid control is performed by applying pressure, vacuum, or neutral states at each hole. Pressure is applied by delivering carrier fluid into the system. Every hole is connected with syringes (3cc Disposable Reservoir System and Barrel Adapter Assembly, EFD) containing DMSO and fluid is pushed by pressure and pulled by vacuum. In order to switch those three states easily, a set of 2-way and 3-way valves (Numatech) is prepared and connected to the syringes. These solenoid valves are computer controlled (Labview 7.1, National Instruments). A pressure controller (VSO-

EP, Parker Pneutronics) is connected at the pressure source to regulate pressure application.

Image processing

All experiments have been performed under stereoscope (Olympus SZX-12) with a digital camera (Nikon Coolpix 4500) for imaging. The camera output is recorded and digitized. High-resolution particle images are taken by Upright Microscope (Zeiss Axioscope) with 10x and 40x objectives. By using image analysis software (ImageJ 1.34s, National Institute of Health), torsional angles between precursor particles are measured. Particle boundaries are found by an edge-detecting tool in the software and afterward, center points are detected by drawing squares and diagonals at each particle's boundary.

Heat transfer simulation

ABAQUS 6.1 was used to perform the heat transfer simulation of 3-D device geometry. The device and channel dimensions (i.e., device size and silicon and glass layer thickness) are identical in size to the actual device used for experiments, and channel design has been simplified. Heat flux is applied to the backside heater area creating boundary conditions. Other remaining areas exposed to the outside are set as natural convection to the air.

Results and Discussion

Particle sintering in a microchannel

Polymer particles are sintered at near glass transition temperature (T_g) of the polymer, and during a sintering process, the particles deform slightly, merging into one body. This occurs as a result of particles tending to lower their surface energy by reducing their surface area. If this sintering occurs in a regular dish or beaker, controlling the shape of sintered particles becomes difficult. However, if a micromold is prepared to trap particles, particular shapes of sintered particles are obtainable. Figure 6.2 shows a schematic illustration of particle deformation and sintering in a microchannel. At low temperatures (e.g., lower than T_g in tens of degrees Celsius) particles become slightly sticky, facilitating adherence to one another. The deformation of particles is not perceptible at this temperature. However, at high temperatures (near to T_g), particles become stickier and softer, deforming more, and therefore, the chain becomes shorter.
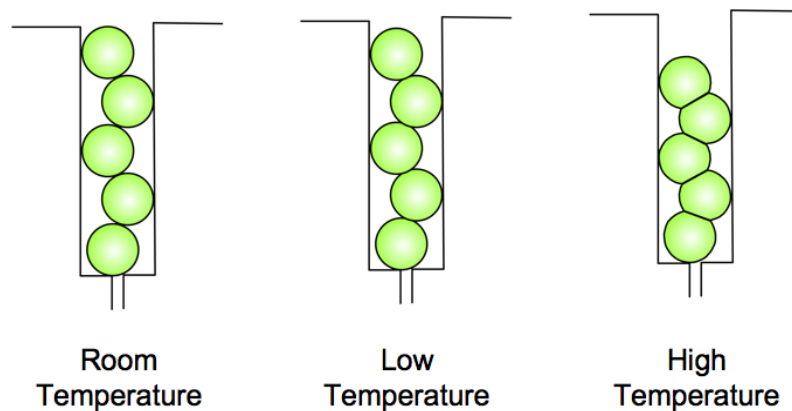

Figure 6. 2. Schematic illustration of particle fusing in a microchannel confinement at high and low temperatures.

Polymer particle sintering in a silicon microchannel with 20 μm polystyrene particles has been tested in this paper. Figure 6.3 shows a fabricated silicon microchannel via deep reactive ion etching. Particles are dragged into the reaction channel by vacuum and sintered in it by increasing the device temperature. An on-chip heater is prepared directly on the backside of the reaction channel. After the sintering has been completed, the flow is reversed and the product is collected at the collection chamber. This device is designed to synthesize linear-shaped particle chains; thus Channel width and depth is approximately 25 μm to allow passage of only one linear chain, and particles stop at the restriction point narrower than the diameter of a particle (i.e, 10 μm in width).
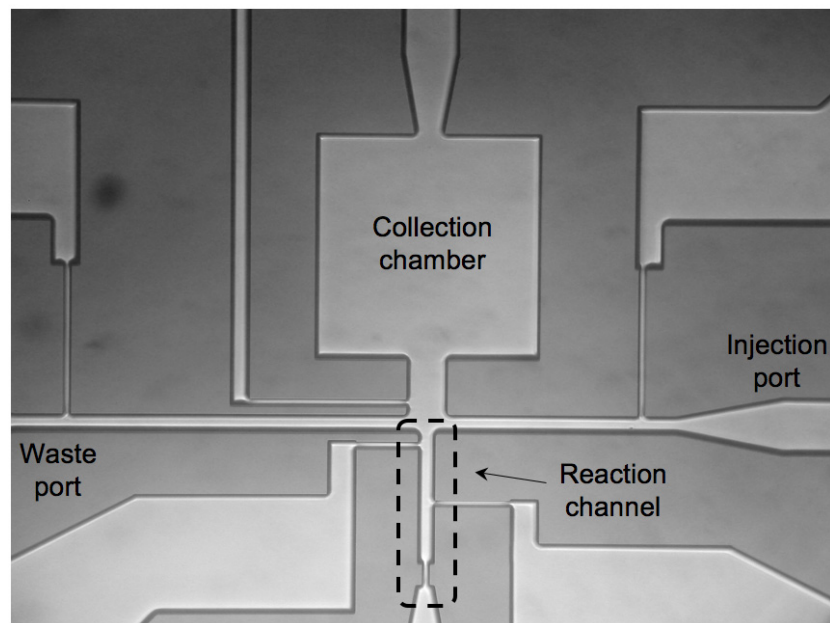

Figure 6. 3. Fabricated silicon channel used for the sintering, showing reaction channel, collection chamber, injection, and waste ports. 4 thin lines represent additional pressure lines, aiding wash, and section isolation (i.e., one near the collection chamber, two at the reaction channel, one near the injection port, and one at the waste port).

The glass transition temperature of a polystyrene particle is about 100°C; therefore, temperature is increased to 80°C to make particles sticky and soft. Figure 6.4 (i) shows stacked 20 μm polystyrene particles in a microchannel. The stack always forms a zigzag shape as entering particles tend to follow the path with the least fluidic resistance[15-18]. The flow line ① has outflow to the channel to wash away any particles above it, and five particles remain below it as shown. Figure 6.4 (ii) is a sintered chain at 80°C and there is noticeable length and boundary change after the sintering is accomplished. In addition, Figure 6.4 (iii) is a sintered chain in a collection chamber, and Figure 6.4 (iv) is a high-resolution image of a sintered chain. As evidenced in the figure, the particle stack order is not disrupted during the sintering process and, interestingly, the shape of the restriction is imprinted at the tail of the chain, proving particles were soft at the sintering temperature.

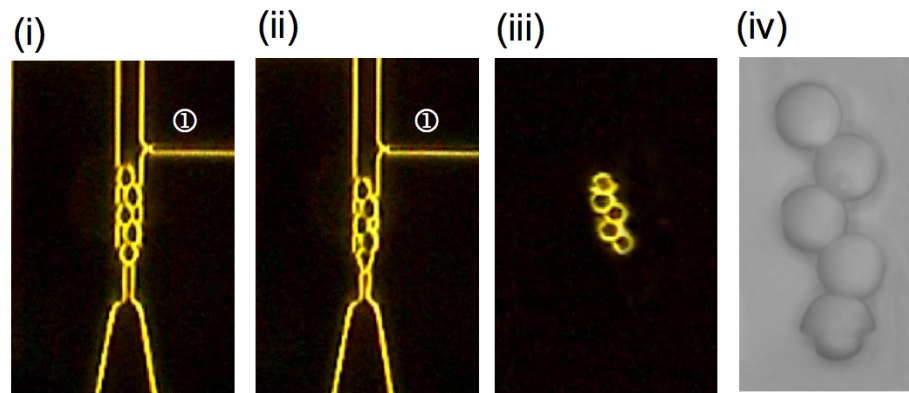**Figure 6. 4. Thermal fusing of 20 μm polystyrene particles in a microchannel. (i) Five stacked particles in a microchannel. (ii) Thermally fused particle at 80 °C. (iii) Fused chain collected in the collection chamber. (iv) High-resolution image of fused chain.**

Understanding heat distribution from the heater is essential as the on-chip heater is fabricated on the backside of the silicon channel. The device is bonded with silicon

and glass, and the heater is fabricated on the bottom side of the silicon to make the fabrication process as simple as possible. Figure 6.5 (i) illustrates a cross-sectional view of the device. The heater temperature (T_H), reaction channel temperature (T_R), and top glass temperature (T_G) are examined to find out the temperature distribution from the heater to the top surface. Figure 6.5 (ii) is the temperature distribution profile and shows quite even temperature distribution at the silicon side, and gradual temperature decrease into the glass side. Higher input power increases the heater temperature (T_H); however, as the temperature increases, the temperature variance between top and bottom surfaces also increase.
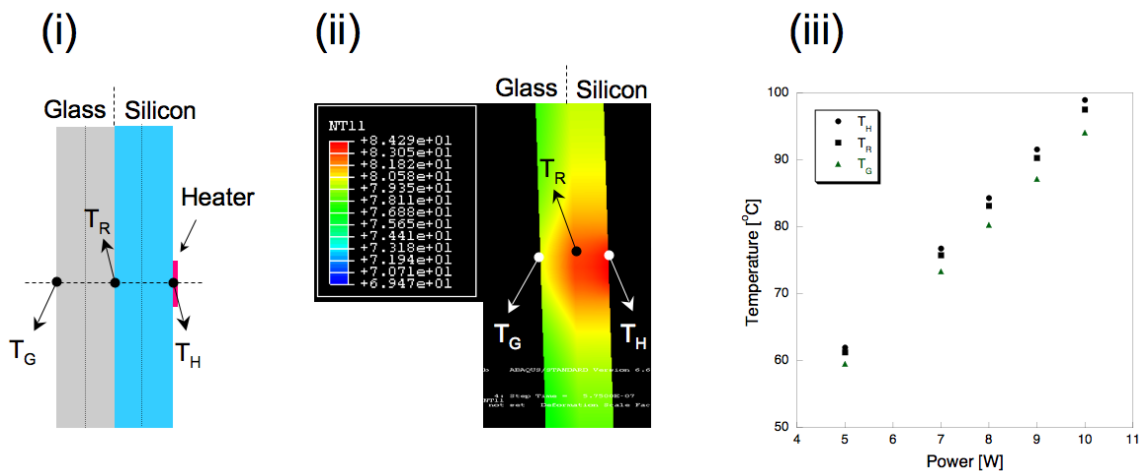
Figure 6. 5. Heat transfer from a backside heater. (i) Device structure illustration. The device is bonded with silicon and glass. The heater is fabricated on the backside of the silicon. Heater temperature is T_H, the temperature of the top silicon surface above the heater is T_R, and the temperature of the top glass surface is T_G. (ii) Temperature distribution along the z-axis from the backside heater (10^6 μm^2 size). (iii) The change of T_H, T_R, and T_G at different power values.
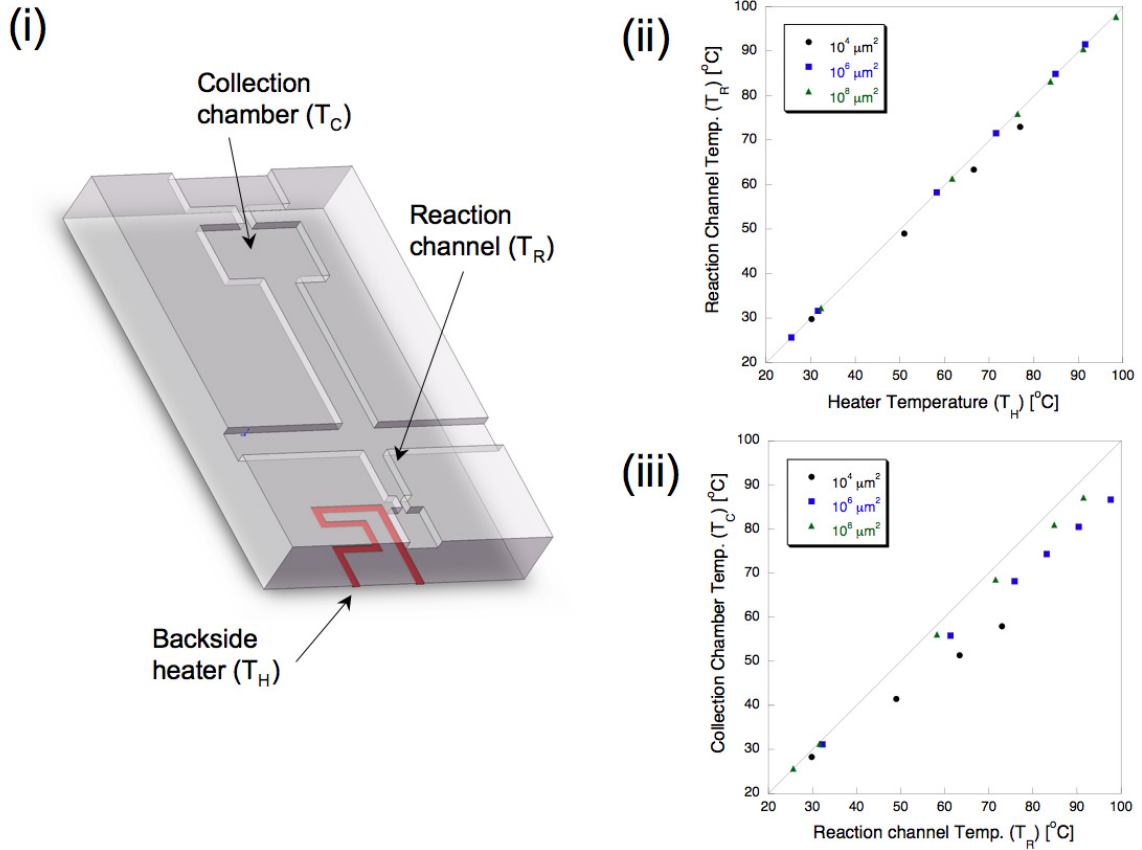
Figure 6. 6. Temperature distribution with different power and heater sizes. (i) schematic diagram of the device's silicon side. The heater temperature is TH, the reaction channel temperature is T_R, and the collection chamber, (1.5 cm distance from the reaction channel), is T_C. (ii) T_R and T_H comparison, employing three different heater sizes; 10^4 µm^2, 10^6 µm^2, and 10^8 µm^2. (iii) Temperature difference between T_R and T_C utilizing three different sized heaters. The straight lines in Figure (ii) and (iii) indicate equal proportions.

The size of the backside heater causes different heat distribution throughout the entire device; therefore, three different heater sizes, 10^4 µm^2, 10^6 µm^2, and 10^8 µm^2 are examined by heat transfer simulation (ABAQUS 6.1). The device size is 7.5 cm^2 (2.5cm X 3.0cm) and heat flux is applied from the backside heater. In order to check the heat distribution, three different temperature points are examined; T_H is the temperature of a backside heater, T_R is the temperature of the top silicon surface directly over the heater,

and T_C is the temperature of the top silicon surface at a distance (i.e., 1.5 cm) from the heater (Figure 6.6(i)).

A larger heater (10^8 μm^2) provides excellent heat distribution throughout the entire device. Figure 6.6 (ii-iii) illustrates plots extracted from the simulation data performed with various heater sizes. The temperature differences between T_H and T_R are negligible when large heaters, 10^6 μm^2 and 10^8 μm^2, are used; however, there is a slight difference ($\sim$3°C) when a small heater (10^4 μm) is employed. The difference augments as the temperature increases (Figure 6.6 (ii)). As shown in Figure 6.6(iii), the 10^4 μm^2 sized heater produces a noticeable difference between T_R and T_C (i.e., about 12°C), while the 10^8 μm^2 size heater only yields a 2~4°C difference. This temperature difference yielded from the 10^4 μm^2 sized heater is useful if a relatively low temperature zone is desired in the same device, without having any particular heat isolation component.

Controlling particle shape

The shape of a sintered particle chain is controlled by varying the sintering temperature. Figure 6.7 illustrates a few particle chains sintered at different temperatures. The glass transition temperature of polystyrene particles is about 100°C, but surprisingly this thermal sintering occurs from 60°C in a microchannel, and at 100°C, the particles are actually burned, and evidence loss of their original shapes (Figure 6.7(i)). The degree of particle deformation increases as the temperature increases, producing a shorter-length, sintered particle chain. Figure 6.7(ii) shows high-resolution images of sintered particle chains, wherein the interface between two particles becomes flatter as the temperature increases. When the temperature elevates above that of 90°C, particles are almost

liquefied, having flowed into the restriction area even without vacuum force from the restriction.

(i)

| 25 °C | 50 °C | 60 °C | 70 °C | 80 °C | 90 °C | 100 °C |

(ii)

| 60 °C | 70 °C | 80 °C | 90 °C | 100 °C |
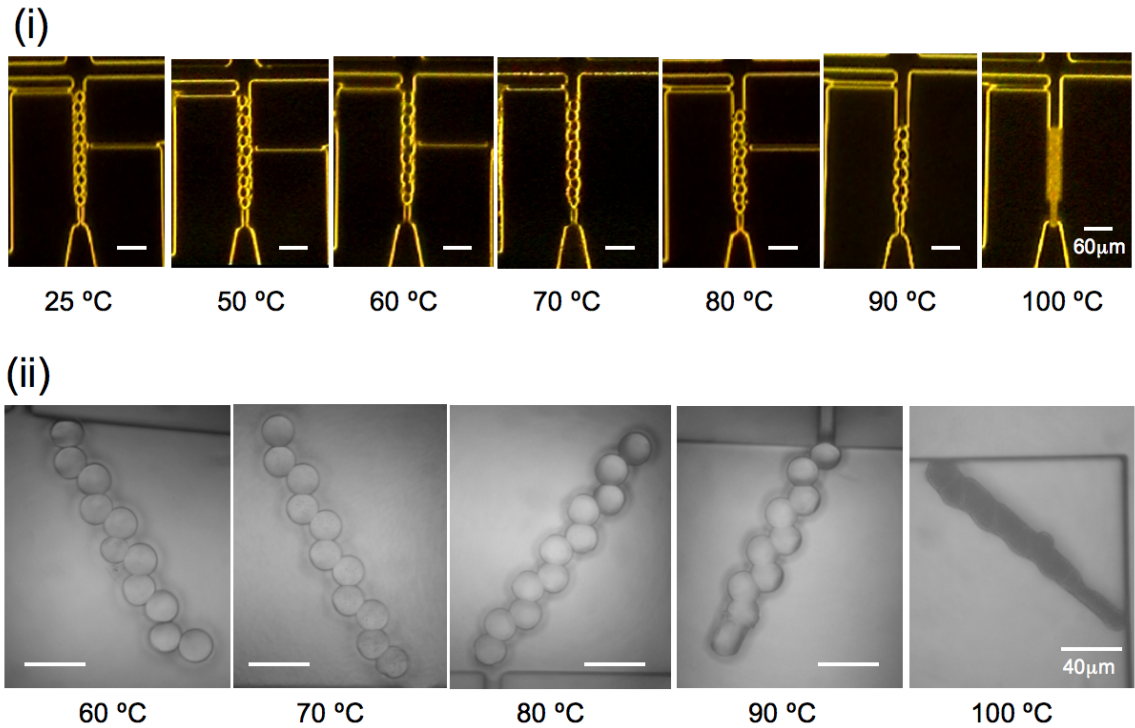
Figure 6. 7. Fused polystyrene particle chains at different temperatures. (i) Particle chains in a microchannel. (ii) High-resolution image of fused particle chains at different temperatures.

The sintering temperature changes the length and the bond angle (i.e., the angle between two adjacent particles) of a particle chain (Figure 6.8(i)). When particles are squeezed during the heating process, they are also pushed to the sidewall of the channel causing the chain to shorten and widen. The angle is calculated from $\sin\alpha = \dfrac{W}{D} - 1$, where W is the width of a channel and D is a particle diameter. The length of 11 particles before sintering is 221.84 μm, becoming about 160 μm at 90°C. The angle before sintering is 23.69° and it became 31° when the temperature reached 90°C. When the

temperature increases above 100°C, the chain is liquefied, subsequently flowing out through the restriction.
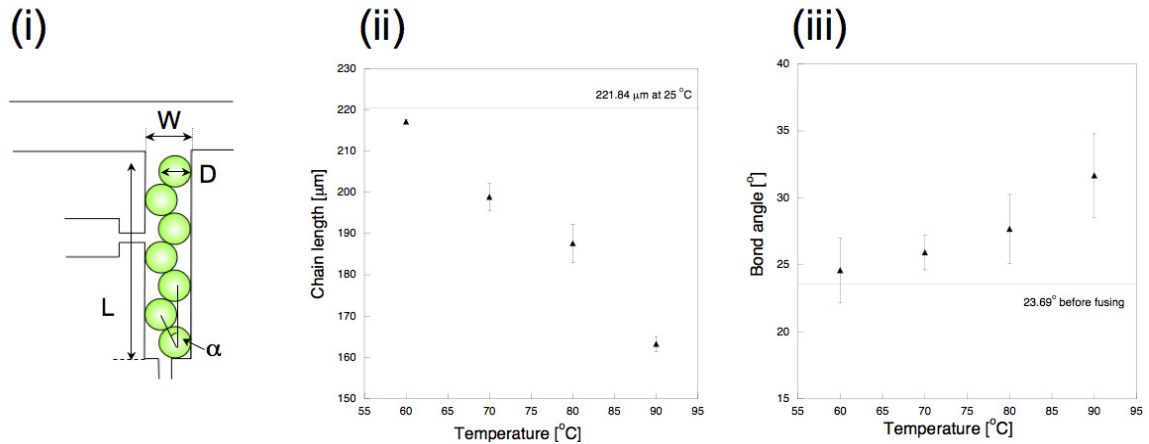
Figure 6. 8. Chain length and bond angle changes at different temperatures. (i) Illustration indicates measured chain length and angle. (ii) Chain length change versus fusing temperature. The line indicates the chain length before fusing (221.84 μm). (iii) Bond angle change versus fusing temperature. The line indicates the angle before fusing (23.69°).

Sintering times are dependent on both number of particles and sintering temperature. A chain with 10 particles takes longer than that of 5 particles, and low temperature takes substantial time to finish the sintering step (Figure 6.9). For example, 10 particles require 140 seconds to fuse at 60°C while 5 particles take only 40 seconds. However, from the 80°C point, both particle chains take less than a second and the difference between those two chains are negligible. At high temperatures (i.e., greater than 70°C), the boundary and chain length change is easily noticed; therefore, the timer was stopped when the change occurred. However, it was not easy to detect the boundary and length change at low temperatures (i.e., 60°C and 65°C), so the chains were pushed

out of the channel to check sintering completion. This confirmation process was iterated with 5 second interval.
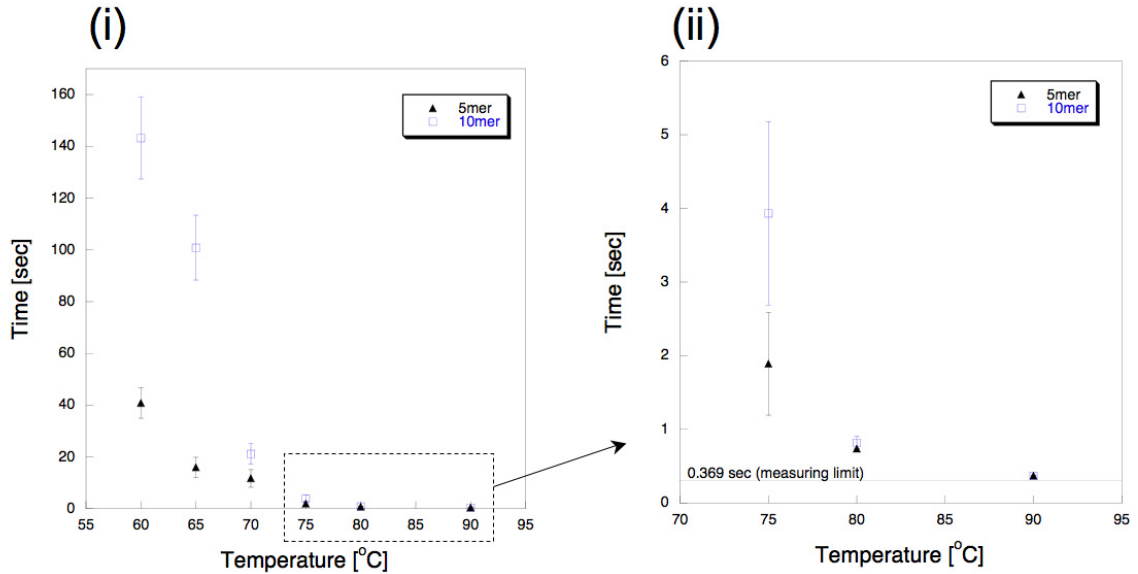
Figure 6. 9. Fusing time at different temperatures. (i) Fusing time at different temperatures. (ii) Enlarged plot of a dash box in figure 8 (i). The line indicates the limit of measuring time (0.369 sec).

One possible reason for the time variance is heater size and location. As can be seen from Figure 6.6(iii), heating from a small heater on the backside is highly localized. Therefore, if the heater does not cover an entire mold channel or if the location is not perfectly aligned, it may take some time to distribute adequate heat for sintering. This process should take longer at lower temperatures. Sintering time at 80°C and 90°C could be less than the indicated time; however, the Labview VI employed for this experiment has a limited measurement time (i.e., 0.369 second).

Multiple particle production
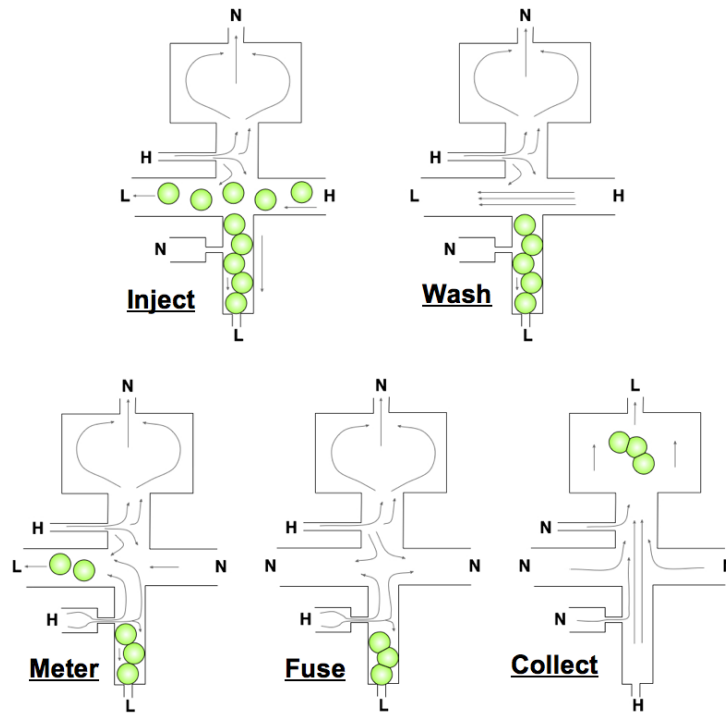
Figure 6. 10. Schematic illustration of the five steps involved in particle manufacturing: Particle injecting, washing, metering, fusing, and collecting. The arrow indicates flow direction. H: High pressure, N: Neutral, L: Low pressure.

This particle-sintering unit is incorporated into the microfluidic system that enables a continuous process for multiple particle chains. Figure 6.10 shows a schematic illustration for manufacturing of multiple particle chains. Particles move by simple three-point pressure control including high, neutral, and low-pressure settings and the continuous process includes five operating steps: injection, washing, metering, sintering, and collecting. Particles are dragged into the shaped channel to form a linear particle chain and other particles are washed away to a waste chamber during the washing step. There is a pressure line to meter the exact number of particles at the channel, and after a metering step, the remained particles are sintered by increasing the temperature of the on-

chip heater. After the sintering is done, the sintered chain is pushed into the collection chamber. There is another pressure line, which is always actuated except a collection step, in front of a collection chamber in order to isolate the collection chamber during an entire process. Therefore, any contaminant particles cannot flow into the collection chamber.

	I	W	M	R	C
1	P	P	N	N	N
2	N	N	P	P	N
3	V	V	V	V	P
4	N	N	N	N	N
5	V	V	V	N	N
6	N	N	N	P	P
7	N	N	N	N	N
8	N	N	N	N	V
9	P	P	P	P	N
10	N	N	N	P	P

• I: Injection, W: Washing, M: Metering, R: Reaction, C: Collection

• P: Pressure, N: Neutral, V: Vacuum
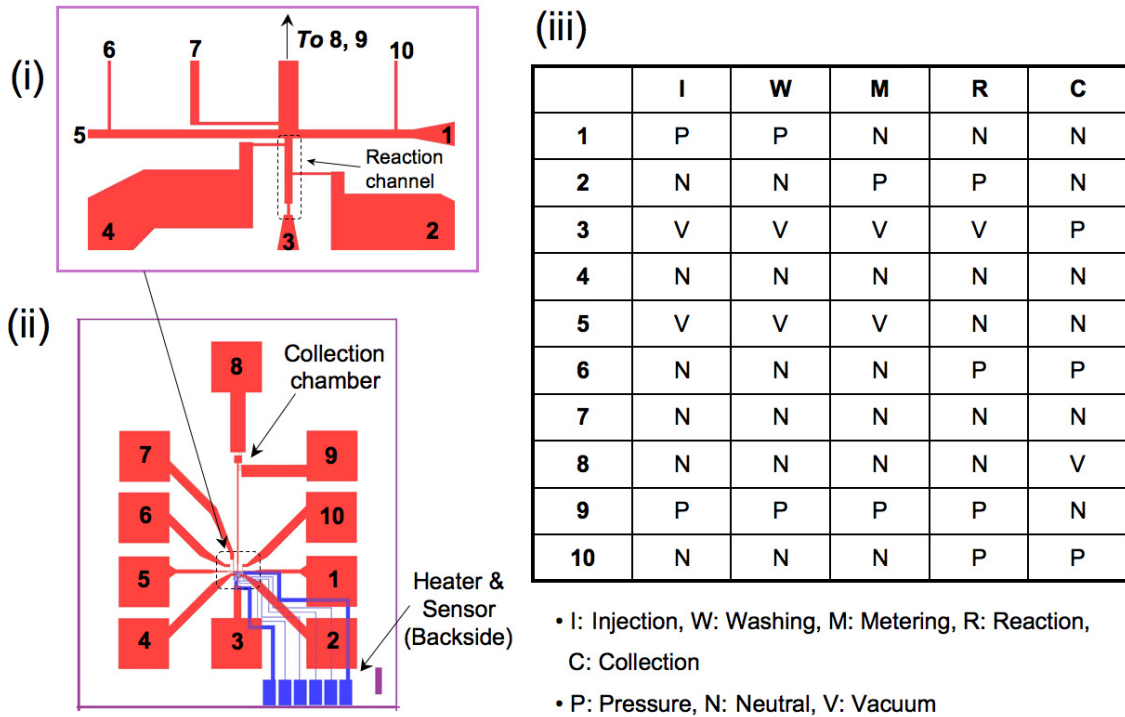
Figure 6. 11. Channel and heater design for multiple processes and corresponding operational table. (i) Main channel geometry for the process. The zoomed image numbers in (i) directly correspond with the numbers in Figure (ii). (ii) Entire design of channel and heater. Heater and sensors are directly under the reaction zone. The collection chamber is 1.5 cm from the reaction zone. (iii) Operational table. I: Injection, W: Washing, M: Metering, R: Reaction, C: Collection. P: Pressure, N: Neutral, V: Vacuum. The numbers in the table correspond to the numbers in figure (ii).

Figure 6.11 illustrates a channel and heater design and an operating table for a multiple process. A small heater and a sensor are fabricated directly under the channel

restriction to achieve maximum heating at that point, and the collection chamber is located approximately 1.5 cm away from the heating zone to ensure a relatively low temperature region. It is important to maintain a low temperature in the collection chamber (i.e., less than 60°C) to obtain individual particle chains. Each hole is connected to syringes that are alternating with pressure, vacuum, and neutral states. Figure 6.11 (iii) is the operating table for a multiple process, while Figure 6.12 shows a high-resolution image of 7 manufactured particles, containing 5 particles in each chain, through the continuous process. The particles are colored either red or blue to distinguish individual particles. As can be seen from the figure, all manufactured particles are highly uniform, exemplifying separate chains.
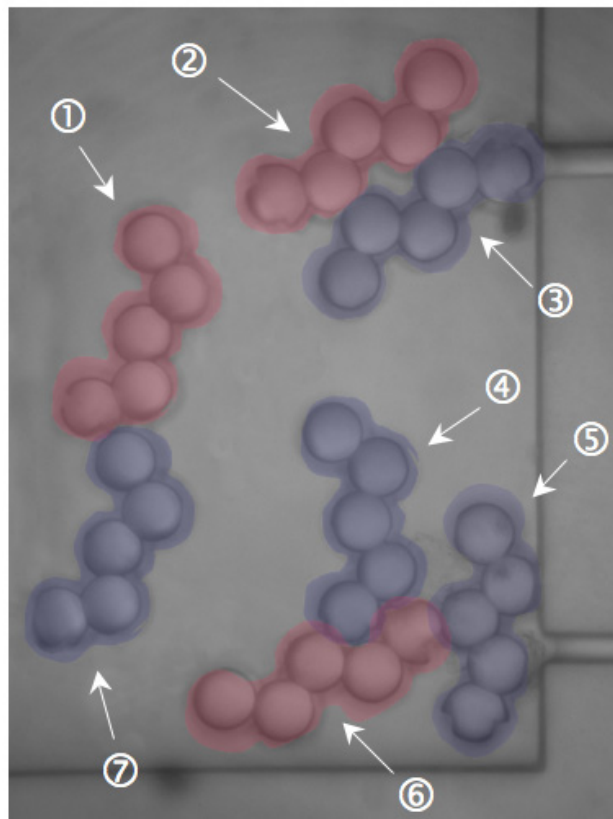
Figure 6. 12. Seven chains, having five particles in each chain, produced via the multiple process. Blue and red coloring is used to distinguish individual particles.

As discussed earlier, the use of a small sized heater (10^4 μm^2) helps to achieve a low temperature collection zone (i.e., approximately 60°C) in a 7.5 cm²-sized device when the temperature of the reaction channel is 73°C. Although the actual heater design is a serpentine shape, the entire heater fits tightly in a 10^4 μm^2-sized square. Thus, the simulation data in Figure 6.6 can be used to understand the temperature distribution, relevant to multiple processing. A particle chain may be sintered at 60°C but the temperature requires an extensive sintering time (e.g., more than 30 seconds). Therefore, it is believed that the short sintering time at 75°C (i.e., approximately 1 second) is safe to obtain all the separate particles in the collection chamber.

Figure 6. 13. Diagram showing backside-etching areas (i.e., A and B) applied to heat transfer simulation to investigate the heat isolation effect. The distance between heating area and collection chamber is 1.5 cm.

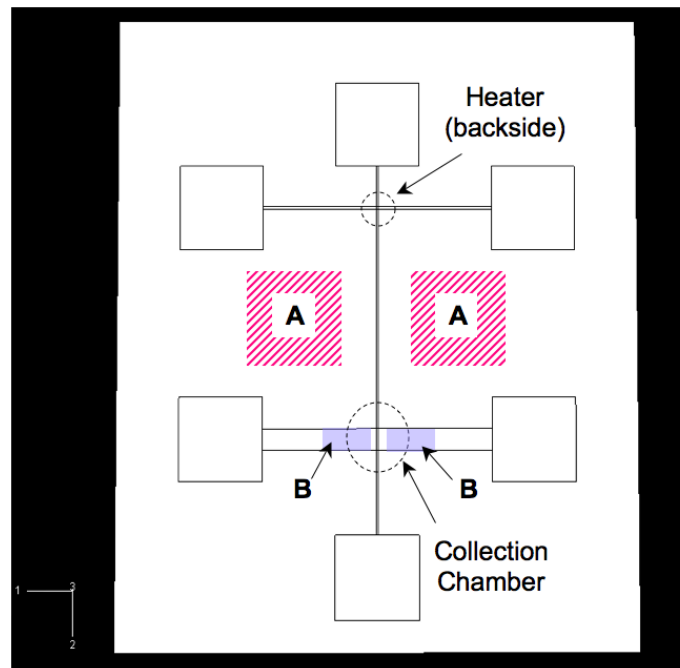| Conditions	T_R	T_C	$T_R - T_C$
Water (k = 0.613 Wm^{-1}K^{-1})	71.7756	61.4034	10.3722
DMSO (k = 0.199 Wm^{-1}K^{-1})	71.8057	61.8723	9.9334
Air (k = 0.0299 Wm^{-1}K^{-1})	71.946	60.3349	11.6111
Backside etching at small A (area: 0.49cm^2, depth: 420μm, remaining Si: 30μm)	73.1799	61.1986	11.9813
Backside etching at large A (area: 1.5cm^2, depth: 420μm, remaining Si: 30μm)	79.5938	60.3525	19.2413
Backside etching at large A (area: 1.5cm^2, depth: 448μm, remaining Si: 2μm)	83.4732	51.3117	32.1615
Backside etching at B (area: 0.1cm^2, depth: 420μm, remaining Si: 30μm)	72.6132	59.4241	13.1891
Backside etching at B (area: 0.1cm^2, depth: 448μm, remaining Si: 2μm)	72.1175	56.4744	15.6431
Backside etching at large A and B (area: 1.6cm^2, depth: 448μm, remaining Si: 2μm)	83.5128	45.8221	37.5907

Figure 6. 14. The temperature difference between TR and TC with different heat isolation conditions, having the same amount of power (10W).

More powerful heat isolation can be achieved by performing backside deep etching in the area between the heater and collection chamber. Heat transfer simulation confirms the effect of backside etching at the 2 different zones (i.e., A and B in Figure 6.13) as well as the effect from different thermal conductivity materials. 1.5 cm distance was placed between the heating area and the collection chamber, as previously illustrated. Figure 6.14 presents data obtained through simulation at the constant power (i.e., 10W).

Due to the heat isolation condition given to the device, the power efficiency differs for each condition, generating different T_R. A lower thermal conductivity material (i.e., air) generates a 2°C greater temperature variance as opposed to a higher thermal conductivity material (i.e., water). This effect is due to higher thermal resistance caused by lower conductivity, hindering rapid temperature increase. However, performing backside etching generates a more influential temperature drop between the reaction channel and the collection chamber (about 37°C as maximum difference) than changing buffers in microchannels.

Backside etching at large A ($1.5cm^2$) yields a recognizable temperature difference (i.e., 32.1615°C) in contrast to small A ($0.49cm^2$). Etching around the collection chamber, area B ($0.1cm^2$), also shows some temperature drop (15.6431°C), but the difference is less than half of the temperature drop yielded by performing backside etching at large A. In addition, two different depths were examined: One was 420 μm, giving a remaining depth of 30 μm in the silicon layer, and the other was 488 μm, yielding a remaining depth of 2 μm in the silicon layer. However, the latter shows a greater difference of only 2° C than the former, lower than expected. Consequently, the combination of backside deep etching at A and B yields maximum temperature drop (i.e., 37.5907°C). These results occur primarily when most of the backside surface, between the heater and the collection chamber, is exposed to air, giving considerable convective heat loss.

Conclusion

In our system, polymer particles are delivered and sintered in a mold type microchannel, using an on-chip microheater. When polymer particles reached a temperature near to the glass transition temperature, those particles became sticky, and adhered together. However, if the temperature elevates above that of the glass transition temperature, particles nearly liquefy, making it difficult to retain their original shape. As shown previously, polystyrene particles start sintering from 60°C and lose their original shape when the temperature reaches the actual glass transition temperature, 100°C. The shape of the chain is controlled by the temperature that is generated from the backside heater. The heater size is one of the important factors to achieve an appropriate temperature gradient for multiple particle manufacturing and more effective heat isolation may be obtained through performing backside etching of the surface between reaction channel and collection chamber.

This system is a novel method to create new types of particle structures. In addition, it is flexible because it employs a simple heating method, thus other polymer materials can also be used. Moreover, the microchannel used as a mold can have various shapes to produce unique structures other than a linear chain, facilitating this system's modification into more complex structures, composed of many different particles, in one sintered structure[17]. The resultant sintered structure can be studied for a myriad of further researches such as self-assembly[16, 19] and developing a unique drug delivery carrier[20, 21]. We can also generate Janus particles[22] and patch particles[23] that possess many functions using this method.

References

1. Upadhyaya, G. S., *Sintered metallic and ceramic materials: preparation, properties, and applications*. Wiley: New York, 2000.

2. Rahaman, M. N., *Ceramic processing and sintering*. M. Dekker: New York, 1995.

3. Narkis, M., Sintering Behavior of Poly(Methyl Methacrylate) Particles. *Polymer Engineering and Science* **1979,** 19, (13), 889-892.

4. Rezaei, M.; Ebrahimi, N. G., Thermal Properties, Rheology and Sintering of Ultra High Molecular Weight Polyethylene and Its composite With Polyethylene Terephthalate. *Polymer Engineering and Science* **2005,** 45, 678-686.

5. Mazur, S.; Beckerbauer, R.; Buckholz, J., Particle size limits for Sintering Polymer Colloids without Viscous Flow. *Langmuir* **1997,** 13, 4287-4294.

6. Childs, T. H.; Berzins, M.; Ryder, G. R.; Tontowi, A., Selective Laser Sintering of an Amorphous polymer - simulations and Experiments. *Proceedings of the I MECH E Part B Journal of Engineering Manufacture* **1999,** 213, (4), 333-349.

7. Kathuria, Y. P., Microstructuring by selective laser sintering of metallic powder. *Surface and Coatings Technology* **1999,** 116-119, 643-647.

8. Kruth, J. P.; Wang, X.; Laoui, T.; Froyen, L., Lasers and materials in selective laser sintering. *Assembly Automation* **2003,** 23, (4), 357-371.

9. Yi, D. K.; Seo, E.-M.; Kim, D.-Y., Fabrication of a Mesoscale Wire: Sintering of a Polymer Colloid Arrayed Inside a One-Dimensional Groove Pattern. *Langmuir* **2002,** 18, 5321-5323.

10. Maki, S.; Harada, Y.; Mori, K., Application of resistance sintering technique to fabrication of metal matrix composite. *Journal of Materials Processing Technology* **2001,** 119, 210-215.

11. Tian, W.-C.; Pang, S. W., Thick and thermally isolated Si microheaters for microfabricated preconcentrators. *J. Vac. Sci. Technol. B* **2003,** 21, (1), 274-279.

12. Lagally, E. T.; Emrich, C. A.; Mathies, R. A., Fully integrated PCR-capillary electrophoresis microsystem for DNA analysis. *Lab chip* **2001,** 1, 102-107.

13. Pal, R.; Yang, M.; Lin, R.; Johnson, B. N.; Srivastava, N.; Razzacki, S. Z.; Chomistek, K. J.; Heldsinger, D. C.; Haque, R. M.; Ugaz, V. M.; Thwar, P. K.;

Chen, Z.; Alfano, K.; Yim, M. B.; Krishnan, M.; Fuller, A. O.; Larson, R. G.; Burke, D. T.; Burns, M. A., An Integrated Microfluidic Devices for Influenza and Other Genetic Analyses. *Lab chip* **2005,** 5, (10), 1024-1032.

14.   Cong, Y.; Zhang, Z.; Fu, J.; Li, J.; Han, Y., Water-induced morphology evolution of block copolymer micellar thin film. *Polymer* **2005,** 46, 5377-5384.

15.   Kumacheva, E.; Garstecki, P.; Wu, H.; Whitesides, G. M., Two-Dimensional Colloid Crystals obtained by Coupling of Flow and Confinement. *Phys. Rev. Lett* **2003,** 91, (12), 128301.

16.   Wu, H.; Thalladi, V. R.; Whitesides, S.; Whitesides, G. M., Using Hierarchical Self-Assembly To Form Three-Dimensional Lattices of Spheres. *Journal of American Chemical Society* **2002,** 124, 14495-14502.

17.   Sung, K. E.; Vanapalli, S. A.; Mukhija, D.; McKay, H. A.; Millunchick, J. M.; Burns, M. A.; Solomon, M. J., Programmable fluidic synthesis of microparticles with configurable anisotropy. *Submitted* **2007**.

18.   Vanapalli, S. A.; iacovella, C. R.; Sung, K. E.; mukhija, D.; Millunchick, J. M.; Burns, M. A.; Solomon, M. J., Assembly and Packing Spheres in Confined Channels for Microfluidic Synthesis of Anisotropic Particles. *Submitted* **2007**.

19.   Glotzer, S. C.; Solomon, M. J., Anisotropy of building blocks and their assembly into complex structures. *Nature Material* **2007,** 6, 557-562.

20.   Tao, S. L.; Desai, T. A., Microfabricated drug delivery systems: from particles to pores. *Advanced Drug Delivery Reviews* **2003,** 55, 315-328.

21.   Champion, J. A.; Mitragotri, S., Role of target geometry in phagocytosis. *PNAS* **2006,** 103, (13), 4930-4934.

22.   Roh, K.-h.; Martin, D. C.; Lahann, J., Biphasic Janus particles with nanoscale anisotropy. *Nature Material* **2005,** 4, 759-763.

23.   Glotzer, S. C., Some Assembly Required. *Science* **2004,** 306, 419-420.

CHAPTER 7
CONCLUSIONS AND FUTURE WORK

Conclusions

The objective of this dissertation was developing simple but versatile control systems in microfabricated devices by employing electrokinetic and fluidic forces. First, the DEP DNA stretching was duplicated and optimized to build a robust electric control system for DNA molecules. Second, a new patterning method was developed to pattern non-traditional materials into microsystems fabricated by traditional methods. Third, a novel anisotropic particle synthesis method is developed through simple fluidic control in complex microchannel geometry, which can be easily employed for other applications.

The first part of this dissertation (Chapter 2), addresses the issues on reproducibility of DEP DNA stretching by enhancing electric field control capabilities. DEP DNA stretching is still not fully understood. However, the findings presented here illuminate that denser electric field and surface with less non-specific adsorption of DNA molecules to the channel walls significantly enhances the reproducibility of DNA stretching, giving a nearly 90% success rate. Nevertheless, more work (e.g., temperature, surface property, and buffer ion dependence on stretching) need to be performed to construct a more stable and fully understood system. Although this stretching system

was not incorporated into a more complex, integrated system for comprehensive DNA analysis devices, the resultant system possesses excellent potential to be included into the integrated system.

Secondly, a novel patterning technique, employable for patterning a vast array of materials, ranging from highly sensitive cells and enzymes to novel materials, whose properties are yet unknown has been developed. This method provides an excellent tool for microfabrication and surface modification due to material flexibility, easy fabrication, and precise alignment. The traditional microfabrication technology involves many harsh chemical treatments and a thermal process, which cannot be used for handling sensitive materials. However, this technique presents great adaptability of traditional MEMS technology by integrating non-traditional materials with traditional microfabricated devices. This method is applicable to the stretching system. Nano-sized enzyme patterns can be prepared between the two electrodes to digest stretched DNA molecules, which can then be used to investigate DNA-protein interaction or to construct an integrated DNA analysis device using DNA cut fragments.

Third, the novel synthesis method is developed for homogeneous and heterogeneous anisotropic microparticles, using a combination of microfluidic control and geometric confinement. This method impacts the anisotropic particle synthesis area as it employs a continuous and programmable process, enabling production of many different unique structures from one synthesis run. Many current techniques depend on either microfluidics or geometrical confinement. The presented method is influential as it is the first approach combining the fluidic control and the geometrical confinement in one system. Although the technique contains some limitations from heating reaction and

scale issues, those limitations will be easily solved in the near future. Another notable advantage of this technique is that it provides excellent flexibility to the system in terms of applicable materials. In this present work, polystyrene particles are the only material tested through the system; however, other molecules or particles (i.e., cells or metallic particles) can also be employed in the same control system for the desired applications.

Future work

The studies conducted in this dissertation raised issues worthy of further investigations in and future researches in both DNA stretching and particle synthesis works. Among those, three further researches on the particle synthesis system would be the most feasible and bring significant impact: (1) Modification of the particle system for the use of smaller particles, and as well for other reaction schemes such as chemical reactions. (2) Development of a valve component to control particle motion in the device. (3) Integration of complete particle synthesis process, commencing with the pre-cursor particle preparation to applications of the synthesized anisotropic particles, and development of a complex barcording system for cell labeling or any desired applications.

First, the particle synthesis method possesses numerous possibilities for further studies, because this method is extremely flexible and applicable to many other particles as previously mentioned. The device used in this work is designed and manufactured for 20 μm size polystyrene particles specifically. However, the size can be reduced to nano-scale for the use of nano particles via nanofabrication techniques such as Focused Ion

Beam Milling and Electron Beam Lithography[1]. Many novel synthesized particles are nano-scale, and each developed particle contains unique chemistries and functions[2-4]. Therefore, if those particles are applied into this system, many other reaction schemes can be incorporated, producing numerous anisotropic particles, which may possess greater functions and usage than the anisotropic microparticles developed in this dissertation. Although the nanofluidic control is expected to be slightly different from the microfluidic control used previously, it is feasible if the pressure drop, the interfacial electrokinetic forces from the channel walls can be overcome, and the thermal motion of nano-sized particles[5, 6].

Second, electrical valves, using charge effects between particles and channel surfaces, are one possible solution to easily control particle motion in the complex microchannel network. Particles in the presented system have been controlled by employing only pressure driven forces, and thus, numerous particles have transported together, which required several washing steps. Therefore, it is supposed that a reduction in the number of washing steps, and increased precision of particle motion control can be achieved if a certain valve component is incorporated in the system, which would control an individual particle's motion. Many valves (i.e., membrane valves and wax or gel valves[7-9]) and single particle trapping controls (i.e., Dielectrophoretic trapping[10, 11]) have been developed recently; however, those methods require more fabrication steps and materials.

Interestingly, particle motions in the tight microchannels have been observed as being considerably dependent on both particle charges and wall charges. (Glass and silicon channel material, as well as many other particles have slight negative charges,

unless modified differently.) When particles were mixed only in DI water, the particles' motions were very slow, tending not to enter tight channel geometry, due to the resistance generated by interaction between particles and wall charges. However, when particles were mixed in salt-contained DI-water, the particle surface charges were shielded by the salt solution. This shielding effect reduced the resistance and particle flow was very fast and smooth, unaffected by tight channel geometry. As a result of this occurrence, development of a simple electric valve component, only using the charge effect between channel surfaces and particles without incorporating any other materials, is most feasible. To facilitate this process, a few square shaped-trapping areas can be prepared in the middle of a tight straight channel. The size of the square would be larger than the width of the tight channel, allowing only one particle to settle there. The squares provide a preferred zone for particle retention, as they contain less charge constraints than tight straight channels. Therefore, when the particles, mixed in DI water, enter into the tight channel, each particle remains in the square, and the trapped particles can be released by pressure pulse, which overcomes the charge effect. That way, we can individually deliver particles, one at a time, into the system.

Third, the anisotropic particle synthesis system can be incorporated into a more complex, integrated system. A complete particle synthesis process can be constructed, commencing from the pre-cursor particle preparation to applications of the synthesized anisotropic particles. Particle generation, via photopolymerization[12] and two-phase flow control[13], has been recently developed, and those two methods are combinable with our synthesis method. In the proposed method, the pre-cursor particle is generated first via either the photopolymerization or two-phase flow control method. Then the particle is

transported and synthesized to obtain unique anisotropic particles. Another integrated system can be prepared with the developed synthesis method. A microbarcoding system has been considered as one feasible application for the synthesized anisotropic particles as the particles can be synthesized with unique sequences (e.g., A-B-A). The barcoded particle can be transported to the specific location in the device for labeling purposes. In this process, a cell group to be labeled meets a barcoded particle at a predetermined channel location. Therefore, the cell can possess specific information and is transportable to either a detection section[14] or a section for other applications such as culturing.

References

1.   Plummer, J. D.; Deal, M. D.; Griffin, P. B., *Silicon VLSI technology*. Prentice Hall: New Jersey, 2000.

2.   Roh, K.-h.; Martin, D. C.; Lahann, J., Biphasic Janus particles with nanoscale anisotropy. *Nature Material* **2005,** 4, 759-763.

3.   Glotzer, S. C.; Solomon, M. J., Anisotropy of building blocks and their assembly into complex structures. *Nature Material* **2007,** 6, 557-562.

4.   Glotzer, S. C., Some Assembly Required. *Science* **2004,** 306, 419-420.

5.   Probstein, R. F., *Physicochemical hydrodynamics*. 2nd ed.; John Wiley & Sons, Inc: New York, 1994.

6.   Nath, P.; Roy, S.; Conlisk, T.; Fleischman, A. J., A System for Micro/Nano Fluidic Flow Diagnostics. *Biomedical Microdevices* **2005,** 7, (3), 169-177.

7.   Pal, R.; Yang, M.; Johnson, B. N.; Burke, D. T.; Burns, M. A., Phase Change Microvalve for Integrated Devices. *Anal. Chem.* **2004,** 76, 3740-3746.

8.   Eddington, D. T.; Beebe, D. J., Flow control with hydrogels. *Advanced Drug Delivery Reviews* **2004,** 56, 199-210.

9.   Unger, M. A.; Chou, H. P.; Thorsen, T.; Scherer, A.; Quake, S. R., *Science* **2002,** 288, 113-116.

10.   Voldman, J., Electrical Forces For Microscale Cell Manipulation. *Annu. Rev. Biomed. Eng.* **2006,** 8, 425-454.

11.   Rosenthal, A.; Voldman, J., Dielectrophoretic Traps for Single-Particle Patterning. *Biophysical Journal* **2005,** 88, 2193-2205.

12.   Dendukuri, D.; Pregibon, D. C.; Collins, J.; Hatton, T. A.; Doyle, P. S., Continuous-flow lithography for high-throughput microparticle synthesis. *Nature Material* **2006,** 5, 365-369.

13.   Xu, S.; Nie, Z.; Seo, M.; Lewis, P.; Kumacheva, E.; Stone, H. A.; Garstecki, P.; Weibel, D. B.; Gitlin, I.; Whitesides, G. M., Generation of monodisperse particles by using microfluidics: Control over Size, Shape, and Composition. *Angew. Chem. -Int. Edit.* **2005,** 44, (5), 724-728.

14.   Pregibon, D. C.; Toner, M.; Doyle, P. S., Multifunctional Encoded Particles for High-Throughput Biomolecular Analysis. *Sience* **2007,** 315, 1393-1396.